Investigation of Bond Behaviour Between GFRP Reinforcing Bars and Concrete Containing Seawater

Mehran Parvizi

Thesis submitted to the University of Ottawa
in partial Fulfillment of the requirements for the
Master of Applied Science in Civil Engineering

Civil Engineering Department
Faculty of Engineering
University of Ottawa

Acknowledgements

I would like to express my sincere gratitude and render my warmest thanks to my supervisor Dr. Martin Noel for his continues support, patience, motivation, enthusiasm and immense knowledge. His friendly guidance and expert advice have been invaluable throughout all stages of the work. I could not have imagined having a better advisor and mentor for my Master program study.

My deepest thanks goes to my parents and sister who with their enormous support and love helped me through all stages of my life.

I would like to acknowledge the lab technical officers at University of Ottawa for their guidance through this research.

Lastly I would like to thanks my friends who helped me through this stage of my life.

Abstract

There has been a growing concern of water scarcity in recent years as global water shortages are increasing. The concrete industry consumes about 2 billion tons of potable water annually. For this reason, seawater has drawn attention as a potential substitute for mixing and curing water for concrete if certain challenges can be addressed. One of the main problems associated with the use of seawater in concrete is the risk of corrosion of internal steel reinforcement. Fibre-reinforced polymer (FRP) bars have been shown to be a viable reinforcement alternative in aggressive environments due to their corrosion-resistant properties. Glass FRP (GFRP) bars, due to their acceptable mechanical properties and reasonable price, are currently the most widely used in industry. GFRP bars are manufactured with a variety of surface configurations having different bond performance in concrete, which influences structural behaviour in concrete flexural elements. Therefore, the viability of GFRP bars with sand coated and spiral deformations in seawater concrete is an important topic for research. In this study the bond behaviour is investigated using two different test methods: 1) pullout specimens, and 2) beam anchorage specimens. The results suggest that there is no significant difference between the short-term bond strength of GFRP bars in seawater concrete compared to normal concrete. Additional research is recommended to explore possible long-term issues.

Keywords: Seawater, Bond, GFRP, Pullout, Beam-anchorage

Contents

List of Figures

List of Tables

Chapter 1 Introduction

1.1 General

The use of fibre reinforced polymer (FRP) reinforcing bars in concrete structures is generally believed to be a suitable alternative to conventional steel bars where corrosion is a major concern to the long-term serviceability of the structure. The use of corrosion-resistant FRP reinforcement enables structural elements like bridge decks to maintain their performance under aggressive environments in the presence of de-icing chemicals, salts, and other corrosive agents. This feature, among other unique advantages including high strength-to-weight ratios and electromagnetic transparency, has encouraged engineers to employ FRP bars in concrete structural members for a wide range of applications [1][2]. Among all different kinds available, Glass FRP (GFRP) is the most well-known type in industry due to its acceptable properties and low cost.

FRP bars are made out of continuous strands of fibres embedded into a resin matrix through a pultrusion process. The resin, which is usually vinyl ester or epoxy, plays an important role in distributing the load among the fibres, as well as forming a protective layer around the fibres keeping them safe from aggressive environments, impact and any other damaging accidents. Unlike steel, FRP is an anisotropic material and its properties vary with direction. Fibre orientation is aligned with the longitudinal axis of the bars, and is thus the direction in which the material has stronger properties (primarily in tension). Due to their attractive and unique properties which include a high tensile strength (1000 to 1500 MPa) and a moderate modulus of elasticity (above 60000 MPa) [3], GFRP bars present a viable option to the construction industry to solve some durability problems which cannot be solved easily using conventional steel bars.

At the same time, there is a growing problem of freshwater shortages in various areas around the world. Freshwater accounts for only 2.5% of the Earth's water, and most of it is frozen; thus water available for drinking is very limited [4]. The problem is intensified due the growing agricultural industry, urban and industrial developments and increased pollution in rivers and lakes. As a result, there is a global scarcity of clean water. The use of potable water in

construction, including for mixing, curing and cleaning in concrete production, implies that less water is available for agriculture and human consumption in these areas as the amount of concrete produced globally is over 10 billion tons each year [5]. These same areas often have an abundant supply of seawater, which, according to most standards, is currently not accepted for use in concrete. To improve the sustainability of the concrete industry, while improving water security and water conservation efforts around the globe (including many impoverished regions), further exploration of the viability of replacing potable water with seawater in concrete production is warranted.

When seawater is used as mixing water in Portland cement concrete (PCC), it is known to change some fresh and hardened properties; for instance, it may result in an decreased slump and increased early age strength, but tends to slightly decrease the long term strength compared to concrete made with normal water. Furthermore, several undesirable chemicals will be incorporated into the PCC microstructure such as sulphates, sodium, magnesium, calcium and potassium ions, and the implications on long-term durability are not well known. While these issues require further study, the main impediment which must be addressed is the high concentration of chlorides present in seawater which results in rapid deterioration of internal steel reinforcement due to corrosion. In light of this, the use of corrosion-resistant FRP bars present a promising alternative for structures made with seawater concrete.

1.2 Research Significance

The presence of chloride ions can accelerate steel corrosion in reinforced concrete because they can penetrate and destroy the non-corroding protective oxide film, which generates the passivation of steel. Corrosion of the steel reinforcement can lead to cracking, spalling, and delamination of concrete, a loss of structural integrity, and various other problems which can significantly reduce the service life and functionality of the structure. Hence, FRP may present a suitable and sustainable alternative in these cases; however, to date, the use of FRP-reinforced concrete containing seawater has not been investigated in detail. This study therefore presents the first major research available on this topic.

In reinforced concrete structures, the forces are transferred between the concrete and rebar through a bonding mechanism which mainly relies on bar surface deformation characteristics and embedment environment. Therefore, the bond mechanism between concrete and reinforcing bars is a key element in determining the flexural behaviour of reinforced concrete members at the serviceability and ultimate levels [6][7]. This mechanism controls the deflection, the width and distribution of cracks, and the ultimate strength of a reinforced concrete member [6][7]. As a result, the bond mechanism between concrete and rebar has been the subject of many different studies, enabling researchers to better understand this mechanism and the affecting factors. In this research, the influence of seawater as mixing water in concrete on the bond behaviour with GFRP reinforcing bars will be investigated.

1.3 Research Objective

The main objective of the current research is to investigate the bond behaviour of GFRP reinforcing bars embedded in concrete made with seawater, in order to understand how this can affect the bond strength and any potential effects that the seawater content might have on bond behaviour. Therefore, two types of testing methods were conducted:

1. Pullout test
2. Beam anchorage specimen

Specifically, the experimental program was designed to investigate the bond strength, bond stress distribution, stress-slip relationship, and development length for GFRP reinforcing bars in concrete made with seawater compared to companion specimens made with conventional tap water. Ultimately, this research aims to provide a critical first step towards the potential use of seawater concrete in construction to support critical water preservation efforts around the globe.

1.4 Thesis Outline

This thesis presents the results of an experimental program investigating the bond behaviour of GFRP bars in concrete with and without seawater. The thesis outline is as follows:

Chapter 1: This chapter aimed to present a brief background on FRP materials, as well as the general motivation behind their increased use in construction Moreover, this chapter highlighted the importance of using seawater in construction projects and its substitution for potable water as the world is moving rapidly toward increasing water scarcity in many regions.

Chapter 2: This chapter presents previous research work done on the use of seawater in concrete mixing, as well as its effects in terms of fresh and hardened concrete properties. Moreover, a review of available literature focusing on measuring bond strength between reinforcing bars and concrete, as well as the use of various test methods are explained in this chapter.

Chapter 3: This chapter focuses on the pullout test program, including a detailed description of the test setup and instrumentation, tested materials, results, and their analysis. Finally, this chapter includes some discussion derived from the test results provided.

Chapter 4: The anchorage beam test is described in this chapter, including the specimen details, test setup, stress-slip curves and analysis. A discussion of the test results and comparison with theoretical models are also provided.

Chapter 5: This chapter summarizes the main conclusions and major lessons learned from conducting the research. Moreover, recommendations for future work are also provided in this section. These recommendations aim to minimize the errors in results from any future work based on the past experience on this project.

Chapter 6: References used in this study are all cited in this chapter.

Chapter 2 - Literature Review

2.1 General

The global construction industry is growing rapidly, building structures and transportation networks that facilitate improved standards of living and develop advanced civilizations. Therefore, this industry requires a huge amount of natural and man-made resources. The most commonly used building material is concrete and worldwide production continues to increase. As a result, improving the sustainability of the concrete industry has been the focus of widespread research efforts in recent years, with a primary emphasis on reducing fossil fuel consumption and greenhouse gas emissions, as well as options for recycling waste to limit dependency on non-renewable natural resources. Significant progress has been achieved in the form of production efficiencies (through the use of alternative fuels and carbon capture technologies) and use of supplementary cementing materials to offset the consumption of carbon-intensive Portland cement in concrete. One issue which has received relatively less attention is the construction industry's reliance on large quantities of clean potable water; whereas most regions in Canada are fortunate to have access to freshwater sources nearby, globally the situation is direr and alternative solutions are needed. It can be argued that, in certain regions, access to clean water is one of the most pressing issues facing humanity today.

Concrete, with its variety of uses, is the most-used material in the construction industry [8], consuming about 2 billion tons of water annually [9] which is almost 9% of the world's industrial demand [10]. This water is mainly used during casting and curing stages, and additional water is also needed for cleaning equipment. At the same time, many experts are warning that water shortages and scarcity will challenge human life for the years to come. According to the World Health Organization (WHO), by 2025 about half of the world's population will live in water-stressed areas [11] (Figure 2.1). Therefore, reducing the amount of potable water used in the construction industry, which would enable agriculture and human consumption to benefit more from the available sources, would be a very wise decision to make. On the other hand, most of these stressed areas are within reasonably close proximity to abundant sources of seawater, which can potentially supply the concrete industry if certain challenges can be overcome. The ions of chloride, sodium, magnesium, calcium and potassium

are the main chemical constituents of seawater [12]. If the seawater contains up to 35,000 ppm of dissolved salts, the predominant salt would be sodium chloride which makes up approximately 88% of the total salt content [12]. A review of the effects of seawater on concrete properties is provided in the following sections.

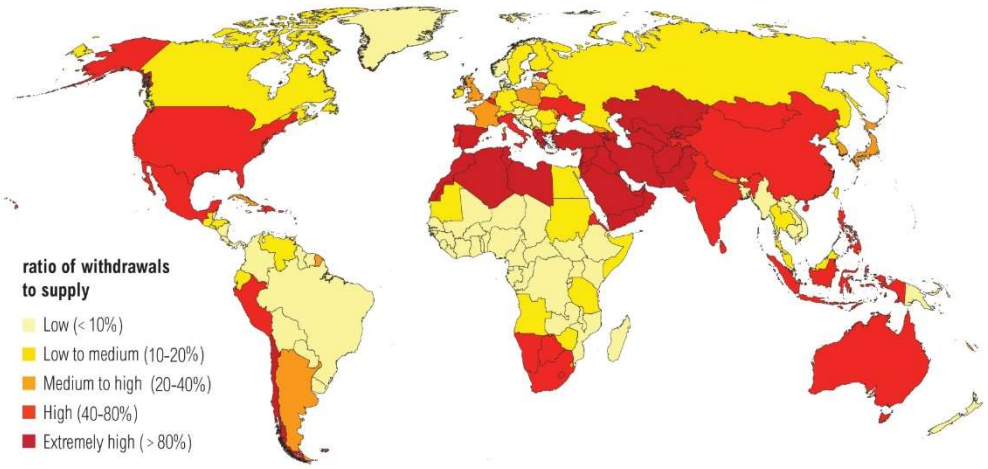

Figure 2.1 Water stressed regions by 2040 [13]

2.2 Seawater Concrete

2.2.1 Fresh Properties

Researchers have reported changes to both the fresh and hardened properties of concrete made with seawater compared to similar mixes made with freshwater. Ghorab et al. [14] found that using seawater for both casting and curing can reduce the initial and final setting times by 25% and 22%, respectively, compared to normal concrete. Similarly, Katano et al. [15] concluded that the setting times for initial and final stages were shorter by 90 and 135 minutes, respectively. Generally, it was concluded that the existence of seawater results in a decrease in the workability as well as the setting time [16][17][14]; this reduction was reported to be about 20% (From 600 mm to 480 mm in slump flow) in comparison with the control mix[18].

However, some researchers showed that suitable chemical admixtures can improve the seawater concrete workability [19].

2.2.2 Hardened Properties

The existing studies reported no major negative effects on mechanical properties of seawater concrete [20][21]. These studies show that a limited portion of salt can help strength gain in concrete [22], while seawater has visible effects mainly on early-age strength [23]. In this regard, Islam et al. [24] found a higher early-age strength of seawater concrete compared to normal concrete which was attributed to the concrete pores being filled by hydration products; conversely, the long-term strength was observed to be slightly reduced, which was related to the leaching out of soft hydration products from the concrete pores [24][20]. Narver [25] concluded that the concrete compressive strength was higher for the first month, but there was a 6% reduction after the third month compared to normal concrete specimens. Likewise, Steinour [26] showed higher early-age compressive strength followed by a 8-15% reduction compared to normal concrete made with potable water. Moreover, several recent studies also confirm the conclusions from the above mentioned researchers [19][21][12][27][28].

On the other hand, Griffin and Henry [22] reported a strength increase at both short and long term stages for seawater concrete. A similar strength increase was also reported by Dewar [29]. Moreover, Shi et al. [30] observed a 22% increase in 28-day compressive strength compared to normal concrete. Park et al. [31] tested different chloride contents ranging from 0 to 1.2% of cement weight, with the results showing that the effect on mechanical properties is negligible, but the drying shrinkage and associated cracking increased notably by increasing the chloride content. In addition, the experiments showed that the seawater concrete characterizations improved by using mineral admixtures such as flyash [32][33][34], and metakaolin [30][14][35].

2.2.3 Durability

Long-term concrete problems arising from the use of seawater as mixing water or curing water can potentially cause several issues during the lifetime of the structure. While the chemical reaction between cement paste and high chloride concentration in seawater is basically negligible and not a concern, the presence of potassium and magnesium sulphates (K_2SO_4 and $MgSO_4$) in sea salt content could potentially cause long-term deterioration by internal sulphate attack, due to the reaction with calcium hydroxide $Ca(OH)_2$, the hydration product of di-calcium silicate (C_2S) and tricalcium silicate (C_3S). The attack mode associated with internal sulphate attack is crystallization which is potentially harmful and damaging. Sodium and potassium ions may also initiate or intensify the alkali aggregate reaction (AAR) if reactive aggregates are used [12]. These long terms effects associated with the use of seawater, as well as potential mitigation measures, have not been thoroughly investigated and continue to present an opportunity for future work.

However, the main drawback of using seawater in structural reinforced concrete applications is the chloride content which has a notable and detrimental effect on internal steel reinforcement. Mohammed et al. [27] tested reinforced cylindrical concrete specimens in a tidal environment for about a 15 year period, and reported that a larger number of corrosion pits with higher depth on steel rebar was seen when seawater was used instead of freshwater in concrete casting. Moreover, other researchers also concluded that the substitution of freshwater with seawater can highly endanger the steel reinforcement and initiate corrosion [36][37]. Shalon and Rapheal [38] stored specimens made with seawater in a moist room and they reported a serious deterioration of steel rebar due to corrosion. In contrast, some researchers like Otsuki et al. [39] reported that the effect of seawater on steel corrosion was negligible following 20 years of exposure tests since there was no obvious change in corrosion depth between seawater concrete and normal concrete. Otsuki also found that the negative effect of chloride ions in seawater decreases over time. Another interesting result was found by Dempsey [40], where it was reported that the dense concrete made with seawater had a negligible influence on steel rebar corrosion.

Although some contrasting results were reported in the literature, steel reinforcement deterioration remains the main concern in using seawater for concrete construction, where it increases the risk of corrosion in reinforcing steel should the structure be exposed to the open air during its service life. Therefore, there is still a controversy over the use of seawater as mixing water in concrete despite the advantages from the perspective of freshwater conservation. Nevertheless, this issue can be addressed through some alternatives.

The steel corrosion problem may be solved either by using seawater concrete only for plain non-reinforced concrete applications, or if reinforcement is necessary as is the case for most structural applications, corrosion-resistant materials such as fibre reinforced polymer (FRP) bars can offer a good solution [41].

2.3 Fibre Reinforced Polymer (FRP) Reinforcement

FRP is a composite material comprised of fibre and resin, where each component keeps its separate identities, but their combination leads to some certain properties and characteristics that are different from the individual constituents. FRP bars are generally classified according to the fibre type used inside the bar: carbon, glass, aramid, or basalt to name a few. Of these, carbon fibres generally have superior strength and stiffness, but glass FRP (GFRP) products have a lower cost and are thus much more commonly used. The fibres generally make up approximately 70-80% of the composite by volume in FRP bars produced by pultrusion. The resin system, which is typically vinyl ester for GFRP composites, plays an important role in binding the fibres together and distributing the load applied to the composite between the fibres. Moreover, the resin system acts as a protection layer around the fibres, presenting a barrier against abrasion, impact, salts, water, and alkalis [42].

Several studies have tried to examine the performance of GFRP products manufactured with vinyl ester resin to understand the probable effects that environment conditions might have on mechanical and physical properties [43][44][45][46]. They concluded that the chemical condition of the polymer matrix has a significant effect on the long-term stability in a seawater environment. Although GFRP reinforcement can resist many aggressive agents, there are still

some challenges for this material in some cases which can include its resistance to sustained loads and alkaline environments, besides being sensitive to elevated temperatures. Some design guidelines have addressed these concerns by using environmental factors which reduce the nominal material strength ensuring that the adequate strength is satisfied for the design [47]. Since many FRP-reinforced concrete designs tend to be governed by serviceability criteria, these strength reductions are not necessarily prohibitive.

FRP materials possess several attractive physical and mechanical properties such as their light weight and their high tensile strength, as well as little to no interference with magnetic and electrical fields (in the case of GFRP), which makes them attractive for a wide range of applications. The main driver for their use, however, remains the ability of FRP bars to resist corrosion which is by far the most common durability problem affecting reinforced concrete structures in cold regions where de-icing salts are used, as well as in marine environments. Moreover, its acceptable long-term performance has been observed under conditions of seawater exposure [48][49][50]. Although the initial cost of FRP bars is relatively high compared to steel, this solution typically presents a long-term savings through reduced maintenance costs and longer service lives which can compensate for its high initial cost [51][52].

GFRP bars are widely used in industry because of their acceptable range of mechanical properties and their low cost compared to other types. Most of the GFRP products available are made out of E or ECR glass fibres and epoxy or vinylester resin. These products are used in many projects and field applications such as parking garages [53], water treatment plants [54], and bridges [55][56][2][1].

The poor corrosion resistance of conventional steel reinforcement motivated and directed the construction industry toward the use of FRP reinforcement as a viable alternative in structural construction which can extend the service life of a reinforced concrete structure. Therefore, in cases where the design is more dependent on the durability requirements of reinforced concrete structures, engineers can count on FRP reinforcement as a reliable substitute. Nevertheless, it is important to note that the relatively low elastic modulus and lack of a yield plateau in their stress-strain curve has made these materials incompatible with conventional design procedures which aim to first initiate the yielding of the reinforcement in structural elements [47].

However, these issues have also been addressed by various building codes (e.g. CSA S806, CSA S6 [57]), and the concrete crushing mode is generally preferred as a more reliable and ductile failure mode in flexural members compared to rupture of the FRP reinforcement. Serviceability criteria, including limits on reinforcement stresses or strains, crack widths, and deflections, are also an important consideration for design. At both the serviceability and ultimate limit states, the behaviour of a reinforced concrete member is significantly affected by the bond behaviour between the concrete and reinforcement, which is further discussed in the following sections.

2.4 Bond Behaviour

The interaction between concrete and reinforcement in reinforced concrete (RC) elements controls most of the element's structural behaviour. This action in FRP RC mainly relies on the bond behaviour and bond stress magnitude developed at the concrete and rebar interface. Several products are currently available in the market with different properties including surface treatment, material stiffness, and cross-sectional shapes, which influences their structural response according to their individual type and characterization. Therefore, improving the available databank with additional tests related to the bond behaviour is vital to generalize bond-slip relationships for unique practical design procedures.

The bond behaviour of steel reinforcement to concrete has been widely studied during the last 40 years, and a huge amount of experimental and numerical work has been done on this subject as reported in available literature [58][59][60][61]. On the other hand, the lack of comprehensive data on alternatives to steel reinforcement and the continual improvement of manufacturing methods and material properties for FRP bars, particularly with respect to surface treatment, is still motivating researchers to investigate various aspects of their behaviour. The evolution of FRP reinforcing bars over the last few decades around the world has established the necessity and importance for the ongoing development of updated design specifications that will enable engineers in concrete industry to employ these materials as reinforcement in concrete structures and accounting for regional factors.

Aiello et.al [62] conducted a series of pullout tests on GFRP and CFRP bars with several deformations like sand-coated and spiral wound bars, and they reported bond strengths in the range of 17 MPa to 24 MPa for 8 mm diameter GFRP spiral wound bars. Moreover, Baena et.al [63] tested several pullout samples where they observed bond strengths of 16.3 MPa, 15.7 MPa, and 22 MPa for GFRP sand-coated bars with #3, #4 and #5 diameters (9.52 mm,12.70 mm, 15.87 mm respectively), respectively.

Moreover, engineers and researchers all over the world are continuing to explore new research directions to better understand the interaction of these materials with concrete with the goal of improving design codes with formulation of the studied behaviours. One example of this ongoing research effort is a 4-year research project called EUROCRETE that investigated the use of FRP reinforcement in concrete structures. Under the EUROCRETE project, two series of experimental tests were conducted to better understand the bond behaviour of FRP reinforcement in concrete elements. The first series of tests included more than 100 specimens for direct pullout tests, whereas nine concrete beams were also tested under four-point bending for the second series [64]. The EUROCRETE project results showed that the average bond strength decreased along the splice length as this length was increased.

In a reinforced concrete element, in order to satisfy an optimal design, a reliable and efficient force transfer between concrete and internal reinforcement is necessary. In the case of a deformed steel bar, this load transfer mainly occurs through three primary mechanisms (Figure 2.2) [7]:

- Chemical adhesion between the bar surface and the surrounding concrete;
- Frictional forces due to the surface roughness of the bar; and,
- Mechanical interlock between the bar surface deformations (ribs) and the surrounding concrete.

Of these mechanisms, mechanical interlock generally provides the largest contribution to overall bond strength.

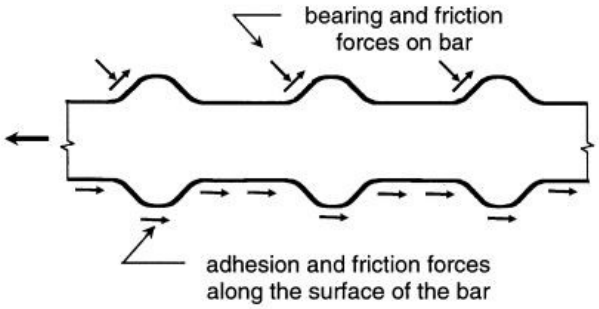

Figure 2.2 Bond Force Transfer Mechanisms [7]

When load is applied to a deformed bar and it begins to slip with respect to its surrounding concrete, the surface adhesion to the concrete is lost, while bearing and friction forces on the ribs and barrel of the bar are mobilized. Initially, the friction forces are increased as the compressive bearing forces on the ribs increase. However, as the slip value increases, friction force on the barrel of the reinforcement is reduced. The forces applied on the reinforcing bar surface are in equilibrium with compressive and shear forces on the concrete contact surfaces.

As shown in Figure 2.3 (a) and (b), these forces may be resolved into tensile forces that can cause cracking perpendicular and parallel to the reinforcement planes [7]. These cracks are able to form a conical failure surface for bars under tension forces. Otherwise they have minor influences on anchorage and development of well-confined reinforcement bars. If the concrete cover or the bar spacing is small, the transverse cracks shown in Figure 2.3(b) will form and lead to splitting cracks, as shown in Figure 2.3(c). In the case that the concrete cover, bar spacing, or transverse reinforcement is sufficient to resist splitting failure, the failure will start by shearing along a surface at the top of the ribs around the bars, which causes a ″pullout″ failure, as shown in Figure 2.3(d). The crushed concrete observed in a region near the bearing surfaces of the bar deformations is very common for both splitting and pullout failures. Finally, some important criteria and limits for bond behaviour are listed below [7]:

- The concrete volume around the bars (concrete cover and bar spacing parameters);
- Concrete properties and mix design;
- The existence of confinement in the form of transverse reinforcement that delays and controls the crack propagation;

- The surface configuration of the bar; and
- The bar geometry (deformation height, spacing, width, and face angle).

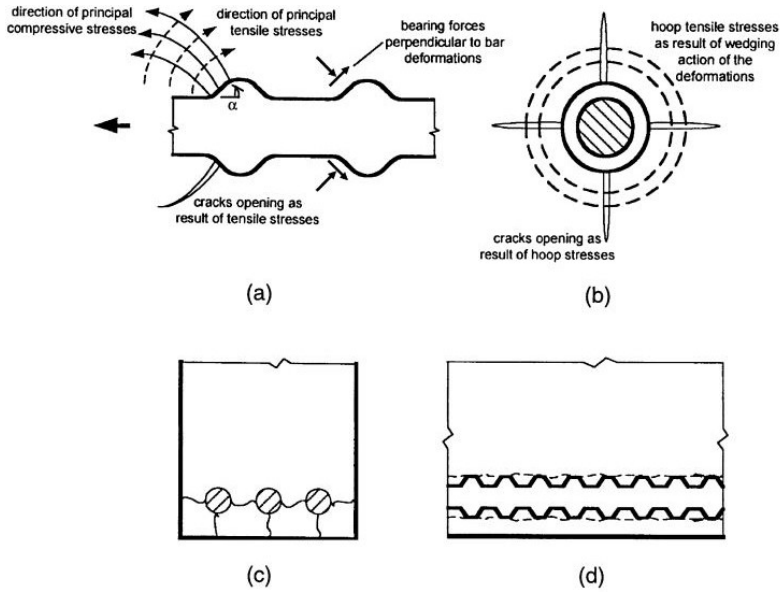

Figure 2.3 Cracking and Damage Mechanism in Bond; (a) side view of a deformed bar with deformation face angle showing formation of Goto Cracks, (b) end view showing formation of splitting cracks parallel to the bar, (c) end view of the member showing splitting cracks between bars and through the concrete cover; and (d) Side view of the member showing shear crack and local concrete crushing due to bar pullout [7]

In the case of FRP reinforcement, the same primary mechanisms are present but the overall behaviour depends on the type of surface configuration of the bar which varies according to each bar manufacturer. Several different types of surface configurations exist; examples include the application of a sand-coating layer bonded to the bar surface (Figure 2.4), and a spiral groove pattern achieved by machining the outer surface of the bar (Figure 2.5). Both of these methods have been shown to successfully improve the bond behaviour of FRP bars embedded in concrete [63][62].

Figure 2.4 GFRP Sand Coated Bar [65]

Figure 2.5 GFRP Spiral bar [66]

Therefore, the bond behaviour between FRP reinforcement and surrounding concrete largely depends on different factors, and is strongly influenced by the bar properties and surface configuration, which contributes to the mechanical interlock of the FRP bars with the concrete, the chemical adhesion between surface treatment and concrete, and the hydrostatic pressure caused by hardened concrete shrinkage against the FRP bars [65].

In Figures 2.6(a) and (b), the bond stress is plotted versus the measured slip for sand-coated, spiral wound, and ribbed FRP rebars, respectively. In the first stage, the chemical adhesion between reinforcement and concrete up to a bond stress of about 2 to 4 MPa, controls the bond mechanism in the concrete and avoids slippage. In the second stage, mechanical interlocking plays an important role in the bond mechanism and the maximum bond stress is typically governed by this phenomenon. When the peak stress is reached, the bar starts slipping out of concrete and subsequently the load decreases; as a result, the mechanical contribution is continuously reduced and, finally, the friction between the bar and the surrounding concrete becomes the predominant bond mechanism. When the non-embedded portion of the bar starts to enter the bonded region, particularly for ribbed bars, the descending portion may be

followed by a further increase of the bond stress, due to wedging action. In Figure 2.6(c) the experimental results for sand-coated FRP bars are presented. Similarly, different stages can be observed, but in this case the bond mechanisms are different than described above. The chemical adhesion is the primary mechanism controlling the initial portion of the curve which is mainly due to the sand applied on the surface; after the loss of chemical adhesion the friction between concrete and reinforcement becomes dominant. The peak bond stress is attained at low slip values, and a sudden drop of the bond stress along increase in the slip value can be observed, after which the curve stabilizes and continues with small fluctuations[62].

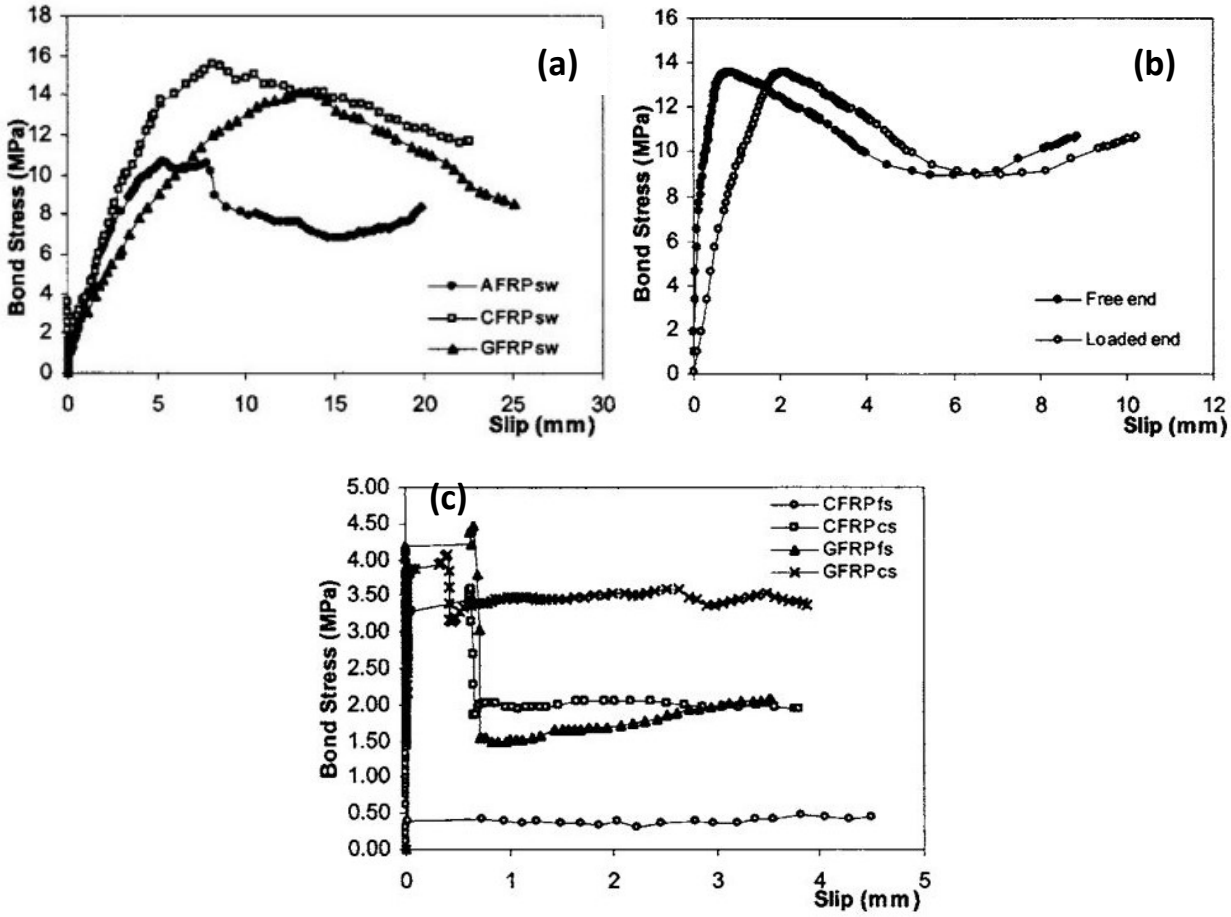

Figure 2.6 Experimental Results; (a) FRP sanded and spiral wound rebars—pullout test—free end; (b) GFRP ribbed rebars—modified pullout test; (c) CFRP and GFRP coarse and fine sanded rebars pullout test—free end[62]

2.5 Bond Test Methods

In order to assess the bond behaviour in reinforced concrete elements, there are a variety of test setups and specimen types that have been used by previous researchers. In Figure 2.7, the four most common test setups are shown. It is important to mention that the bond behaviour is significantly influenced by the testing configuration.

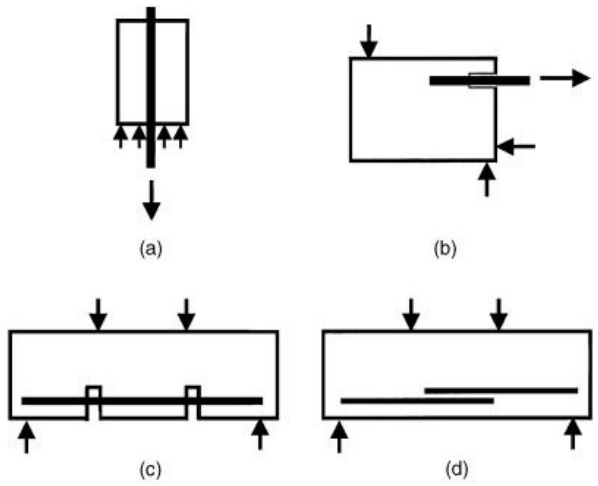

Figure 2.7 Schematic of: (a) Pullout Specimen; (b) Beam-end specimen; (c) Beam anchorage specimen; and (d) Splice specimen [7]

The pullout specimen (Figure 2.7(a)) is popular among researchers because of the simplicity of the test setup and its ease of fabrication. In some cases, transverse reinforcement is added to limit splitting when the bar is under tension. The main intent of this bond test is to draw the bond stress-slip curves at the loaded and free ends of FRP bars subjected to a pullout load.

Two main configurations are typically used for the pullout test setup: The Losberg (1963) and the RILEM/CEB/FIP (1978) arrangements shown in Figure 2.8, both of which are used commonly for the evaluation of bond for steel and FRP bars [64]. The RILEM configuration is also recommended by ASTM D7913/7913M-14 [66].

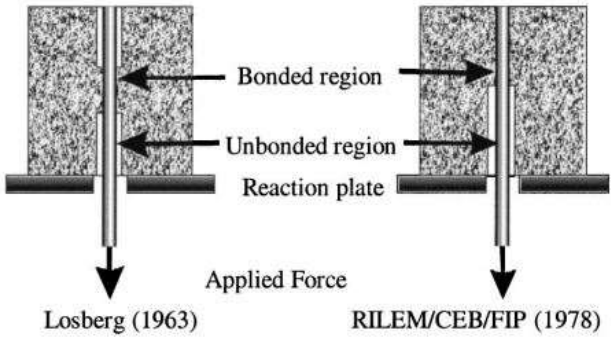

Figure 2.8 Typical Pullout Tests [64]

This test configuration shows the least realistic results among the four methods shown in Figure 2.7 because in reality and actual construction, the stress fields in the concrete are different compared to the specimen built according to this test setup. Unlike reinforcing bars placed in a flexural member, when the bar is pulled and placed in tension with this setup the concrete surface is placed in compression by the loading plate. As a result, compressive struts form between the support points for concrete and the surface of the reinforcing bar passing through the concrete block which will tend to enhance the bond strength.

Therefore, the resulting stress state differs notably from most reinforced concrete elements, in which both the reinforcing bar and its surrounding concrete are in tension. Moreover, the bar ribs bearing surfaces are under a compressive force due to the bar movement relative to the concrete, not because of the basic load application. In cases where bar surface properties like epoxy coatings or the bar surface strength are necessary, the compression force applied to the bar surface in the pullout test causes less applicability of the test results to structural design. Therefore, in determining the development length, the sole use of pullout test results is inappropriate and not recommended [7]. It is useful, however, for direct comparisons of the influence of certain parameters, such as, for instance, concrete mixture properties.

The test results from the remaining specimen types shown in Figure 2.7 (b) through (d) show more realistic bond stress distributions for application to actual structures. The modified cantilever beam, or beam-end specimen, shown in Figure 2.7(b), offers a relatively simple test that generally has a great similarity with the stress state experienced by reinforced concrete flexural members; through this test method, both the reinforcement and the surrounding

concrete are simultaneously placed in tension. To reach the desired stress state, there should be sufficient distance between the compressive force and reinforcing bar, which should be approximately equal to the embedment or bonded length of the bar within concrete. To prevent any conical failure surface from happening, a small portion of the bar close to the surface is unbonded. The specimen shown in Figure 2.7(b), designed to satisfy the requirements like spacing between the bar and the compressive force and reinforced to ensure bond failure rather than other types of failures (e.g. shear and flexural), is described in ASTM A 944 [66]. Shear reinforcement is used in the specimen in order to cut off any probable longitudinal splitting cracks that start occurring at bond failure. The bond strengths reported through this test method have a great proximity to those specimens designed to represent full-scale reinforced concrete elements behaviour. Beam anchorage and splice specimens shown in Figure 2.7 (c) and (d), respectively, are designed to measure the full-scale specimen's development and splice strengths. The anchorage specimen represents a member with a flexural crack and a specified bonded length at both ends of the beam. Based on concerns about the increased normal stresses present at the bar surface due to the reaction forces, which may increase the bond strength relatively, a number of beam anchorage specimens have been designed in such a way that reactions are displaced laterally from the beam centerline. The splice specimen, which has very similar bond strength to the beam anchorage specimens, is designed to have the splice length in the constant moment region. Because of simplicity in fabrication and more realistic stress-state, the data from such tests are mainly used to establish the current design procedure and provisions for development length and splice length in design codes such as ACI 318 [7].

Bond force-slip and bond stress-slip curves are used to help better understand the bond strength and behaviour of reinforcing bars embedded in concrete. In their most commonly used form, the curves are drawn based on known bar forces, obtained in the beam-end and beam anchorage test methods (Figure 2.7(b) and (c)). The bar forces are compared with the measured slip of the reinforcing bar, relative to the concrete at either the loaded or unloaded end of the

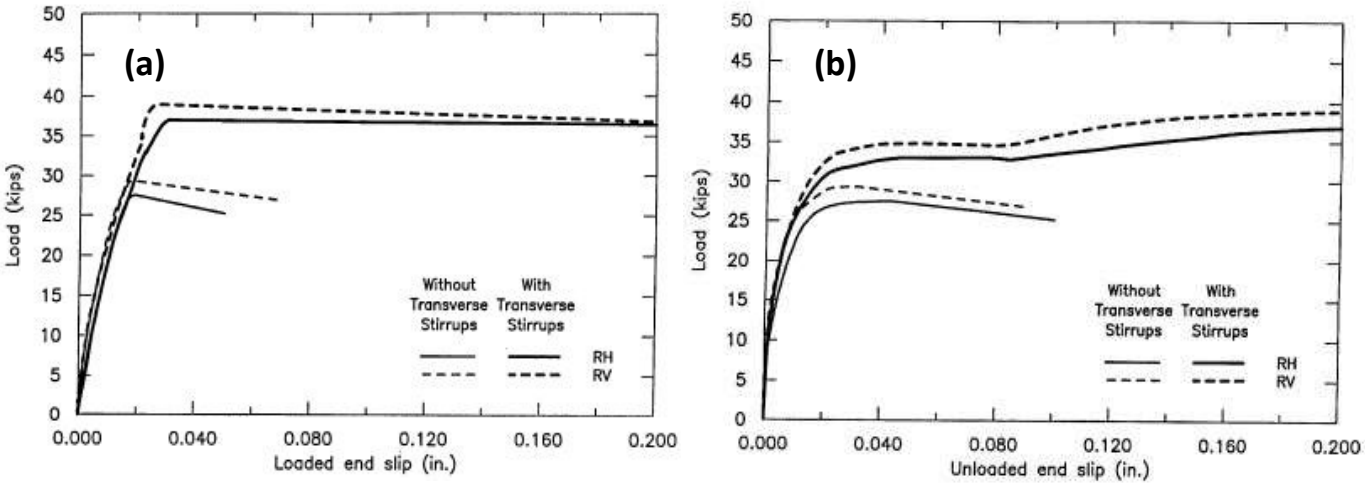

Figure 2.9 Load-Slip Curves of No.8 ASTM A 615 reinforcing bars in an ASTM A 944 beam-end specimen: (a) Average loaded end load-slip curve; (b) Average unloaded load-slip curve [7]

reinforcing bar. In Figure 2.9(a) and (b), examples of steel bar force-loaded end and unloaded end slip curves for beam-end specimens are drawn. A lower initial stiffness was observed on the loaded end bond force-slip curve than the unloaded end curve. The difference shows the elongation of reinforcing bar between the two points of slip measurement as well as the slip which initiates at the loaded end.

The general shape of a bond stress versus slip curve for a monotonically loaded pullout test is shown in Figure 2.10, and actual test results for a CFRP bar are shown in Figure 2.11. Bond force and its related stress-slip curves showing the bond strength, are structural properties that largely depend on both the bar geometry and concrete element details like cover, transverse reinforcement and the state of stress in concrete around the bar. As shown in Figure 2.9 (a) and (b) and 2.11 (a) and (b), bond force and bond stress-slip curves have a very steep slope initially because of the adhesion to the concrete [7]. After the adhesion breaks down, most of the force is transferred by mechanical interlock up to the peak bond stress value, or bond strength. The bond stress then decreases (either gradually or suddenly, depending on the bar surface characteristics) before reaching a somewhat stable residual strength value governed by bar friction.

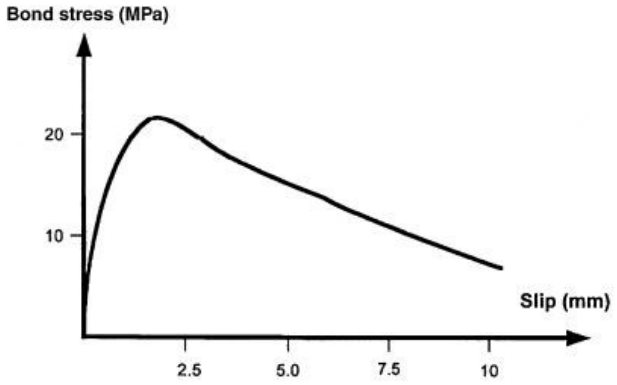

Figure 2.10 Bond Stress-Slip Curve For Pullout Test [7]

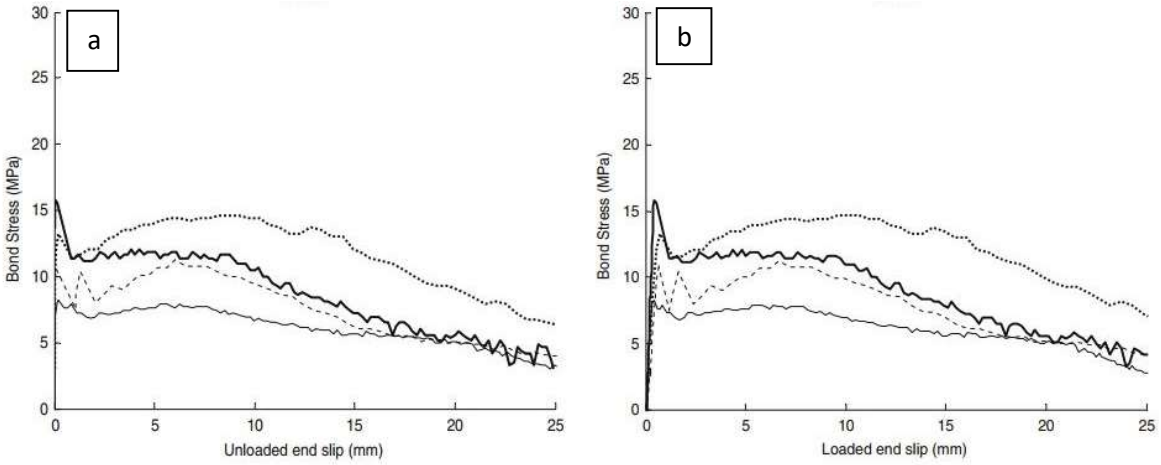

Figure 2.6 Representative Bond-Slip Curves; (a) Unloaded End, (b) Loaded End [63]

Lei et.al [67] conducted research on the pullout bond behaviour between concrete and FRP bar exposed to seawater conditions. Assuming a uniform distribution for bond stress along the embedded length of the bar in concrete, the bond strength was calculated. The bond strength between the FRP bars and coral concrete experienced different degrees of reduction after long immersion periods in seawater. Increases in immersion time caused the surfaces of GFRP and CFRP bars to gradually deteriorate, which contributed to the expansion of the surface resin over time and finally the bond between the bars and the coral concrete degraded. Under normal temperatures the bars embedded in the seawater concrete can exhibit good bonding performance and corrosion resistance. However, higher temperature of the soaking seawater caused the bond strength reduction (Figure 2.12) between the bars and the concrete, because of the resin degradation and the glass fibres severe erosion.

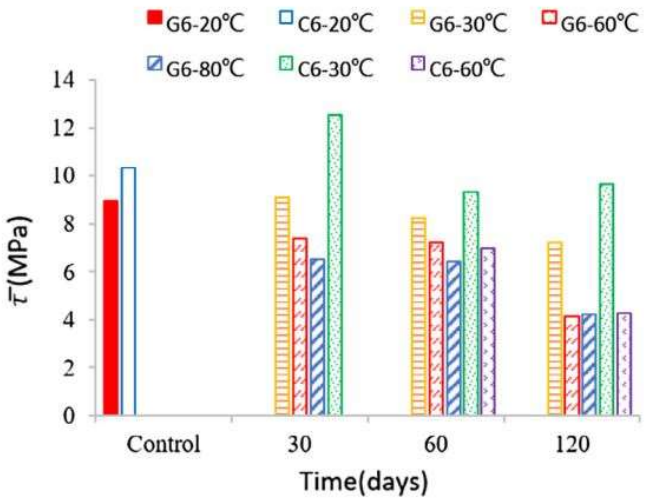

Figure 2.12 Bond Strength vs Time [67]

2.6 Summary

In this chapter, previous research related to the use of seawater in concrete was summarized, and the bond behaviour of FRP reinforcing bars in concrete was reviewed. In summary, the following general observations may be noted:

- Many regions around the world are facing water shortages which presents a significant threat to human lives and livelihoods in affected areas. For this reason, reducing the water consumption of the construction industry is imperative;
- The use of seawater as mixing water in concrete tends to reduce workability and setting time of concrete. This effect can typically be mitigated with the use of admixtures if necessary to provide the desired fresh state behaviour;
- The early age strength of concrete made with seawater tends to be slightly higher than similar mixes made with tap water. However, the long term strength of concrete made with seawater may be slightly lower than a similar mix with normal water. In most cases, the result is likely of negligible importance but may require modifications to a mix design in some cases, and/or the use of mineral admixtures to achieve the desired result;
- The long-term durability of concrete made with seawater still requires further research. While most researchers agree that the high chloride content is detrimental to the

integrity of steel-RC structures due to the increased risk of corrosion, other potential long-term issues have not been thoroughly studied;

- To address the issue of corrosion, one option is to remove the steel reinforcement altogether and replace it with a corrosion-resistant alternative. FRP reinforcement has been used in a wide range of structural applications for precisely this reason. However, the behaviour of FRP-RC members containing seawater has not been investigated;
- The structural behaviour of RC members is strongly dependent on the bond transfer between concrete and reinforcement. The mechanism of bond transfer is influenced by several parameters including the bar surface configuration, and properties of the surrounding concrete. The present research aims to investigate, for the first time, the bond behaviour of various GFRP bars in concrete made with seawater.

Chapter 3 Pullout Test

3.1 General

The bond behaviour between concrete and reinforcement may be assessed through a variety of different test methods as described in Chapter 2. Among these, the standard pullout test as defined by ASTM D7913/D7913M-14 [68] is one of the simplest test methods designed to directly compare the influence of certain parameters on bond strength using cube-shaped concrete specimens with an embedded bar having a short specified bonded length (typically five times the bar diameter). The bond stress-slip response may be plotted to present the peak and residual bond strength values for a given set of variables. In this research, five replicate specimens were casted for each combination of three important variables, namely concrete type (i.e. prepared with either normal tap water or seawater), bar size (i.e. nominal bar diameter of either 12 mm or 16 mm), and bar surface configuration (i.e. sand coated or spiral groove deformations). In total, 40 cubes were prepared and tested to analyze their bond behaviour, as summarized in Table 3.1.

Table 3.1 Test Matrix

Bar Type	Concrete Type	Bar Diameter (mm)	Number of Specimens	Total
Sand Coated	Normal	12	5	20
Sand Coated	Normal	16	5	
Spiral	Normal	12	5	
Spiral	Normal	16	5	
Sand Coated	Seawater	12	5	20
Sand Coated	Seawater	16	5	
Spiral	Seawater	12	5	
Spiral	Seawater	16	5	

3.2 Materials

3.2.1 FRP Bars

The FRP bars used in this study were commercially available reinforcing bars comprised of glass fibres with vinyl ester resin (i.e. GFRP bars) as they are the type most commonly implemented in real civil engineering projects. Two different surface configurations were considered, namely sand coated and spiral deformations (Figure 3.1). The bars used in the pullout specimens were 75 centimeters long with nominal diameters of either 12 or 16 mm, and their average batch-specific mechanical as well as geometric properties provided by the manufacturers are summarized in Table 3.2 (note that these are measured properties, not design values).

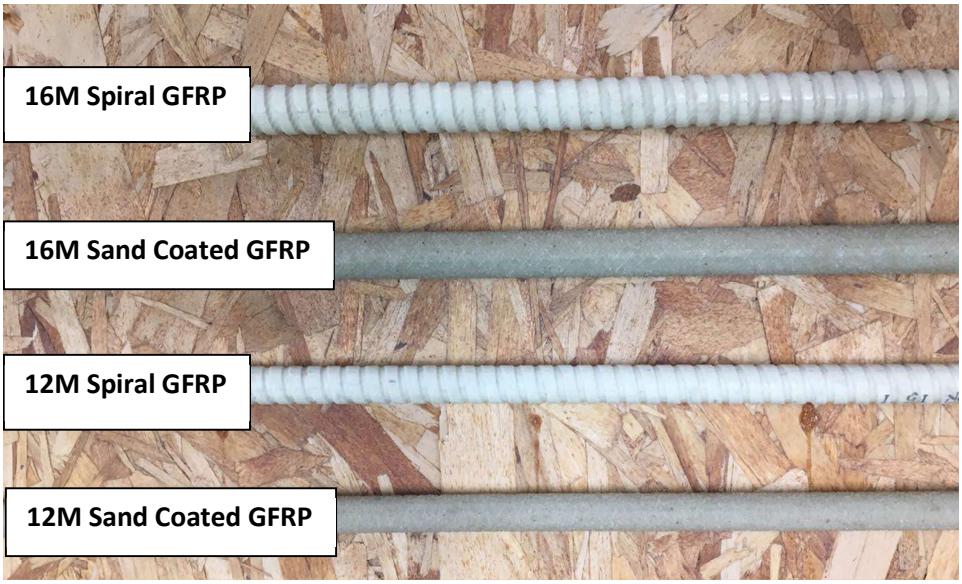

Figure 3.1 GFRP Bars

Table 3.2 GFRP Bar Properties

Property	12M Sand-Coated Bar	16M Sand-Coated Bar	12M Spiral Bar	16M Spiral Bar
Longitudinal Tensile Strength (MPa)	1424	1503	1405	1339
Longitudinal Tensile Modulus (MPa)	62679	61872	65380	66320
Transverse Shear Strength (MPa)	241	245	249	258
Cross-Sectional Area (mm^2)	149	227	133	209

3.2.2 Formwork

ASTM D7913/D7913M-14 [66] states that the specimens for the standard pullout test should be concrete cubes with 20x20x20 centimeters width, length and height. Moreover, it mentions that for each bar type and concrete mix design, a minimum of five similar cubes are needed. Therefore, two series of formwork (Figure 3.2), each with five cubes, were built out of melamine-coated wood. As the bar had to pass through the specimen, a hole was made at both ends of each cube; at the unloaded end the hole was equal to the bar diameter and at the loaded end the hole was slightly larger to accommodate the de-bonding element (in this case, PVC pipe). Since the ASTM D7913/D7913M-14 recommendation for the bonded length in the concrete specimen is $5d_b$ (where d_b is the bar diameter), the remainder of the bar was de-bonded in each specimen using PVC pipe. The de-bonding element is placed at the loaded end of the cube in order to minimize the confining effects of the loading plate on the bond behaviour. The formwork was caulked very precisely to limit any cement paste leakage, and some 3D-printed washers were used to stabilize the bars in the center of each cube through the PVC pipes.

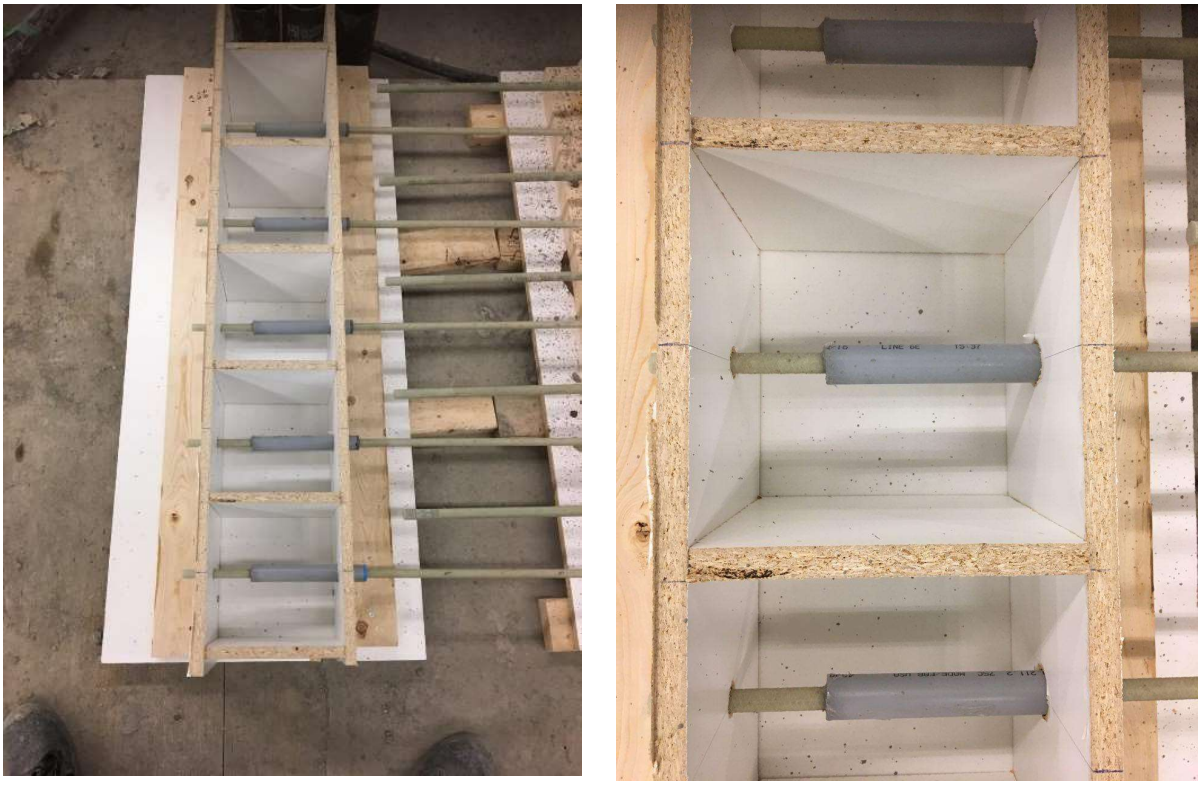

Figure 3.2 Formwork

3.2.3 Concrete

The concrete used in this project was mixed in the civil engineering laboratory according to the mix design listed in Table 3.3 with a target 28-day compressive strength of 30 MPa:

Table 3.3 Concrete Mix Design

Materials	Weight (kg/m^3)
Type GU Cement	340
W/C	0.58
Water (Freshwater/Seawater)	190
Fine Aggregates	750
Coarse Aggregates	1050

Type GU cement was used as the binder in the concrete, while crushed limestone with a 19 mm maximum nominal size conforming to ASTM C33/33M-18 was used as coarse aggregate.

Regular tap water was used to cast control concrete for comparison purposes, while the mixing water for the seawater concrete was prepared according to ASTM D1141-98 [4] which is the standard for the preparation of substitute ocean water and is mainly used for oil contamination, detergency evaluation and corrosion testing. ASTM D1141-98 states that the sea-salt used to make the seawater substitute should have the chemical composition mentioned in Table 3.4. Prepared sea-salt meeting these requirements was purchased for use in this project.

Table 3.4 Sea-Salt Composition

Compound	**Concentration, g/L**
NaCl	24.53
$MgCl_2$	5.2
Na_2SO_4	4.09
$CaCl_2$	1.16
KCl	0.695
$NaHCO_3$	0.201
KBr	0.101
H_3BO_3	0.027
$SrCl_2$	0.025
NaF	0.003
$Ba(NO_3)_2$	0.0000994
$Mn(NO_2)_2$	0.0000340
$Cu(NO_3)_2$	0.0000308
$Zn(NO_3)_2$	0.0000096
$Pb(NO_3)_2$	0.0000066
$AgNO_3$	0.00000049

The prepared sea-salt was added to distilled water in order to produce the required volume of seawater for mixing concrete. In accordance with ASTM D1141-98, the water pH was then adjusted to 8.2 by adding 0.1N solution of hydrochloric acid (Figure 3.3).

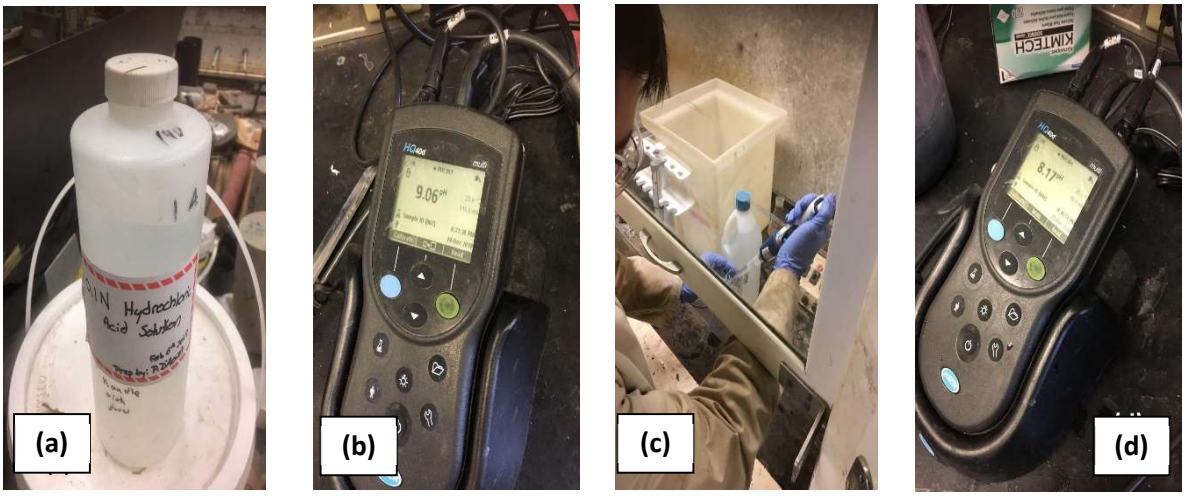

Figure 3.3. pH Adjustment Sequence; (a) 0.1 N HCl solution; (b) Seawater pH before Adjustment; (c) Adding 0.1N HCl Solution; (d) Adjusted pH

Finally, the aggregates were also measured (Figure 3.4) and the concrete was ready to be casted.

Figure 3.4 Measured Aggregates

After mixing, the concrete was placed and condensed in the formwork (Figure 3.5). Concrete cylinders were also prepared for each batch in order to measure the compressive strength. The curing process started after demolding and continued for 28 days; during this time the specimens were kept under a wet cloth and plastic sheet.

Figure 3.5 Specimen Fabrication

3.3 Test Setup

The machine used to test the pullout specimens was a Universal Testing Machine (UTM) (Figure 3.6), which has the ability to load the specimens monotonically under a controlled rate, and at the same time keeps recording the data coming from the displacement transducers attached to the machine ports. The standard pullout test setup is shown schematically in Figure 3.7, with the actual specimen in the test frame shown in Figure 3.8. The concrete cube was held in place using a steel cage (Figure 3.8), while the long side of the bar was secured to the top crosshead of the machine using an anchorage pre-stressing wedge system sitting on a steel plate (Figure 3.9). Once the specimen was in place, the test was performed under displacement control at a constant rate of 0.02 mm/s in accordance with ASTM D7913/7913M-14 [68]. The test specimens were instrumented with two linear variable displacement transducers (LVDTs) attached to the bar on the top side and another one to the bottom side (Figure 3.10), each measuring the loaded end and unloaded end slips, respectively.

The test was initiated by inserting the test fixtures into the testing machine and adjusting the steel cage height and level. Subsequently, the specimen was placed in the cage and the machine top crosshead was lowered in order to pass the bar through the top plate and pre-stressing wedge system sleeve to install the pre-stressing wedge system on the bar. After attaching the anchor to the bar, the machine crosshead was moved upward slowly to adjust the height of the specimen in the cage until the top surface of the specimen came into contact with the steel cage plate in order to keep the specimen fixed while the bar was pulled. Finally, the test was started at a rate of 0.02 mm/sec speed, while LVDTs at the loaded end and unloaded end were recording the slip.

Figure 3.6 Universal Testing Machine

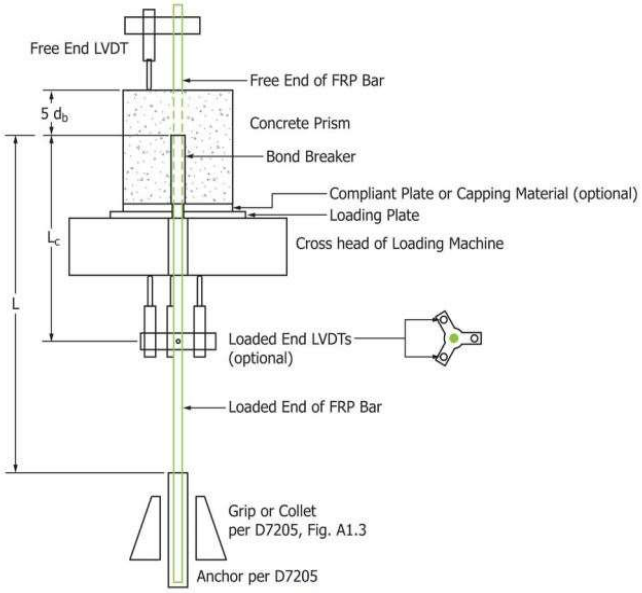

Figure 3.7 Pullout Test, ASTM 7913/7913M-14 Recommendation

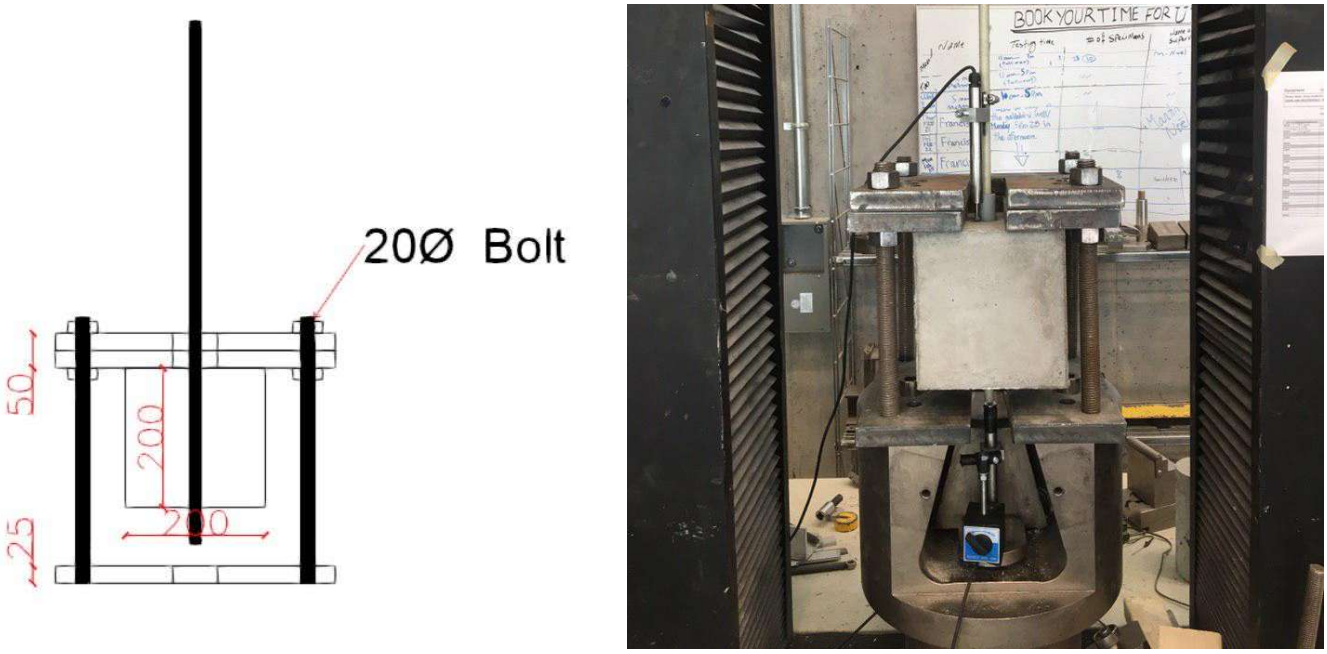

Figure 3.8 Test Setup Steel Cage

Figure 3.9 Top Head, Anchorage Pre-Stressing Wedge System

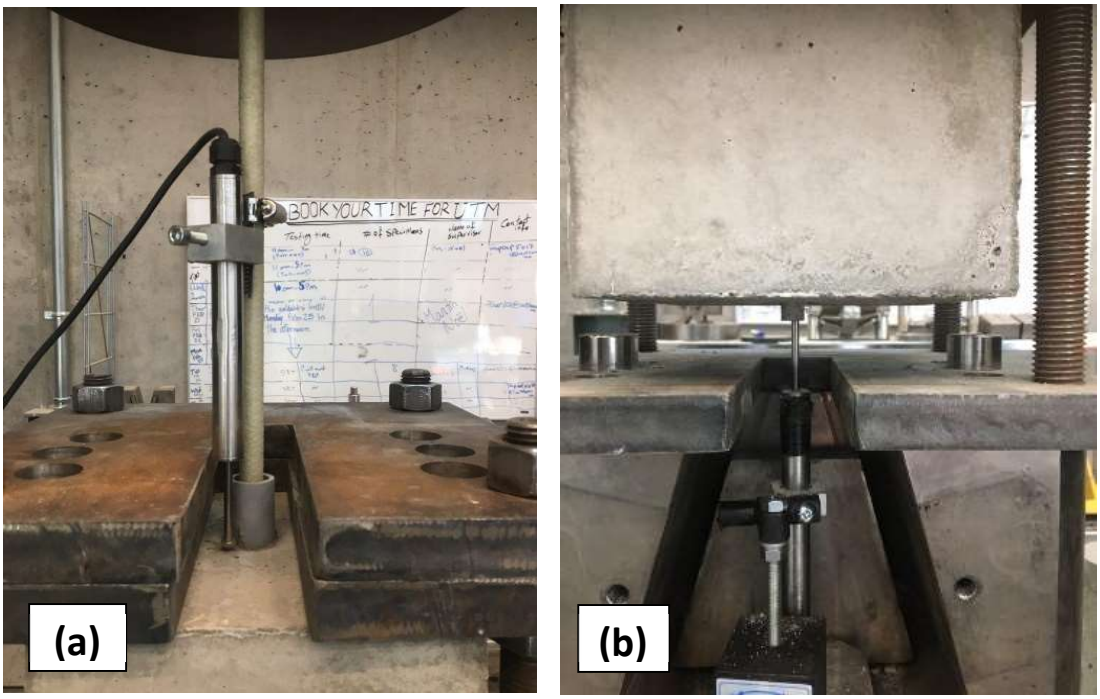

Figure 3.10 LVDTs Attached to: (a) Top; (b) Bottom

3.4 Results

3.4.1 Concrete Properties

The average concrete slump values and compressive strength results at 28 days are summarized in Table 3.5 for batches number 1 to 4 which were casted for the pullout specimens. All of the slump and 28-day strength values were quite similar for all four batches. There was no noticeable reduction in workability for the seawater mixtures compared to the control batches.

Table 3.5 Concrete 28-Day Compressive Strength

Batch Name	28-day Compressive Strength (MPa)	Slump (cm)
Normal Concrete Sand Coated bar	41.0	13.0
Seawater Concrete Sand Coated bar	41.1	13.5
Normal Concrete Spiral bar	40.0	12.5
Seawater Concrete Spiral bar	39.2	14.0

Figure 3.11 shows the compressive strength gain over time for normal and seawater concrete at 7, 14, 21, and 28 days for batches number 5 and 6. These additional batches were prepared mainly to compare the concrete compressive strength gain over time and for the beam tests described in Chapter 4. It can be observed that the seawater concrete had higher initial strength values at 7 days, but the 28 day strengths were almost the same for all batches. This result is similar to that reported by other researchers as discussed in Chapter 2.

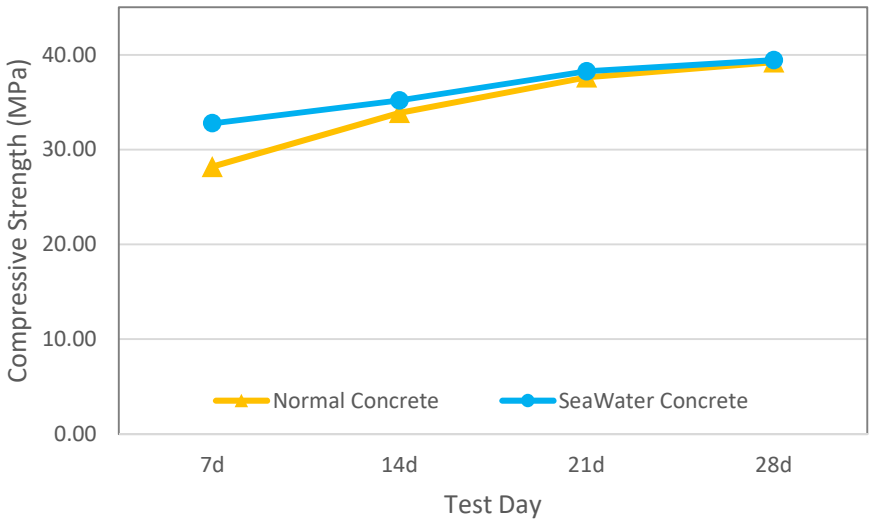

Figure 3.11 Compressive Strength Gain Curve

3.4.2 Pullout Tests

The pullout test was performed on 40 specimens made with seawater and normal concrete. The test results are listed below in Tables 3.6 and 3.7, while selected bond stress-slip curves at the loaded and unloaded end of the specimens are plotted in Figures 3.13 to 3.16. The remaining bond stress-slip curves are provided in Appendix A. The bond stress was attained by using Equation 3.1:

$$u = \frac{P}{\pi d_b L_e} \qquad \text{Eq. 3.1}$$

Where:

$u = Bond\ Stress\ (MPa)$

$P = Appied\ Tension\ Force\ (N)$

$d_b = Bar\ Diameter\ (mm)$

$L_e = Bonded\ Length\ equal\ to\ 5d_b$

A correction was applied to the slip readings from the top LVDT to subtract the small elastic elongation between the point where the LVDT was attached to the bar and the starting point of bonded length in the concrete. This correction was obtained by multiplying this distance by the bar strain (calculated using the known GFRP bar modulus of elasticity and the force in the bar) and subtracting this value from the top LVDT readings.

Some variability is observed in the bond strength values within each group, but overall a consistent response and shape of the stress-slip curve was obtained (see Appendix A). At the loaded end, a steep slope is observed up to the peak load at which point the bar lost its bond with the concrete and the bond stress decreased sharply to a relatively steady residual level where the bond behaviour was ruled by the friction between concrete and the bar. The unloaded end response was similar, except that the slip initiates after the peak bond stress is reached once the entire bar is mobilized. During the post-peak friction-dominated portion of the curve, the bond stress fluctuated slightly but generally either remained fairly stable (sand-coated bars, see Figure 3.13) or decreased very gradually (spiral bars, see Figure 3.15). The residual bond strength values provided in Tables 3.6 and 3.7 correspond to the bond stress at a measured unloaded end slip of 10 mm; this value was selected because the rate of change in stress at this stage was very low as the stress had more or less stabilized. The test continued until the LVDTs reached their maximum travel distance of approximately 30 mm.

The observed bond behaviour was slightly different for the two bar surface configurations (Figure 3.17). The sand-coated bars tended to experience higher average peak loads than the spiral bars which is likely due to improved adhesion to the surrounding concrete, but also tended to display slightly more variability as observed in the COV values. Moreover, the post-peak behaviour of the sand-coated bars showed a relatively constant level of friction in terms of bond stress with very small fluctuations, while the spiral bar ribs exhibited more of a wedging effect which was manifested by greater fluctuations and a greater reduction in bond stress as the bar was pulled out of the concrete with a resultantly lower residual bond strength. Examination of the bars after the test showed that the bar deformations were sheared off in the case of both sand-coated and spiral deformations (Figure 3.12).

Figure 3.12 Bar Deformation after Pullout

The bars with 16 mm nominal diameters tended to have slightly higher average bond strengths than the 12 mm bars, except in the case of sand-coated bars with seawater concrete. Comparing the normal and seawater concrete mixtures, the observed bond behaviours were quite similar. For 12M sand-coated bars, the seawater concrete showed a slightly higher peak and residual bond strength than the mixtures made with normal concrete, while for 16M sand-coated bar specimens this trend was reversed. Meanwhile, the average peak bond strength for 12M spiral bars in seawater concrete was lower than the that of the same bar in normal concrete, while the opposite was true for 16M bars. The variation and statistical significance of these differences will be further explored in the following sections.

On a small number of occasions during the test when the bond stress was approaching its peak, a slight slippage occurred in the anchorage system gripping and applying load to the bar which caused a sudden drop in load. In one case (namely 12M sand-coated bar #4 in normal concrete), some data was unfortunately lost and the peak load was not recorded as shown in Table 3.6.

Table 3.6 Sand Coated GFRP Bar with Normal and Seawater Concrete

Specimen	Normal Concrete Peak Bond Strength (MPa)	Seawater Concrete Peak Bond Strength (MPa)	Normal Concrete Residual Bond Strength (MPa)	Seawater Concrete Residual Bond Strength (MPa)
12M #1	10.57	14.69	5.27	8.81
12M #2	18.39	15.45	8.80	5.93
12M #3	15.99	13.37	7.79	7.26
12M #4	**	15.24	**	8.41
12M #5	16.48	18.25	8.24	9.01
12M Average	**15.35**	**15.40**	**7.5**	**7.8**
COV	**0.21**	**0.10**	**0.18**	**0.15**
16M #1	12.10	16.06	7.15	6.75
16M #2	19.09	15.73	10.29	7.20
16M #3	12.90	12.71	9.77	5.13
16M #4	17.50	14.60	11.39	7.19
16M #5	20.00	13.22	12.36	4.00
16M Average	**16.32**	**14.46**	**10.19**	**6.05**
COV	**0.18**	**0.09**	**0.17**	**0.21**

***Lost data*

Table 3.7 Spiral GFRP Bar with Normal and Seawater Concrete

Specimen	Normal Concrete Peak Bond Strength (MPa)	Seawater Concrete Peak Bond Strength (MPa)	Normal Concrete Residual Bond Strength (MPa)	Seawater Concrete Residual Bond Strength (MPa)
12M #1	13.00	10.00	3.98	1.45
12M #2	11.89	7.56	3.11	1.86
12M #3	9.48	10.52	1.93	2.85
12M #4	12.48	10.56	2.51	2.05
12M #5	12.42	10.94	3.25	2.09
12M Average	**11.85**	**9.92**	**2.95**	**2.06**
COV	**0.10**	**0.12**	**0.23**	**0.22**
16M #1	13.36	13.04	3.30	3.47
16M #2	12.75	11.85	2.91	2.66
16M #3	13.38	13.24	4.34	3.32
16M #4	13.63	15.32	4.37	2.82
16M #5	12.58	14.13	3.39	3.92
16M Average	**13.40**	**13.52**	**3.66**	**3.23**
COV	**0.03**	**0.09**	**0.16**	**0.14**

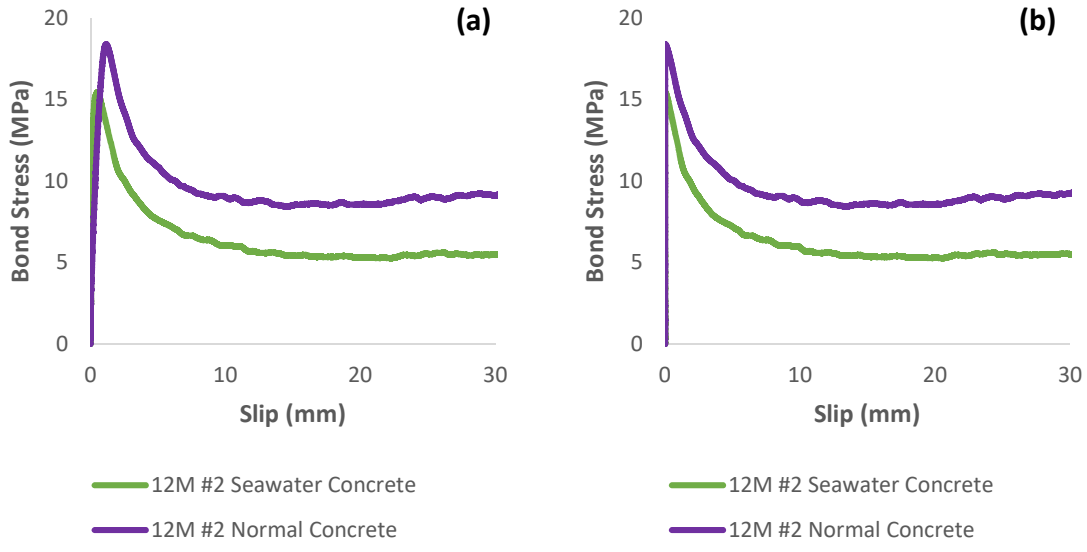

Figure 3.13 Example Stress-Slip Curves; (a) Loaded End, (b) Unloaded End, 12M Sand Coated Bar, Normal Concrete Vs Seawater Concrete

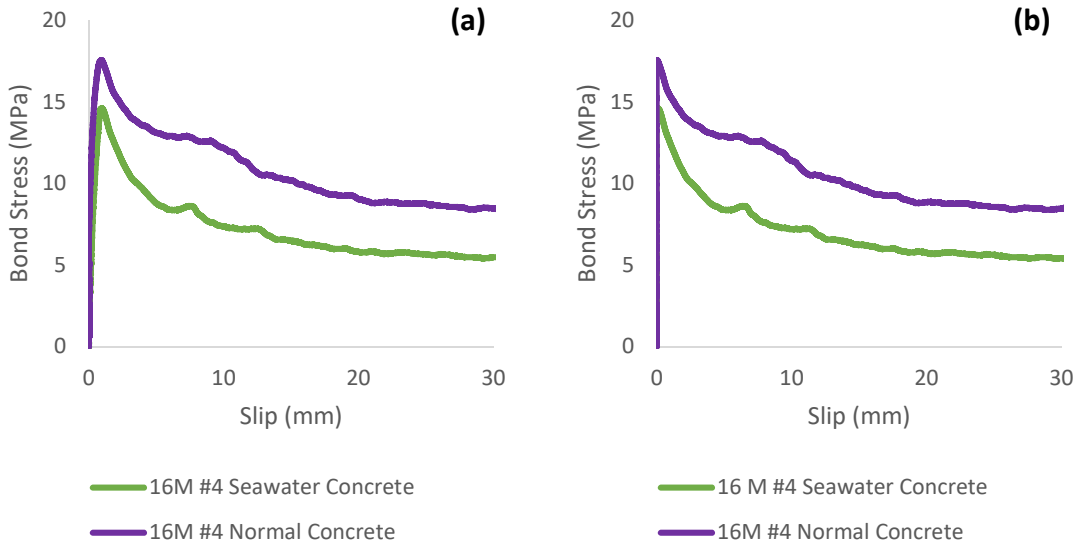

Figure 3.14 Example Stress-Slip Curves; (a) Loaded End, (b) Unloaded End, 16M Sand Coated Bar, Normal Concrete Vs Seawater Concrete

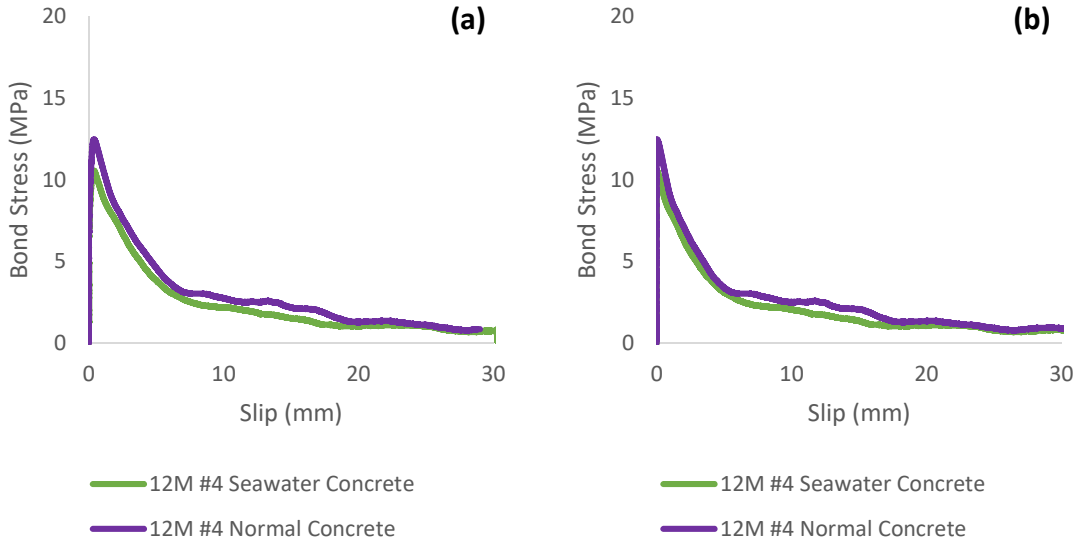

Figure 3.15 Example Stress-Slip Curves; (a) Loaded End, (b) Unloaded End, 12M Spiral Bar, Normal Concrete Vs Seawater Concrete

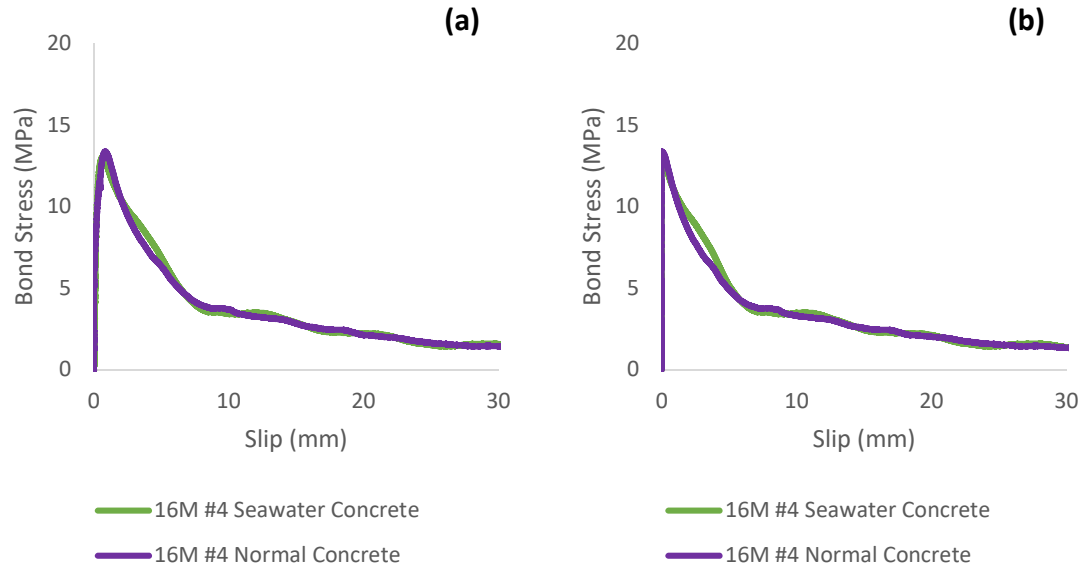

Figure 3.16 Example Stress-Slip Curves; (a) Loaded End, (b) Unloaded End, 16M Spiral Bar, Normal Concrete Vs Seawater Concrete

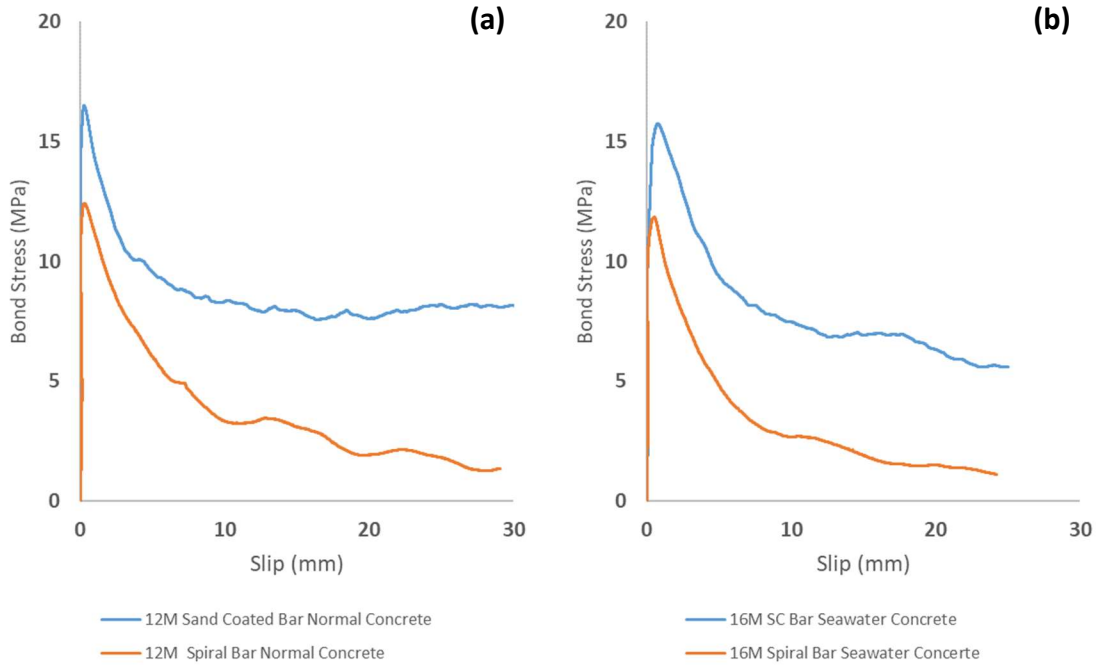

Figure 3.17 Example Stress-Slip Curves, Sand-coated vs Spiral Surface Configuration; (a) 12M with Normal Concrete, (b) 16M with Seawater Concrete

Figures 3.18 compare the idealized curves for all sample groups using the average peak bond strength and residual bond strength reported in Table 3.6 and 3.7. Through these curves it can be observed that due to the bar adhesion to the concrete, the bond stress increases very sharply

and after reaching the maximum bond strength the bond stress decreases until it stabilizes with only small fluctuations for sand coated bar, but the spiral bar descending branch continues to decrease as the bar loses its deformation during the loading.

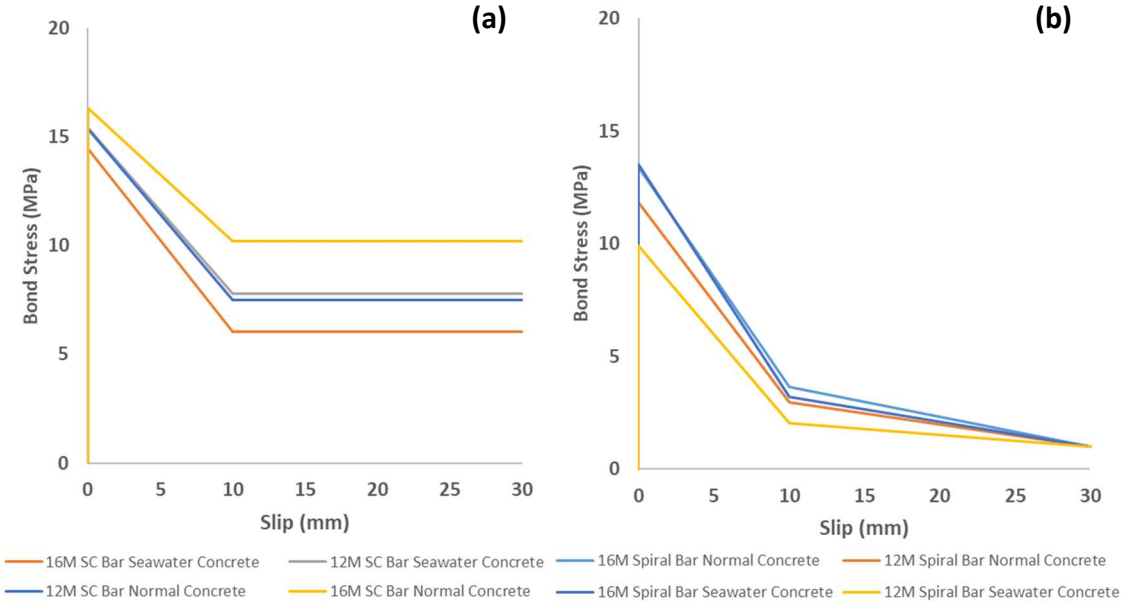

Figure 3.18 Stress-Slip Curves; Unloaded End; (a) Sand Coated Bars Normal and Seawater Concrete, (b) Spiral Bars Normal and Seawater Concrete

3.5 Analysis and Discussion

3.5.1 ANOVA Test

An analysis of variance (ANOVA) test is a statistical method used to determine whether differences in the results from two or more sets of data are significant. In this case, the results obtained from the seawater concrete are compared to those made with normal tap water. In an ANOVA test, the null hypothesis is valid only when the sample means are equal or do not have any significant difference. However, the alternate hypothesis is valid when at least one of the sample means vary from the rest of the sample means. In another words, in the case of two samples, the null hypothesis assumes that both sample means are equal while the alternate hypothesis considers that the sample means are different.

To understand the measure of the level of significance in difference between two data sets, the following values need to be calculated (the present analysis is based on a significance level of 0.05 which indicates a 5% risk of concluding that a difference exists when there is no actual difference):

Between group variability ($MS_{between}$):

The Between-Group-Variability shows the variations between the distributions of two or more individual groups or sets of data. Therefore, each set is looked at and the difference between its mean ($\overline{x_i}$) and the grand mean ($\overline{x_G}$) is calculated in order to understand the variability. If the data distributions are very close or overlap in some areas, the grand mean and individual means will be very similar; however, if the distributions are far from each other then the difference between the means and grand mean will be significant. By having the sample means and grand means, the between group variability **$MS_{between}$** is calculated in a similar manner as the standard deviation. Moreover, each squared deviation $(\overline{x_1} - \overline{x}_G)^2$ should be weighed by the size of the sample (n_i), hence each squared deviation will be multiplied by each sample size and then summed together. This action name is the Sum-of-squares for between-group variability ($SS_{between}$) which is calculated from Equation 3.2:

$$SS_{between} = n_1(\overline{x_1} - \overline{x}_G)^2 + n_2(\overline{x_2} - \overline{x}_G)^2 + n_3(\overline{x_3} - \overline{x}_G)^2 + \ldots..n_k(\overline{x_k} - \overline{x}_k)^2 \qquad \text{Eq. 3.2}$$

The sum-of-squares for between-group variability is then divided by the degrees of freedom ($df_{between}$), which in this case is defined as the number of samples (k) minus 1.

Finally, the between group variability is given by Equation 3.3:

$$MS_{between} = \frac{n_1(\overline{x_1} - \overline{x_G})^2 + n_2(\overline{x_2} - \overline{x_G})^2 + n_3(\overline{x_3} - \overline{x_G})^2 + \cdots..n_k(\overline{x_k} - \overline{x_k})^2}{k-1} \qquad \text{Eq. 3.3}$$

Within group variability (MS_{within}):

The Within-Group-Variability refers to the variations resulting from differences among various data points within an individual group. Therefore, the variability between the individual points in each sample is calculated first and each sample is assessed on its own. The interaction between different samples or groups is not considered at this stage. This value is obtained by calculating how much each data point within a group differs from its own sample

mean. Therefore, the squared deviation of each value $(x_{i1} - \overline{x}_1)^2$ is calculated from its sample mean $(\overline{x}_1)$ and summed together. This number is called the sum of squares for within-group variability shown through Equation 3.4 as follows:

$$SS_{Within} = \sum(x_{i1} - \overline{x}_1)^2 + \sum(x_{i2} - \overline{x}_2)^2 + \ldots..\sum(x_{i2} - \overline{x}_k)^2 = \sum(x_{ij} - \overline{x}_j)^2 \qquad \text{Eq. 3.4}$$

Similar to between-group variability, the sum of squared deviations is divided by the degrees of freedom (df_{within}) in order to find a less-biased estimator for the average squared deviation. This is called the mean square MS_{within}. In this case, the degrees of freedom are defined as the sum of the sample sizes (N) minus the number of samples (K) given by Equation 3.5:

$$MS_{Wit} = \frac{\sum(x_{i1} - \overline{x}_j)^2}{N - K} \qquad \text{Eq. 3.5}$$

F-statistic:

The F-ratio defines whether the means of different samples are significantly different or not. The lower the F-Ratio, the more similar the sample means are. The F-statistic is obtained from Equation 3.6:

$$F_{Statistic} = \frac{Between\ group\ variablity}{Withi\quad group\ variablity} \qquad \text{Eq. 3.6}$$

The F-statistic is compared to an F-critical value (for a specific α/significance level which is usually taken as 0.05); if it is more than F-critical then we can conclude that the difference is significant and therefore the null hypothesis can be rejected.

A one-way ANOVA test was performed in this study via the Excel data analysis tool. The control concrete and seawater concrete compressive strength values at 7, 14, 21, and 28 days were first compared through this test and in each case the differences were found to not be statistically significant (i.e. $F<F_{crit}$) for a significance level of 0.05 (Table 3.8 and 3.9). In other words, statistically speaking, the short term concrete compressive strength was not significantly affected by the substitution of seawater in place of normal tap water up to 28 days.

Moreover, in order to have a statistical comparison, a one-way ANOVA test was similarly performed on the pullout test peak strength values to understand their difference statistically, and the results are shown in Table 3.10 and 3.11. As the ANOVA test result shows, the

difference in peak bond strength between the control and seawater concrete was also found to be not statistically significant since $F < F_{crit}$ in all cases.

Finally, an ANOVA test was also conducted for the residual bond strength values where the curve reaches a reduced and relatively stable or gradually reducing bond stress dominated by bar friction. For this analysis, the residual bond stress value was assumed to correspond to an unloaded end bar slip of 10 mm. The corresponding ANOVA test is presented in Table 3.12 and 3.13. Similar to the previous tests, the results for residual bond strength were also found to be not significantly different ($F<F_{crit}$) between normal concrete and seawater concrete, except for the 16M sand-coated bar. In this single case, it was found that $F>F_{crit}$ which implies that the seawater concrete did demonstrate a different post-peak behaviour compared to the normal concrete samples.

Table 3.8 Concrete Compressive Strength ANOVA Test

7d

Anova: Single Factor

SUMMARY

Groups	*Count*	*Sum*	*Average*	*Variance*
Normal Concrete	3.00	84.67	28.22	6.23
Seawater Concrete	3.00	98.35	32.78	10.69

ANOVA

Source of Variation	*SS*	*df*	*MS*	*F*	*P-value*	*F crit*
Between Groups	31.19	1.00	31.19	3.69	0.13	7.71
Within Groups	33.84	4.00	8.46			
Total	65.03	5.00				

14d

Anova: Single Factor

SUMMARY

Groups	*Count*	*Sum*	*Average*	*Variance*
Normal Concrete	3.00	101.71	33.90	12.81
Seawater Concrete	3.00	105.61	35.20	3.47

ANOVA

Source of Variation	*SS*	*df*	*MS*	*F*	*P-value*	*F crit*
Between Groups	2.54	1.00	2.54	0.31	0.61	7.71
Within Groups	32.56	4.00	8.14			
Total	35.10	5.00				

21d

Anova: Single Factor

SUMMARY

Groups	*Count*	*Sum*	*Average*	*Variance*
39.05	2.00	73.92	36.96	7.22
37.60	2.00	77.20	38.60	0.72

ANOVA

Source of Variation	*SS*	*df*	*MS*	*F*	*P-value*	*F crit*
Between Groups	2.69	1.00	2.69	0.68	0.50	18.51
Within Groups	7.94	2.00	3.97			
Total	10.63	3.00				

28d

Anova: Single Factor

SUMMARY

Groups	*Count*	*Sum*	*Average*	*Variance*
Normal Concrete	3.00	117.70	39.23	11.26
Seawater Concrete	3.00	118.30	39.43	0.34

ANOVA

Source of Variation	*SS*	*df*	*MS*	*F*	*P-value*	*F crit*
Between Groups	0.06	1.00	0.06	0.01	0.92	7.71
Within Groups	23.21	4.00	5.80			
Total	23.27	5.00				

Table 3.9 Concrete Compressive Strength ANOVA Test Result Summary

Age (days)	**F**	**F_{crit}**
7d	3.69	7.71
14d	0.31	7.71
21d	0.68	18.51
28d	0.01	7.71

Table 3.10 Pullout Peak Load ANOVA test

12 M Sand coated

Anova: Single Factor

SUMMARY

Groups	*Count*	*Sum*	*Average*	*Variance*
Normal	4.00	61.43	15.36	11.26
Seawater	5.00	77.00	15.40	3.19

ANOVA

Source of Variation	*SS*	*df*	*MS*	*F*	*P-value*	*F crit*
Between Groups	0.004	1.00	0.004	0.006	0.98	5.59
Within Groups	46.55	7.00	6.65			
Total	46.56	8.00				

16 M Sand coated

Anova: Single Factor

SUMMARY

Groups	*Count*	*Sum*	*Average*	*Variance*
Normal	5.00	81.59	16.32	13.03
Seawater	5.00	72.32	14.46	2.20

ANOVA

Source of Variation	*SS*	*df*	*MS*	*F*	*P-value*	*F crit*
Between Groups	8.59	1.00	8.59	1.13	0.32	5.32
Within Groups	60.91	8.00	7.61			
Total	69.50	9.00				

12 M Spiral

Anova: Single Factor

SUMMARY

Groups	*Count*	*Sum*	*Average*	*Variance*
Normal	5.00	59.27	11.85	1.92
Seawater	5.00	49.58	9.92	1.85

ANOVA

Source of Variation	*SS*	*df*	*MS*	*F*	*P-value*	*F crit*
Between Groups	9.39	1.00	9.39	4.99	0.06	5.32
Within Groups	15.05	8.00	1.88			
Total	24.44	9.00				

16 M Spiral

Anova: Single Factor

SUMMARY

Groups	*Count*	*Sum*	*Average*	*Variance*
Normal	5.00	65.70	13.14	0.20
Seawater	5.00	67.58	13.52	1.68

ANOVA

Source of Variation	*SS*	*df*	*MS*	*F*	*P-value*	*F crit*
Between Groups	0.35	1.00	0.35	0.38	0.56	5.32
Within Groups	7.52	8.00	0.94			
Total	7.87	9.00				

Table 3.11 Pullout Test Peak Load ANOVA Test

Bar Type	F	F_{crit}
12M Sand-Coated	0.006	5.59
16M Sand-Coated	1.13	5.32
12M Spiral	4.99	5.32
16M Spiral	0.38	5.32

Table 3.12 Residual Bond Strength ANOVA Test

12M Sand Coated

Anova: Single Factor

SUMMARY

Groups	*Count*	*Sum*	*Average*	*Variance*
12 M Normal Sand Coated	4.00	30.09	7.52	2.42
12 M Seawater Sand Coated	5.00	39.43	7.89	1.65

ANOVA

Source of Variation	*SS*	*df*	*MS*	*F*	*P-value*	*F crit*
Between Groups	0.29	1.00	0.29	0.15	0.71	5.59
Within Groups	13.86	7.00	1.98			
Total	14.15	8.00				

16M Sand Coated

Anova: Single Factor

SUMMARY

Groups	*Count*	*Sum*	*Average*	*Variance*
16 M Normal Sand Coated	5.00	50.97	10.19	3.89
16 M Seawater Sand Coated	5.00	30.26	6.05	2.04

ANOVA

Source of Variation	*SS*	*df*	*MS*	*F*	*P-value*	*F crit*
Between Groups	42.87	1.00	42.87	14.45	0.01	5.32
Within Groups	23.74	8.00	2.97			
Total	66.61	9.00				

12M Spiral

Anova: Single Factor

SUMMARY

Groups	*Count*	*Sum*	*Average*	*Variance*
12 M Normal Spiral	5.00	14.78	2.96	0.60
12 M Seawater Spiral	5.00	10.30	2.06	0.26

ANOVA

Source of Variation	*SS*	*df*	*MS*	*F*	*P-value*	*F crit*
Between Groups	2.01	1.00	2.01	4.64	0.06	5.32
Within Groups	3.46	8.00	0.43			
Total	5.47	9.00				

16M Spiral

Anova: Single Factor

SUMMARY

Groups	*Count*	*Sum*	*Average*	*Variance*
16 M Normal Spiral	5.00	18.31	3.66	0.43
16 M Seawater Spiral	5.00	16.19	3.24	0.26

ANOVA

Source of Variation	*SS*	*df*	*MS*	*F*	*P-value*	*F crit*
Between Groups	0.45	1.00	0.45	1.31	0.29	5.32
Within Groups	2.77	8.00	0.35			
Total	3.22	9.00				

Table 3.13 Summarized ANOVA Test Result on Residual Bond Strength

Bar Type	**F**	**F_{crit}**
12M Sand-Coated	0.15	5.59
16M Sand-Coated	14.5	5.32
12M Spiral	4.64	5.32
12M Spiral	1.31	5.32

3.5.2 Discussion

The test results presented in this chapter show that the short-term bond strength of GFRP reinforcing bars embedded in seawater concrete may be considered to be similar to normal concrete. This is supported by ANOVA tests that found that the compressive strength values and peak bond strengths were not significantly different between the two concrete types, regardless of bar size or surface configuration type. It is also worth noting that the peak and residual bond stress ranges summarized in Table 3.6 and 3.7, and the specimen behaviour observed in the stress-slip curves, showed a close resemblance to past studies on the bond behaviour of GFRP with conventional concrete (e.g. Okelo et al. [71], Achillides et al. [64]

and Aiello et al. [62]). Therefore, the potential use of GFRP reinforcement with seawater concrete appears promising, at least with respect to short term structural behaviour. Moreover, the concrete compressive strength gain behaviour was similar to most of the past experimental results reported by other researchers over a 28-day period as discussed in Chapter 2. It should be mentioned, however, that this study did not consider other important concrete mechanical properties such as tensile strength, elastic modulus, or shear behaviour, which are recommended for future studies.

Given that the response of flexural reinforced concrete members at both ultimate and serviceability limit states are greatly dependent on bond behaviour between concrete and reinforcement, these results suggest that GFRP-reinforced concrete members made with seawater concrete may be reasonably expected to have a fairly similar overall short-term behaviour as similar members made with normal tap water (although further testing is needed to verify this point). If GFRP-reinforced seawater concrete can be demonstrated as an acceptable and reliable alternative in areas facing freshwater shortages, but with access to seas and oceans, it could have a considerable positive impact to improve water security in these regions.

Although the ANOVA tests determined in almost all cases that the seawater concrete was not significantly different from the normal tap water concrete, one exception was noted as the 16M sand-coated bar embedded in seawater concrete was found to have a lower residual bond stress compared to the normal concrete group. It is not immediately evident why this result is different from the others, although it should be noted that comparing the stress values at a slip of 10 mm was an arbitrary choice and the results may have been different if another value had been used. Furthermore, in most practical cases the residual bond strength is not a critical design parameter, since bond failures are avoided due to their brittle nature. Hence, this result is not considered to greatly affect the overall findings of this chapter.

Although the pullout test results presented in this chapter showed an acceptable behaviour, there remain concerns about the long-term behaviour of seawater concrete. Therefore, it is highly recommended that the bond behaviour between GFRP bars and seawater concrete be assessed after a longer period of time to observe any possible changes.

Moreover, as mentioned in Chapter 2, the pullout test results are not directly applicable to the design of larger members and should not be relied on as the only means of assessing the bond behaviour in concrete. For this reason, it is highly recommended that the bond performance be tested using a different and more realistic test configuration. The following chapter of this thesis is dedicated to this topic.

Chapter 4 Beam Anchorage Test

4.1 General

While the pullout tests presented in Chapter 3 are useful for comparing the influence of individual parameters on bond behaviour, they are generally not suitable for designing actual structural members for the reasons discussed in Chapter 2. For this reason, a series of beam anchorage tests were also performed to more accurately reflect the behaviour of FRP reinforcing bars in flexural concrete members. This specimen type is very similar in appearance to normal beams, except that only a specified length of the bar is bonded to the concrete in the end regions and the rest of the bar is intentionally de-bonded. Therefore, the beam is designed to have two identical bonded lengths at both ends, and the middle section of the bar is encased in a PVC pipe. Moreover, two pockets were located adjacent to the bonded lengths in order to facilitate the placement of LVDTs and strain gauges (Figure 4.1). Finally, the portion of the bar extending beyond the centerline of the support was also de-bonded to minimize the beneficial effect of support confinement on the bar anchorage.

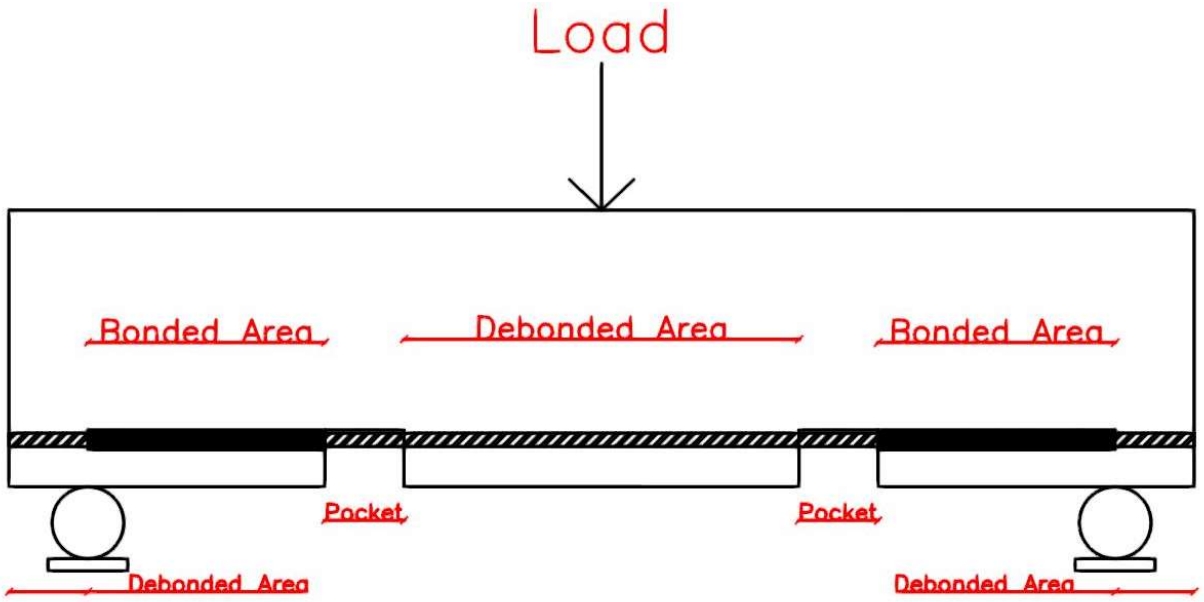

Figure 4.1 Schematic of Bond Anchorage Specimen

4.2 Materials and Fabrication

4.2.1 Reinforcement

The FRP bars used in this part of the study were 1500 mm long GFRP bars with spiral deformations and a nominal diameter of 16 mm (Figure 4.2 (a)) for longitudinal reinforcement and 20 mm for stirrups (Figure 4.2 (b)). The mechanical properties are shown in Table 4.1 and Table 4.2. The selected shear reinforcement diameter was chosen mainly because of the producer technical issues with its machine, which limited the diameter selection, therefore the minimum bar diameter could be 20 mm.

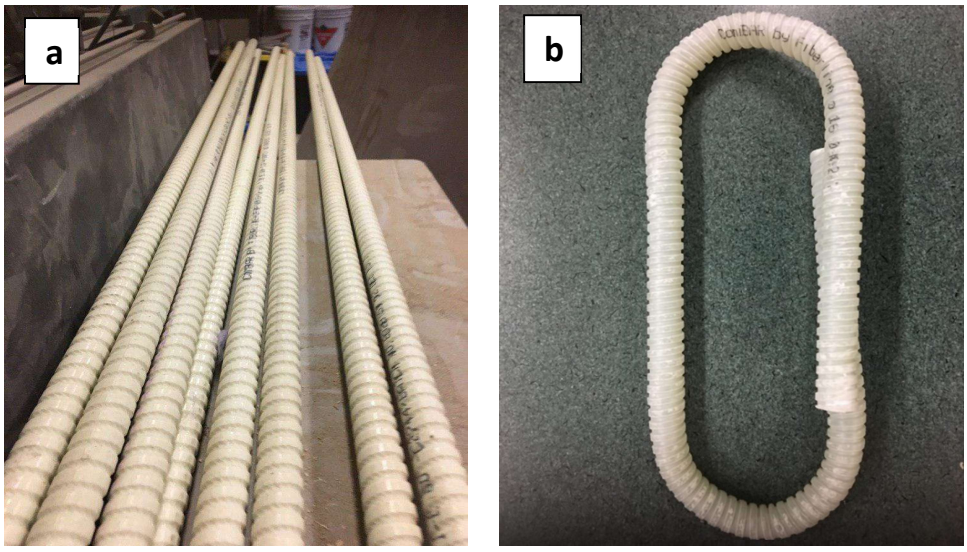

Figure 4.2 GFRP Bars: (a) Longitudinal Reinforcement (b) Stirrup

Table 4.1 16M Spiral GFRP Bar Properties

Mechanical Property	Average Value
Longitudinal Tensile Strength (MPa)	1339
Longitudinal Tensile Modulus (MPa)	66320
Transverse Shear Strength (MPa)	258
Cross-Sectional Area (mm)	209.34

Table 4.2 20M Spiral GFRP Stirrups Mechanical Properties

20M bar	Design Value (MPa)
Ultimate Tensile Strength (Straight Portion)	900
Ultimate Tensile Strength (Bent Portion)	550
Longitudinal Tensile Modulus	>50000

4.2.2 Formwork

Each beam had a length of 1.5 m with cross-section dimensions of 350 mm height by 150 mm width. Formwork which was suitable for the above-mentioned dimensions was built out of melamine wood with the capacity of 3 anchorage beams (Figure 4.3).

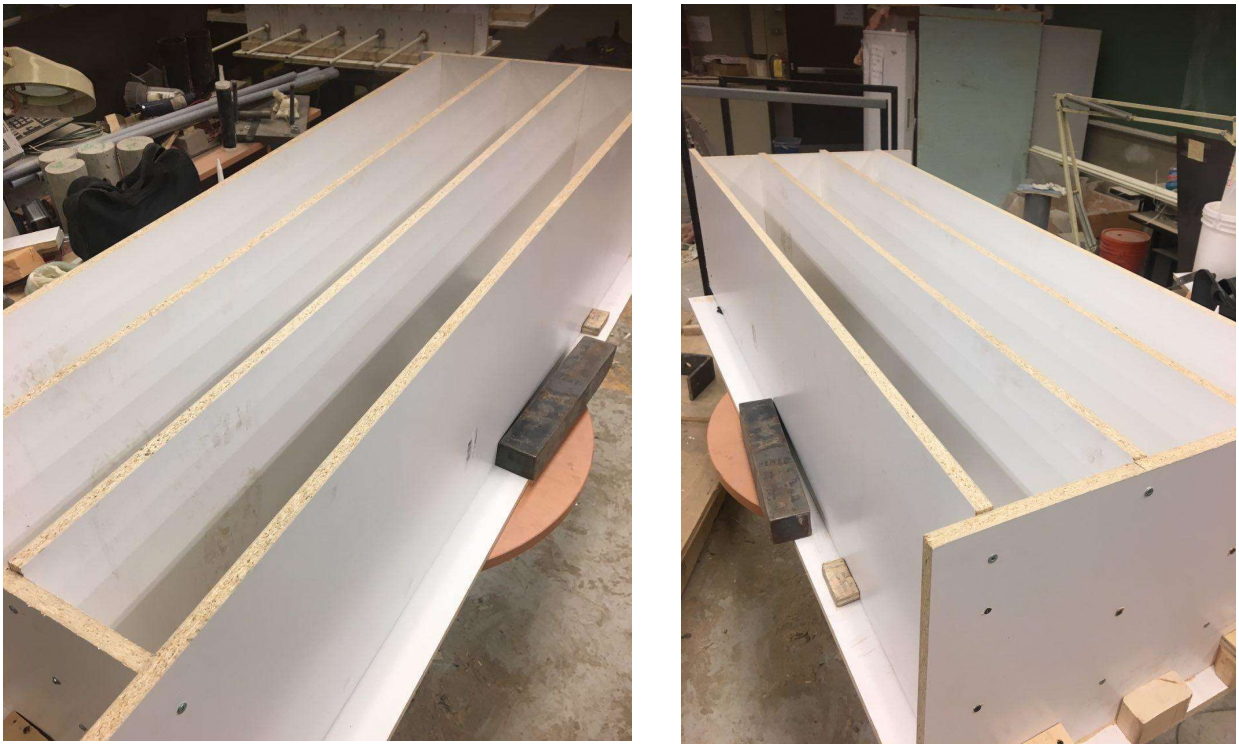

Figure 4.3 Beam Formwork

4.2.3 Concrete

The concrete used for casting the beam specimens had the same properties, mix design and casting procedure as discussed in Chapter 3. Three beams were prepared with a control concrete mix, and three were prepared with seawater as the concrete mixing water.

4.3 Beam Specimen Details

A total of six beam anchorage specimens were fabricated and tested. A single reinforcing bar was placed in the tension zone with a clear concrete cover of 35 mm, and a second bar was placed in the compression zone to facilitate the construction of the reinforcing cage (Figure 4.4). The stirrups were spaced at 150 mm throughout the beam.

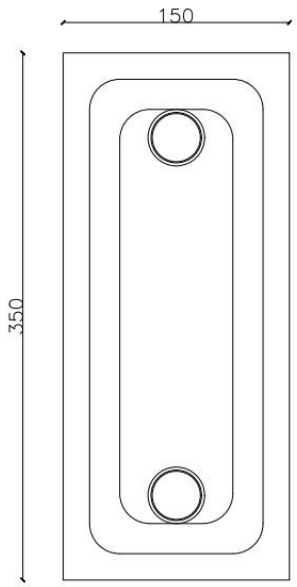

Figure 4.4 Beam Cross Section

The beams were made with either regular or seawater concrete, and the length of the bonded region was varied from 30 to 50 cm (Table 4.3, Figure 4.5). The values of embedment length were selected considering the theoretical development length of 97 cm (as discussed later), in conjunction with an expected safety factor of approximately 2 based on literature and engineering judgment. It is worth noting that the bonded length for the same bars in the pullout

test configuration described in Chapter 3 was only 8 cm. A summary of the test matrix for this portion of the study is provided in Table 4.3.

Table 4.3 Bonded Length

Beam Number	Bar Type	Concrete Type	Bonded Length (cm)
B1	GFRP	Normal	30
B2	GFRP	Normal	40
B3	GFRP	Normal	50
C1	GFRP	Seawater	30
C2	GFRP	Seawater	40
C3	GFRP	Seawater	50

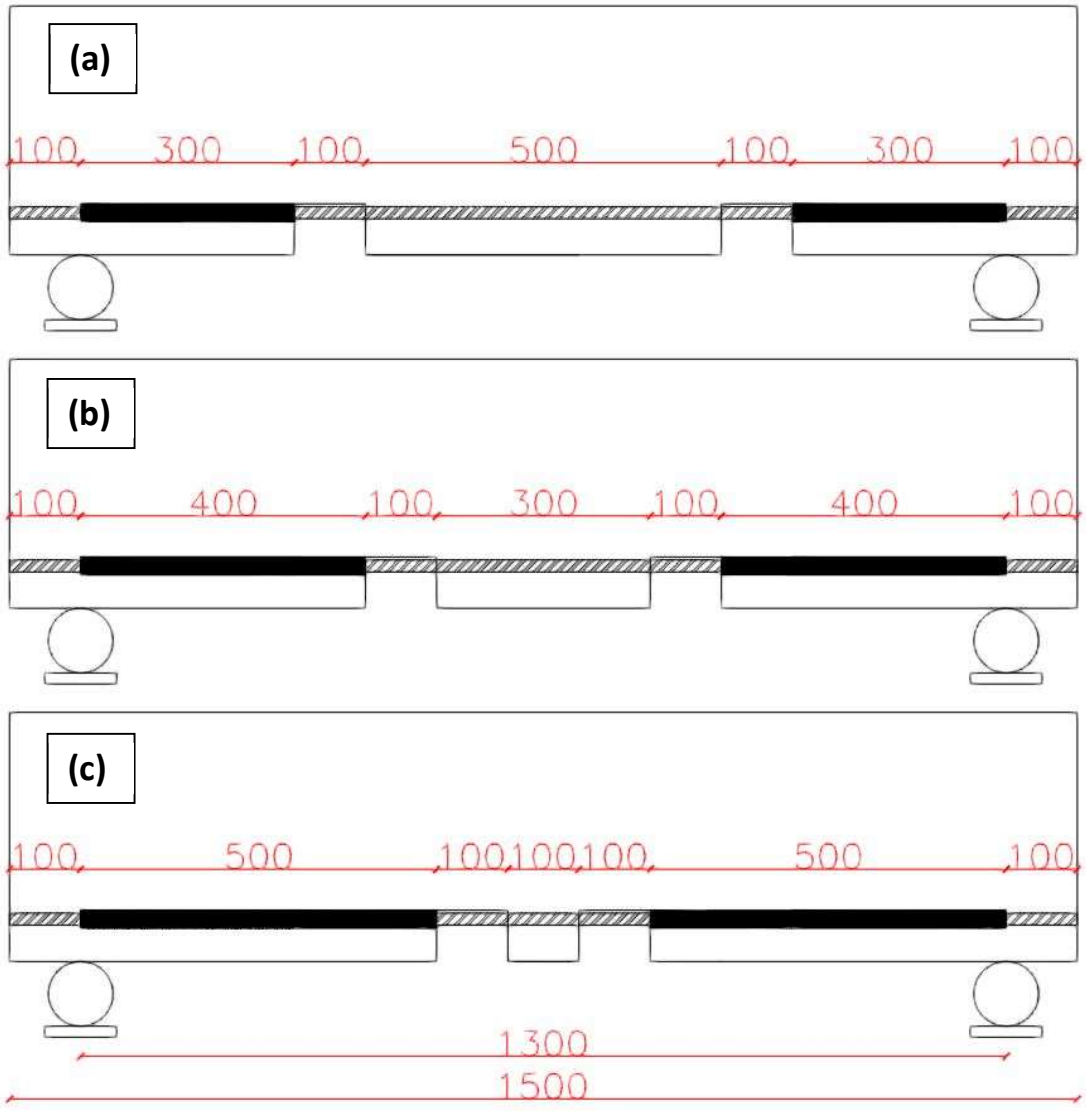

Figure 4.5 Beam Sketch (dimensions in mm)

4.4 Instrumentation

The strain gauges used are shown in Figure 4.6 with 350 ± 10 Ohm resistance and lengths of either 2 mm or 6 mm, depending on their location. The length of the strain gauges applied to the embedded portions of the bar was intentionally limited to minimize any interference with the bond transfer to the surrounding concrete. Strain gauges were attached at 100 mm spacing along the bonded length at both ends of the beam as shown in Figure 4.7 with a 50 mm gap from the starting point of the bonded length. In order to measure the strain in the bar along the de-bonded area, and to confirm the maximum tensile force in the bar, another 2 strain gauges (Figure 4.7), were attached to the GFRP tension reinforcement after casting within the pockets located near the beam mid-span. Prior to attaching the strain gauges, a small portion of the spiral ribs was carefully sanded down to reach the core longitudinal fibres of the bar.

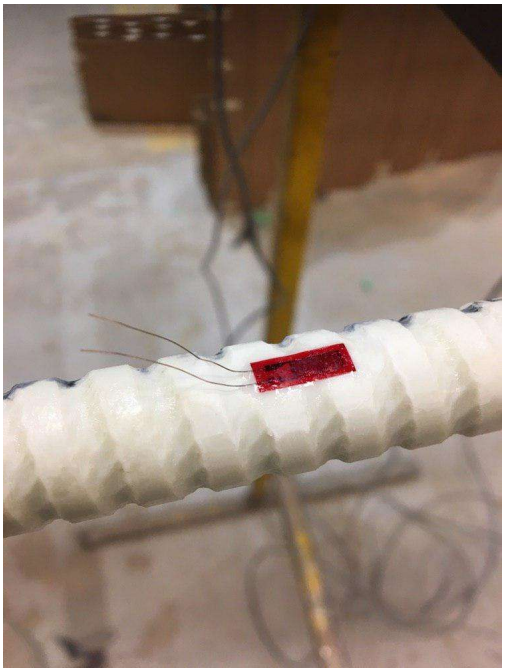

Figure 4.6 Strain Gauges

Moreover, for measuring the amount of slip at the loaded (i.e. midspan) and unloaded ends, four cable transducers were attached to the beam as shown in Figure 4.7.

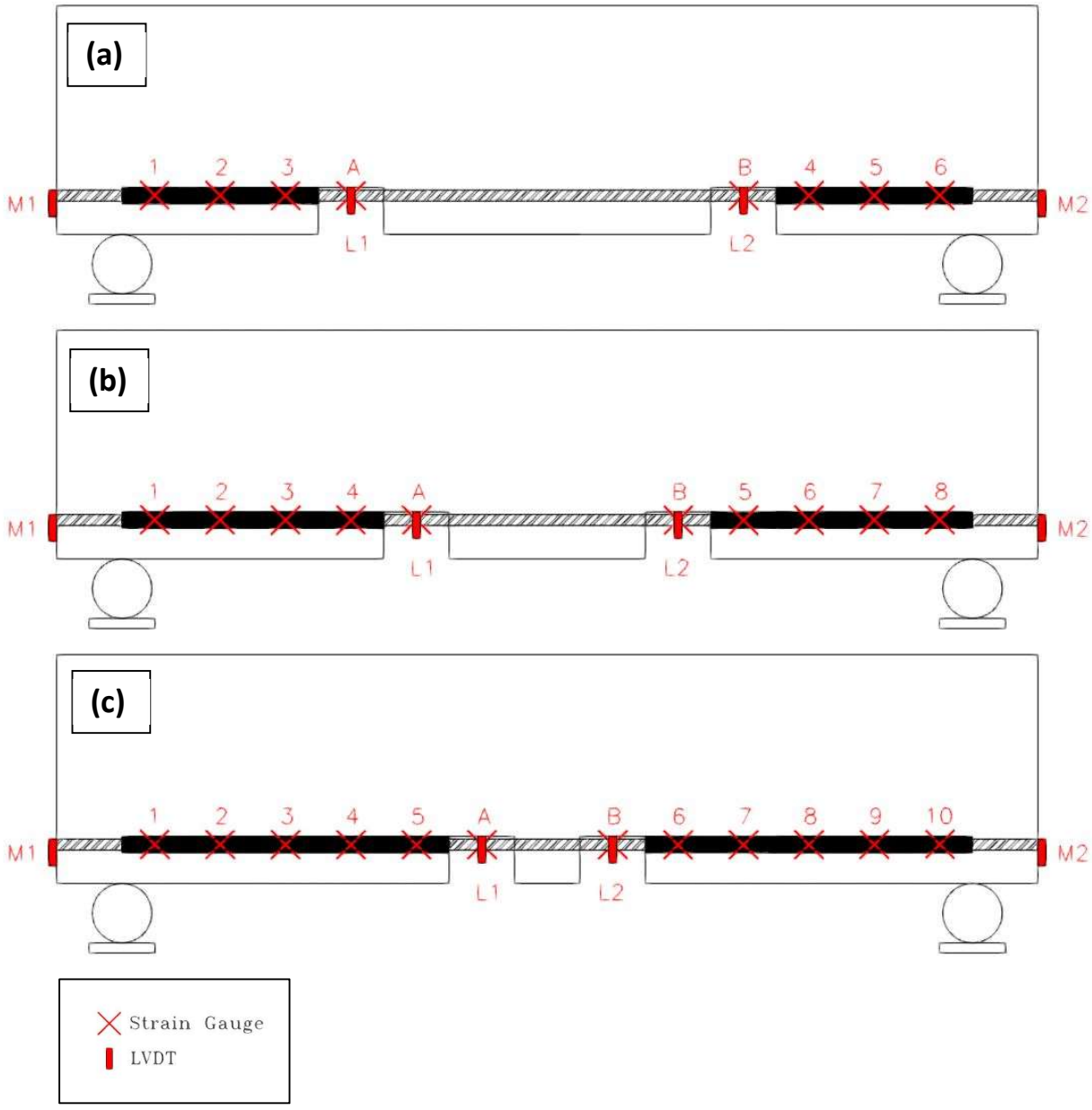

Figure 4.7 Schematic showing strain gauge and LVDTs locations; (a) 300 mm bonded length; (b) 400mm bonded length; (c) 500mm bonded length

The beams were placed on two roller supports and tested in a 3-point-load configuration with the load applied slowly at midspan using a manual jack. A load cell at midspan was used to monitor and record the applied load. The strain gauges were attached to the data acquisition

system for recording the strain during the test, and the cable transducers were attached to the bar at four locations as shown in Figure 4.8.

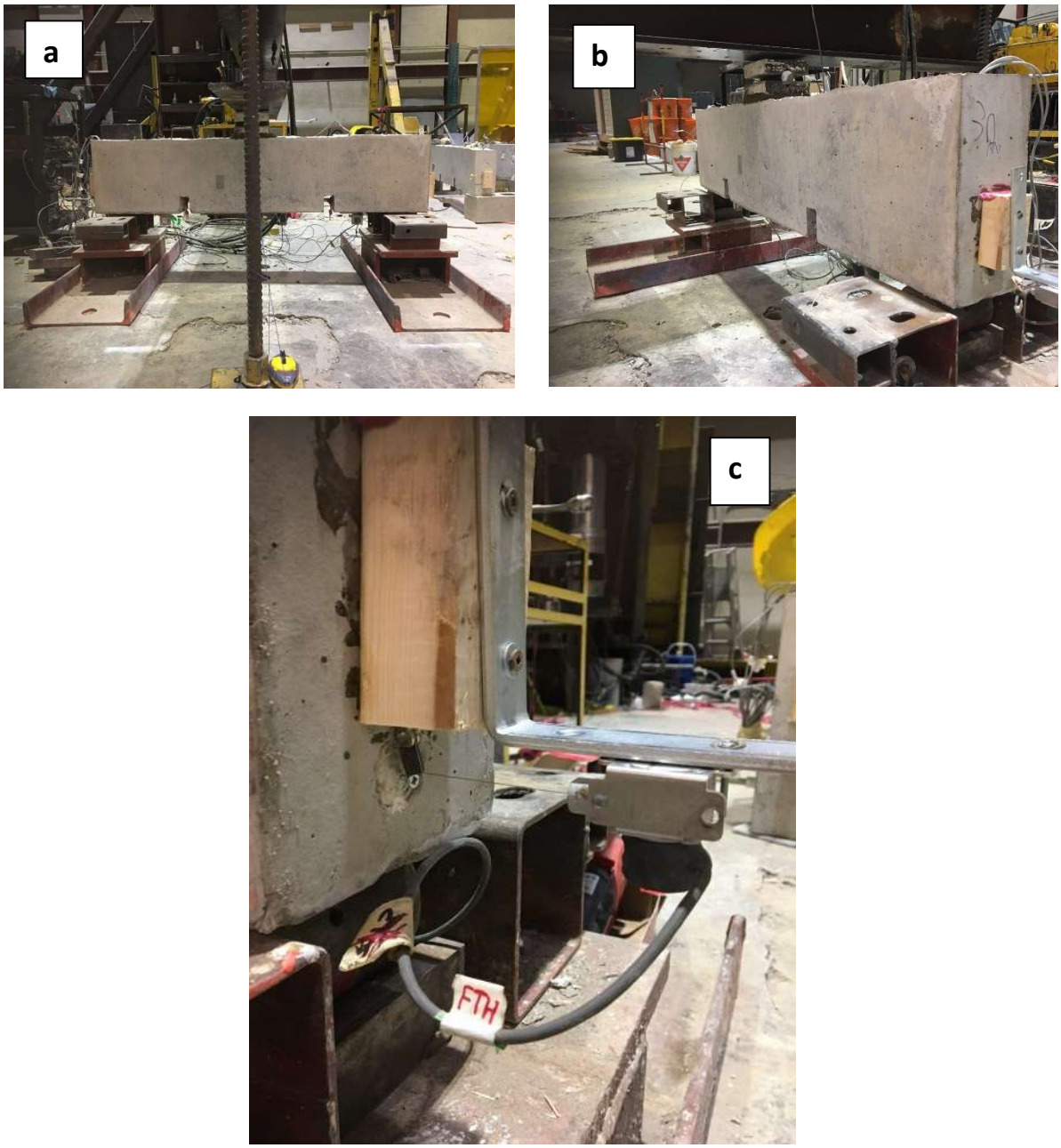

Figure 4.8 Beam Testing: (a and b) Beam Test Setup, (c) LVDT Installation

4.5 Results

4.5.1 Failure Mode

As the applied load was gradually increased, a single flexural crack typically formed at the beam mid-span (Figure 4.9), which continued to widen throughout the test. As the tension force in the bar increased at midspan, the loaded end displacement transducers began to record some initial slip and the bar strains nearest to the midspan began to increase. At a certain point, longitudinal splitting cracks appeared along the bottom surface of the beam in the bonded regions, which initiated near the pockets in the beam and propagated outward toward the supports (Figure 4.10). The load continued to increase until the beam finally failed with a sudden large slip occurring at the unloaded end of one side of the beam (Figure 4.11). At the moment of failure, the concrete immediately adjacent to the pocket often cracked which shifted the location of the cable transducer fixed to the bottom of the beam. This explains the post-peak slip readings at the loaded end which in some cases appeared lower than the unloaded end, or even decreased, which does not accurately represent the observed behaviour.

Figure 4.9 First Flexural Crack

Figure 4.10 Longitudinal Crack Propagation

Figure 4.11 Unloaded End Slippage; (a) Before Slippage, (b) After Slippage

For the beams with the longest embedment length of 50 cm, diagonal shear cracks also appeared prior to failure (Figure 4.12). Although this did not change the final mode of failure which occurred by bar slip, it is apparent from the results that a diagonal compression strut was formed extending outward from the loading point and the tension zone concrete between the pocket and the shear crack was not fully engaged at failure. This is a likely reason for the

observed results in which the increase in bonded length did not always correspond to a similar increase in failure load (F_u) as seen in Table 4.4.

Figure 4.12 Shear Crack at Failure

Table 4.4 Beam Failure Loads, F_u

Property	Normal Concrete			Seawater Concrete		
	30 cm	**40 cm**	**50 cm**	**30 cm**	**40 cm**	**50 cm**
F_u (kN)	91.00	88.36	93.61	79.78	85.26	98.13
Max Bar Force (kN)	99.35	96.37	102.10	87.02	92.99	107.03
Tensile strength (kN)	225	225	225	225	225	225
Percent (%)	44.15	42.80	45.3	38.6	41.32	47.56

The bar force was calculated from the applied load assuming a linear elastic cracked section analysis as the concrete compression strain in the beams was relatively small (the maximum concrete strain in compression was calculated to be 0.001 at failure). The bar force is derived from the applied moment at midspan according to Equations 4.1 to 4.3:

$$k = \sqrt{(n\rho)^2 + 2n\rho} - n\rho \qquad \text{Eq. 4.1}$$

Where:

$$n = \frac{Efrp}{Ec} \qquad \text{Eq. 4.2}$$

Then:

$$T = \frac{M}{d - \frac{kd}{3}} \qquad \text{Eq. 4.3}$$

Where:

$d = Effective\ Depth\ (mm)$

$kd = Neutral\ Axis\ Depth\ (mm)$

$\rho = \frac{A_{frp}}{bd}$

$E_c = Concrete\ Modulus\ of\ Elasticity\ (MPa) = 4500\sqrt{f'_c}$

$T = Bar\ Force\ (N)$

4.5.2 Force-Slip Curves

The tension force-slip curves of the bars are shown in Figures 4.13 to 4.18 for both the loaded and unloaded regions of every single beam. Large post-peak slips corresponding to anchorage failure were only observed at one end of each of the beams, since after failure the load decreased significantly with one side resisting load by friction only. Approximately 1 to 2 mm of slip were typically observed at the loaded ends of the bars before failure, and the sudden failure did not necessarily occur at the same side that was displaying the higher pre-failure slip values. After the anchorage failure, the load usually reached a greatly reduced and relatively

stable residual level dominated by bar friction, which was usually about 40-50% of the peak force.

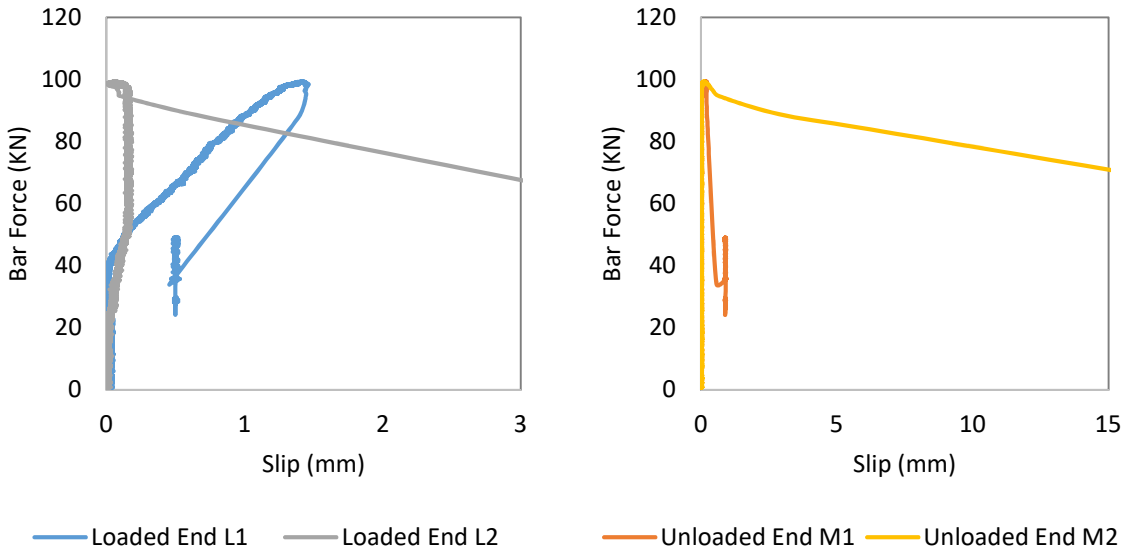

Figure 4.13 Force-Slip Curve, Normal Concrete, 30 cm Embedment Length

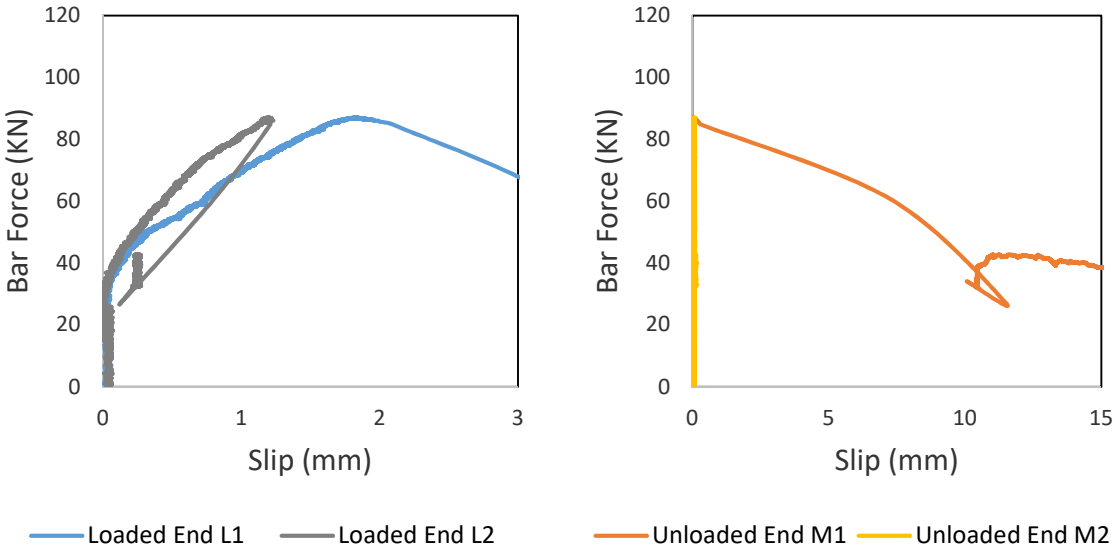

Figure 4.14 Force-Slip Curve, Seawater Concrete, 30 cm Embedment Length

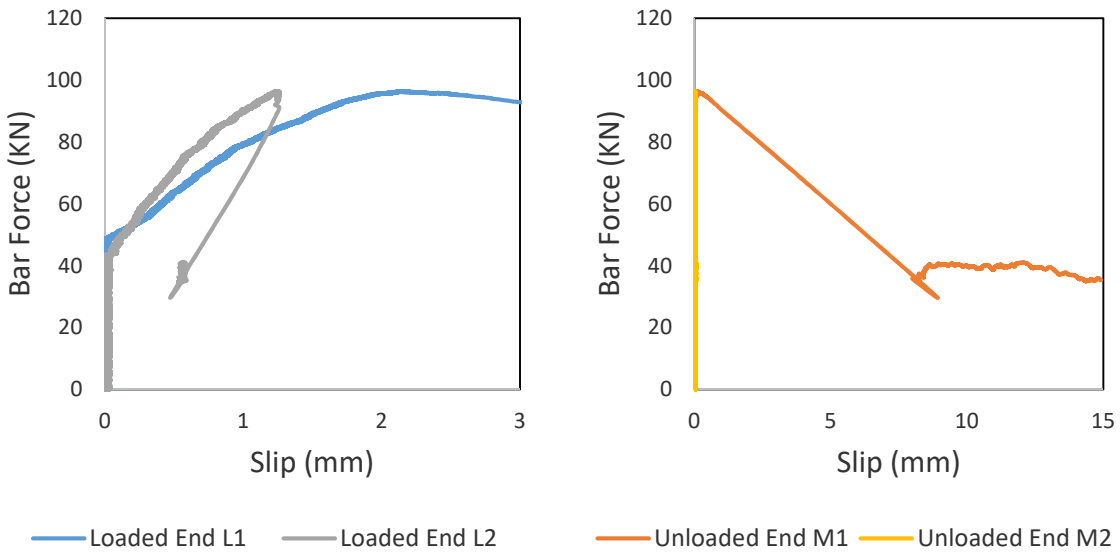

Figure 4.15 Force-Slip Curve, Normal Concrete, 40 cm Embedment Length

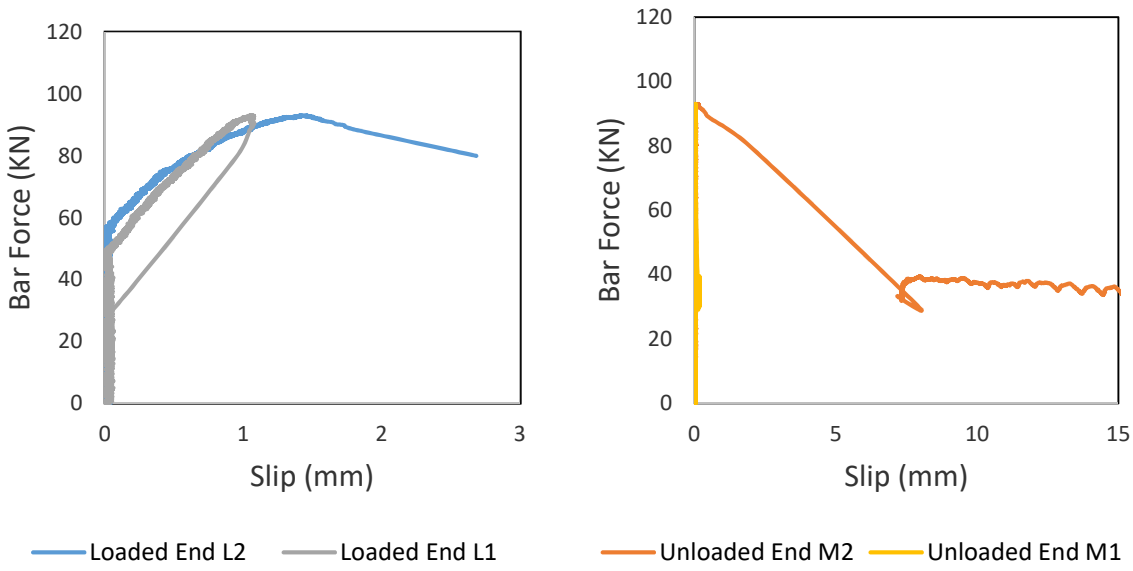

Figure 4.16 Force-Slip Curve, Seawater Concrete, 40 cm Embedment Length

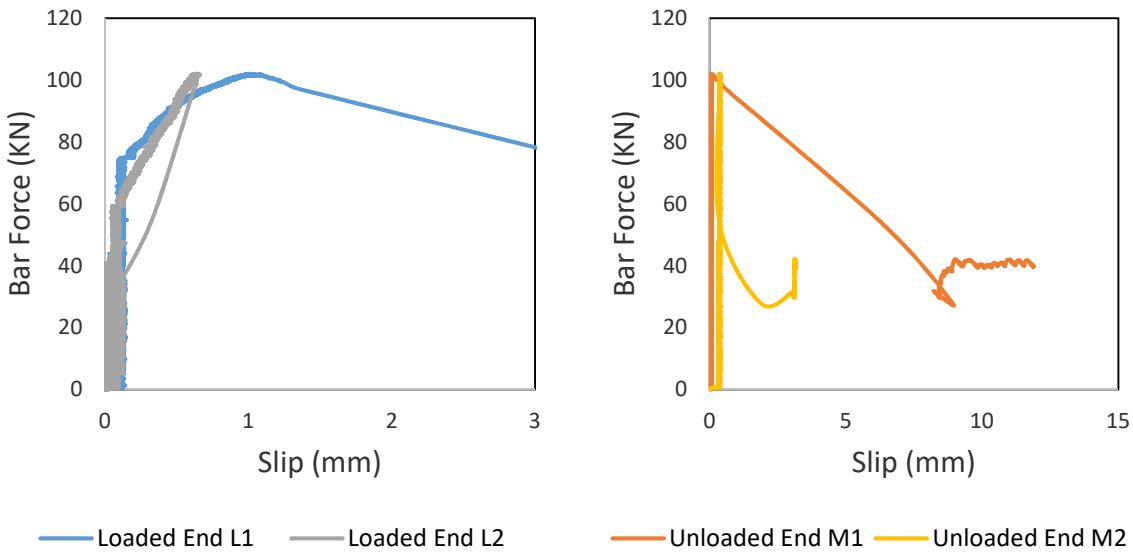

Figure 4.17 Force-Slip Curve, Normal Concrete, 50 cm Embedment Length

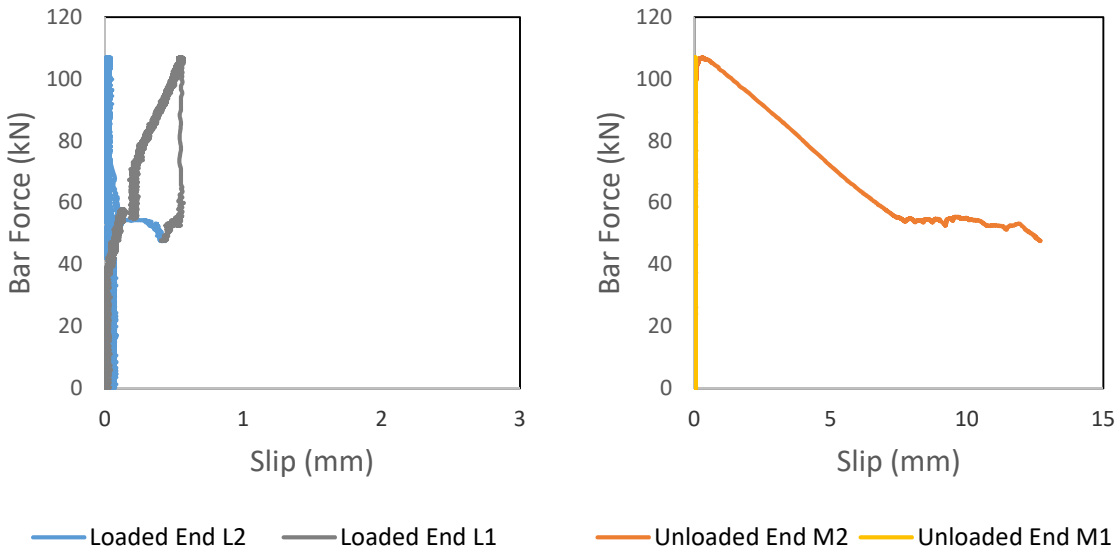

Figure 4.18 Force-Slip Curve, Seawater Concrete, 50 cm Embedment Length

As previously discussed, the failure load did not increase substantially with increasing embedment length, which is likely attributed to the formation of a diagonal shear crack and concrete strut outside of the beam pockets.

4.5.3 Strain Distribution

The strain gauge numbering is shown in Figure 4.19, while the measurements from the strain gauges are plotted in Figures 4.20 to 4.25 for each strain gauge at different bar force levels. At lower force levels, only the strain gauges nearest to the midspan were engaged. As the applied load increased, a somewhat linear variation in strain was observed in the strain gauges along the bond length. Prior to failure, as the longitudinal bond crack propagated toward the beam ends, a non-linear strain variation was often observed as the peak bond stress shifted towards the supports.

It is worth mentioning that during the casting one of the strain gauges was damaged; therefore, there is no reading recorded for strain gauge #5 in Figure 4.22. Moreover, in a couple of instances the strain readings unexpectedly decreased just prior to failure, which is thought to be the result of a possible de-bonding between the strain gauge and the bar (such as #7 in Figure 4.24 and 4.25). These unreliable values were not considered in further analysis.

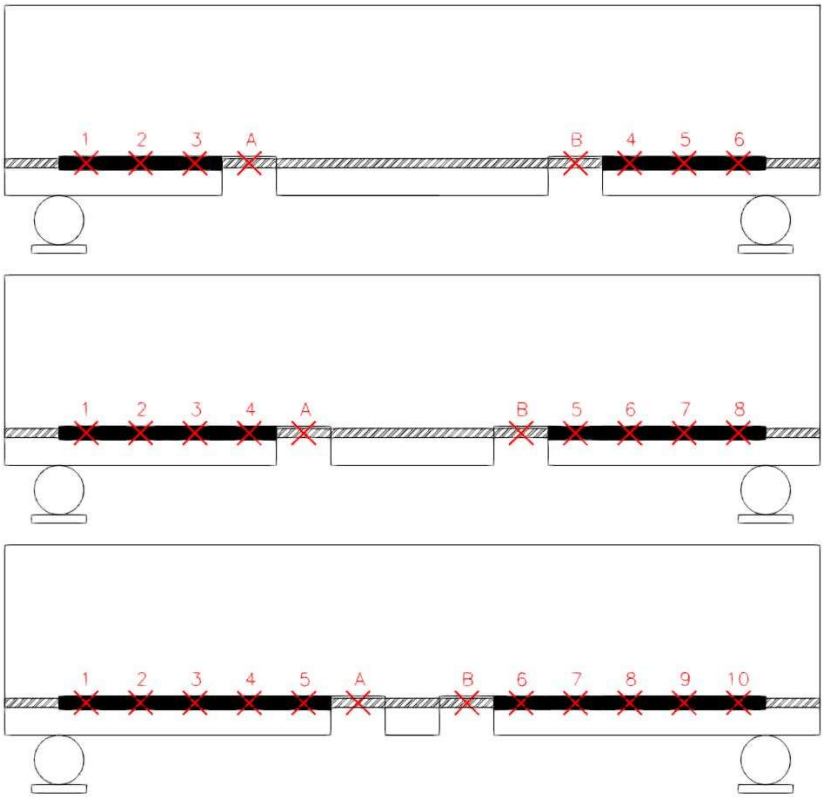

Figure 4.19 Strain Gauge Numbering

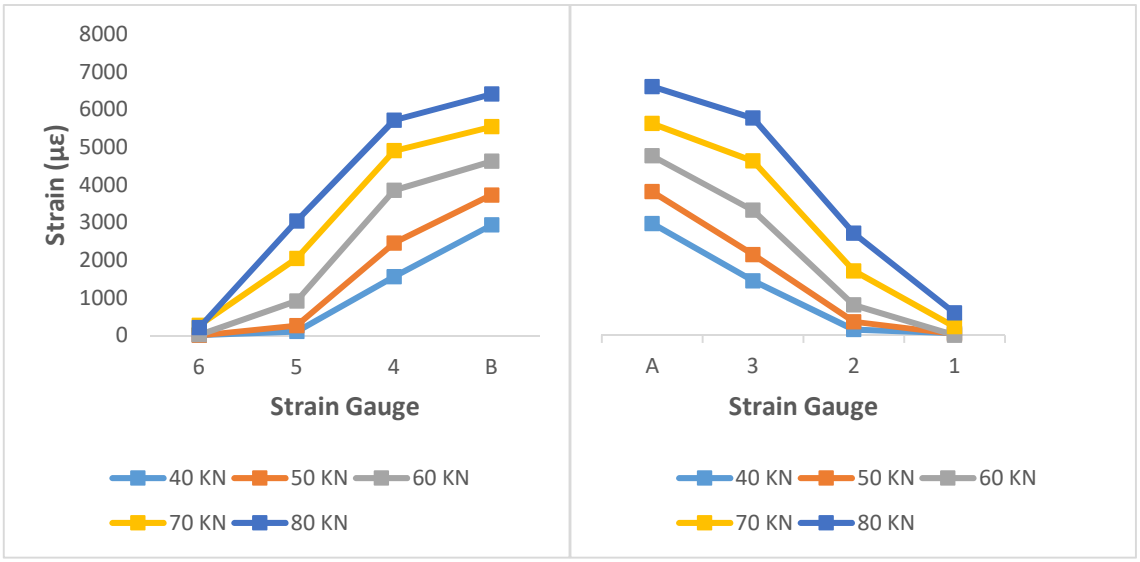

Figure 4.20 Strain Gauge Readings, Normal Concrete with 30 cm Embedment Length

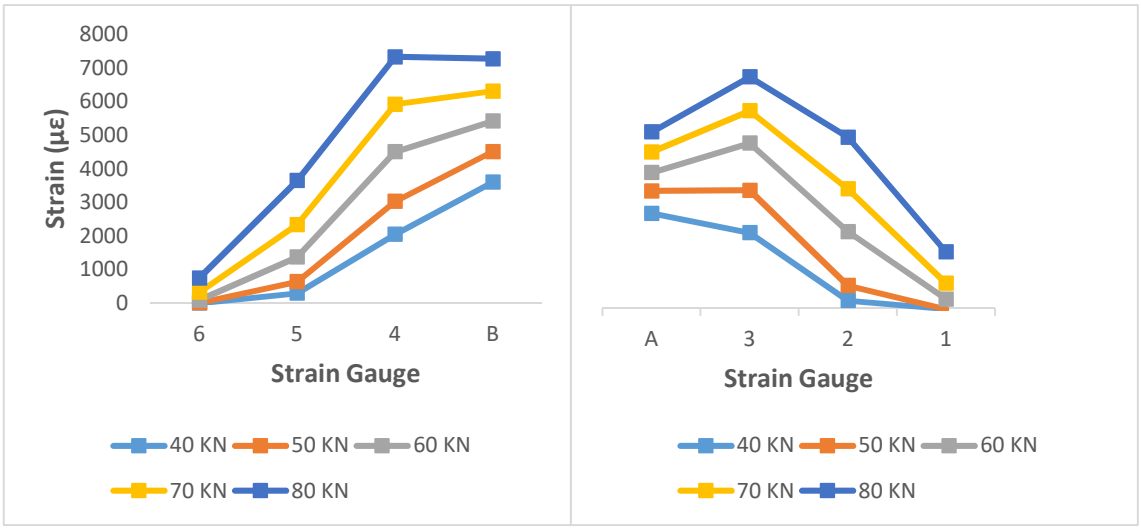

Figure 4.21 Strain Gauge Readings, Seawater Concrete with 30 cm Embedment Length

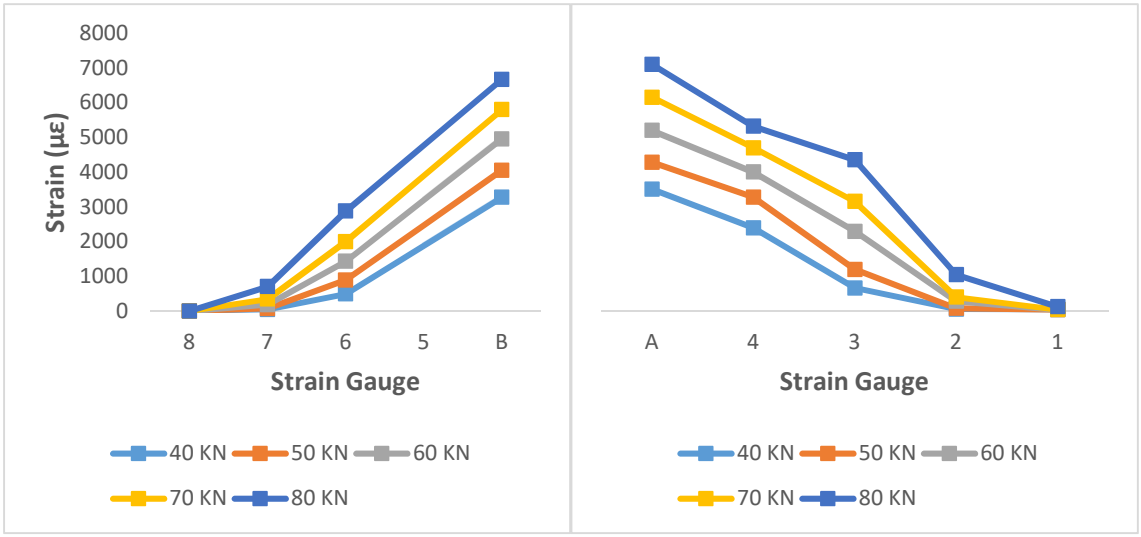

Figure 4.22 Strain Gauge Readings, Normal Concrete with 40 cm Embedment Length

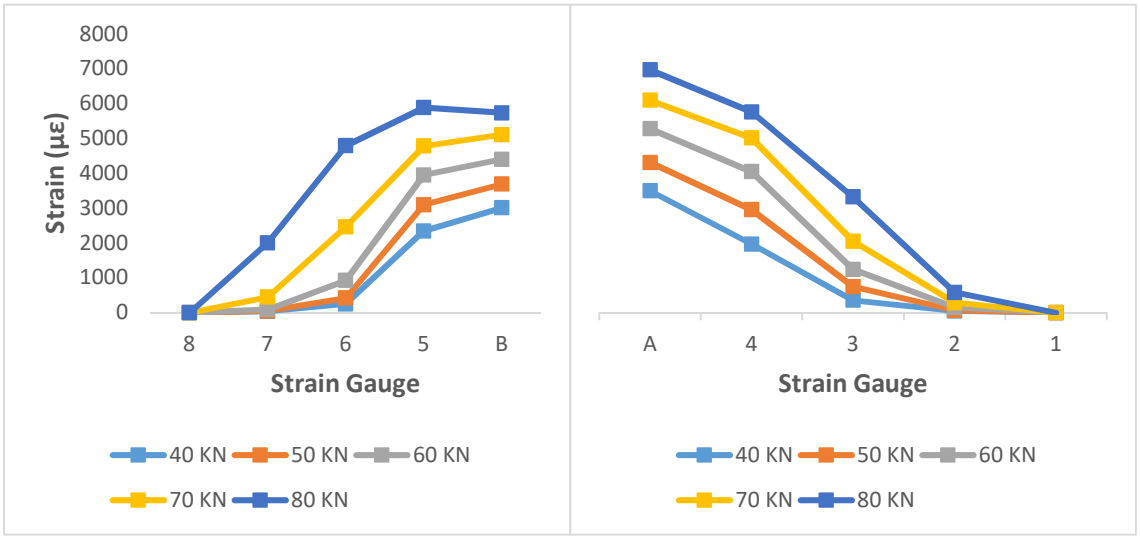

Figure 4.23 Strain Gauge Readings, Seawater Concrete with 40cm Embedment Length

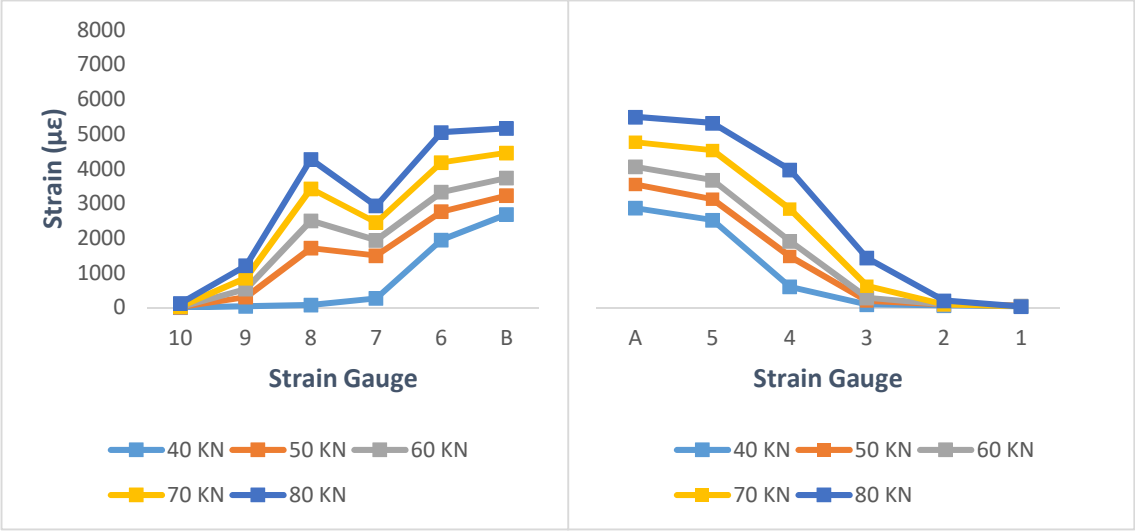

Figure 4.24 Strain Gauge Readings, Normal Concrete with 50 cm Embedment Length

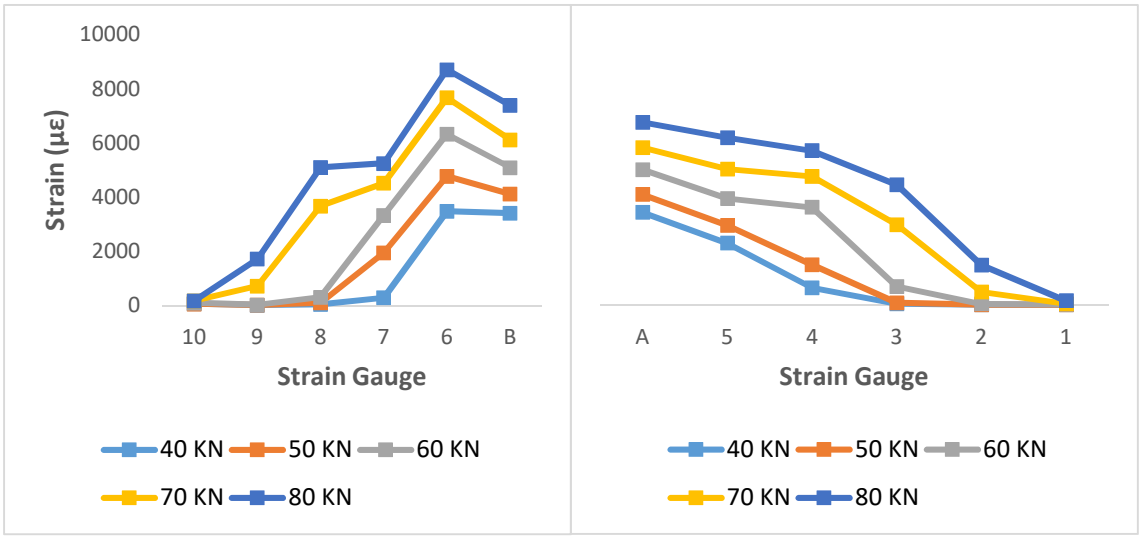

Figure 4.25 Strain Gauge Readings, Seawater Concrete with 50 cm Embedment Length

4.6 Analysis

4.6.1 Bond Strength

Relying on the recorded strain measurements and using the known GFRP bar properties like modulus of elasticity and cross sectional area, the difference in bar forces between two strain gauges can be used to obtain an approximate bond stress distribution along the embedded portion of the bars.

The bond stress distribution plotted in Figure 4.26 to 4.31 may be obtained according to Equations 4.4 to 4.7:

Strain difference between 2 points:

$$\Delta\varepsilon = \varepsilon_2 - \varepsilon_1 \qquad \text{Eq. 4.4}$$

$$\Delta\sigma = \Delta\varepsilon \times \mathrm{E} \qquad \text{Eq. 4.5}$$

Then:

$$\Delta F = \Delta\varepsilon \times E \times A \qquad \text{Eq. 4.6}$$

$$\tau = \frac{\Delta\varepsilon \times E \times A}{100 \times \pi \times D} \qquad \text{Eq. 4.7}$$

Where:

$\Delta\varepsilon = Strain\ Difference$

$\Delta\sigma = Stress\ Difference$

$E = Modulus\ of\ Elasticity\ (MPa)$

$A = Bar\ Cross\ Sectional\ area\ (mm^2)$

$100\ (mm) = Distance\ Between\ Strain\ Gauges$

$\tau = Bond\ Stress\ (MPa)$

$D = Bar\ Diameter\ (mm)$

It can be observed from Figures 4.26 to 4.31 that the bond stress is initially highest near the midspan, but the peak bond stress gradually shifts away from the midspan as the bar starts to slip and the longitudinal splitting crack begins to propagate. The bond stress nearest the pocket tended to reduce close to zero at failure. At the highest load levels, the peak bond stress was typically observed near the midpoint of the embedded portion of the bar just prior to failure. The peak bond stress tended to be approximately 10 MPa in all cases. As expected, this is slightly less than the peak bond stress values obtained in the pullout tests reported in Chapter 3.

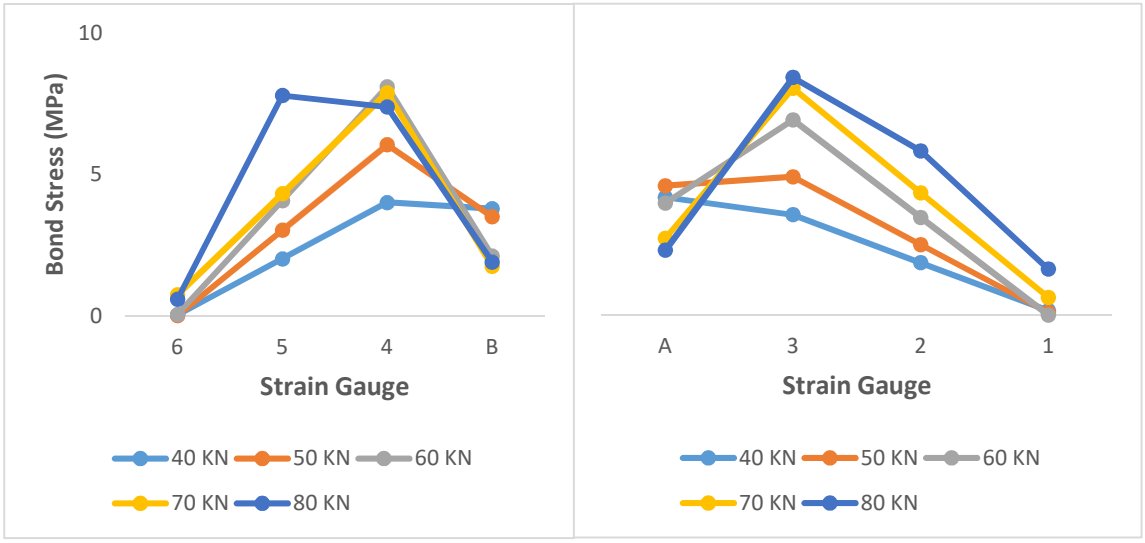

Figure 4.26 Normal Concrete Bond Stress Distribution, 30 cm Embedment Length

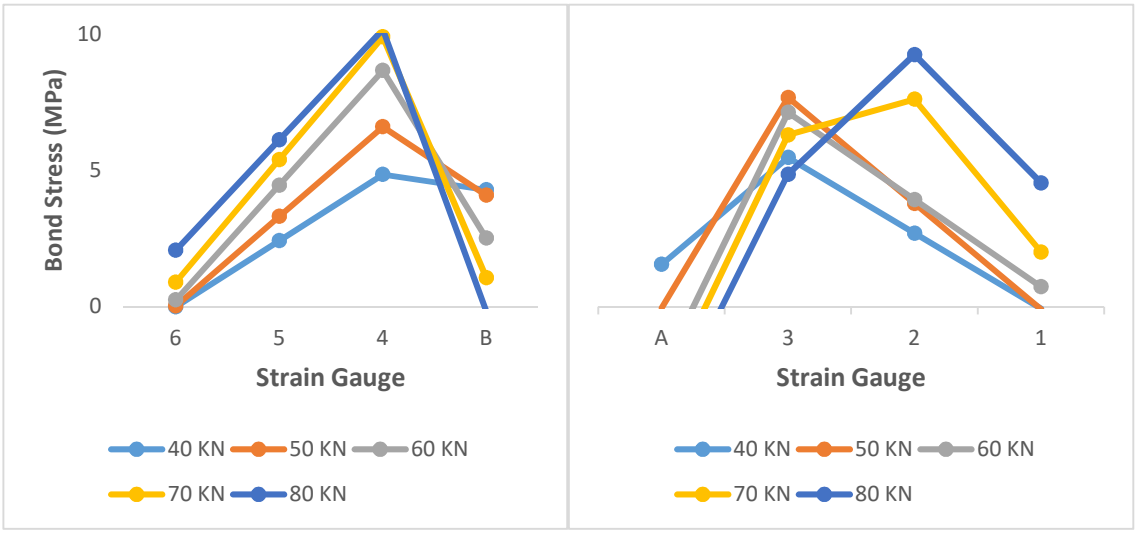

Figure 4.27 Seawater Concrete Bond Stress Distribution, 30 cm Embedment Length

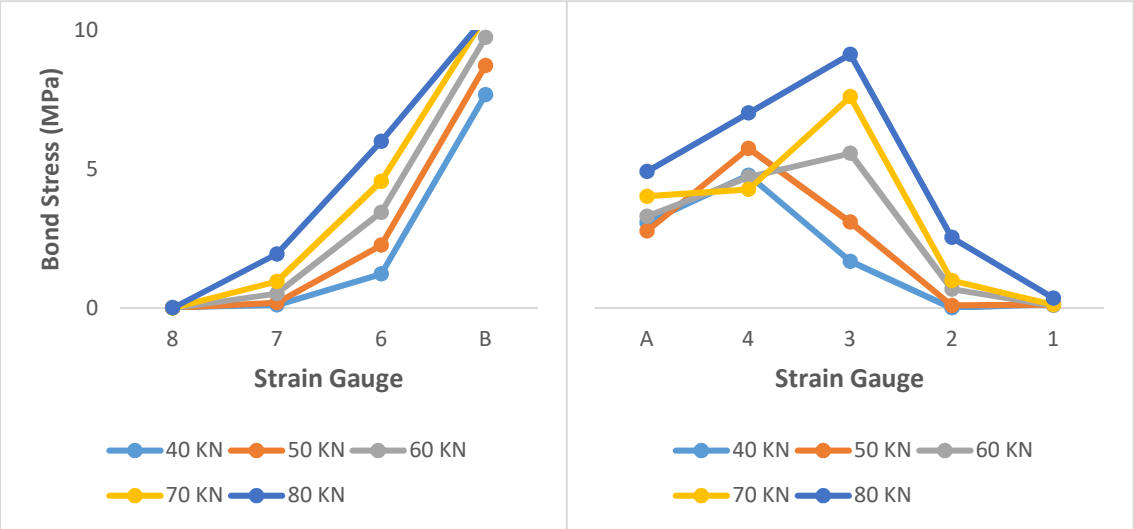

Figure 4.28 Normal Concrete Bond Stress Distribution, 40 cm Embedment Length

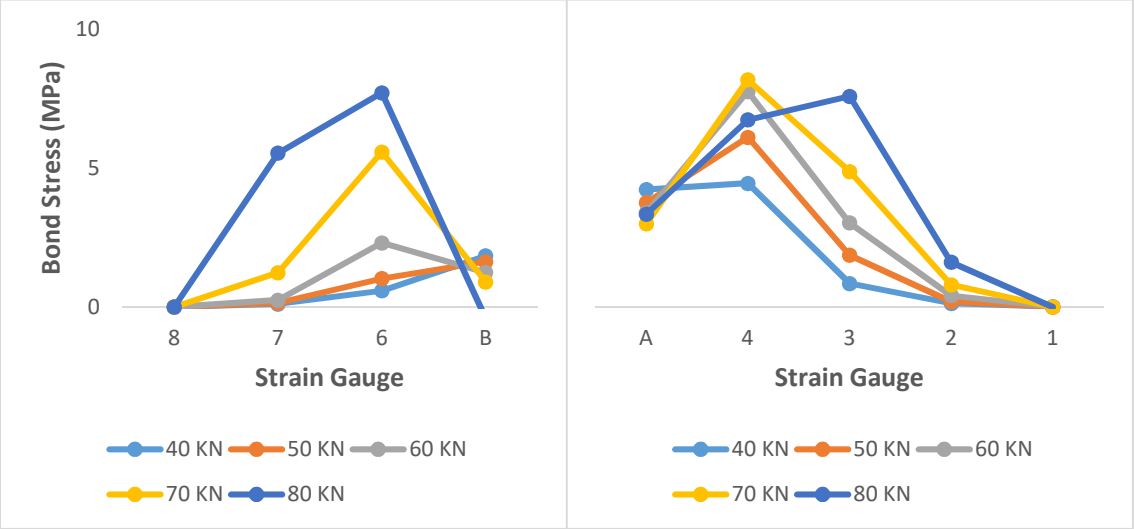

Figure 4.29 Seawater Concrete Bond Stress Distribution, 40 cm Embedment Length

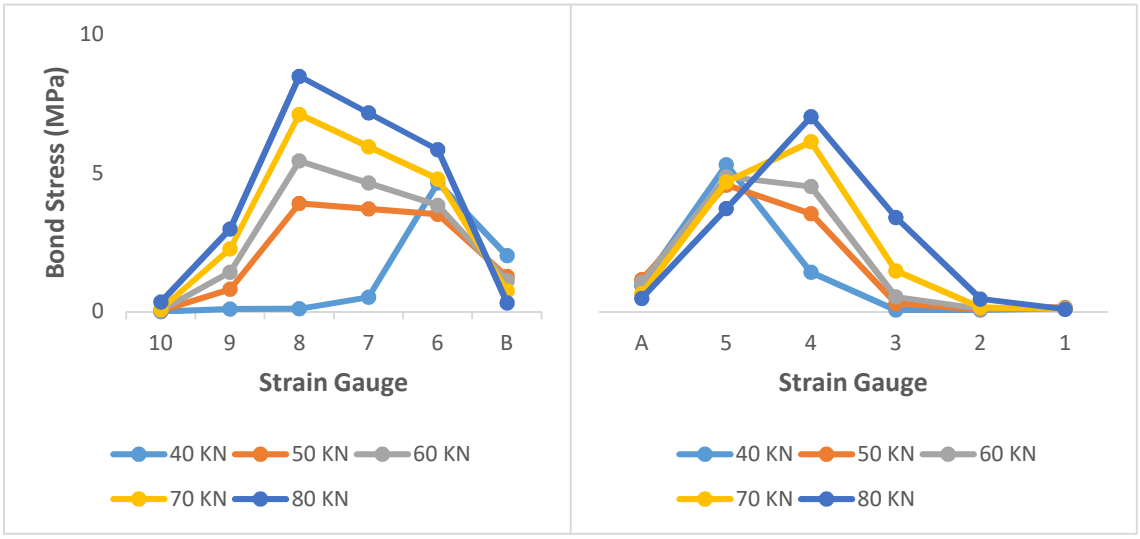

Figure 4.30 Normal Concrete Bond Stress Distribution, 50 cm Embedment Length

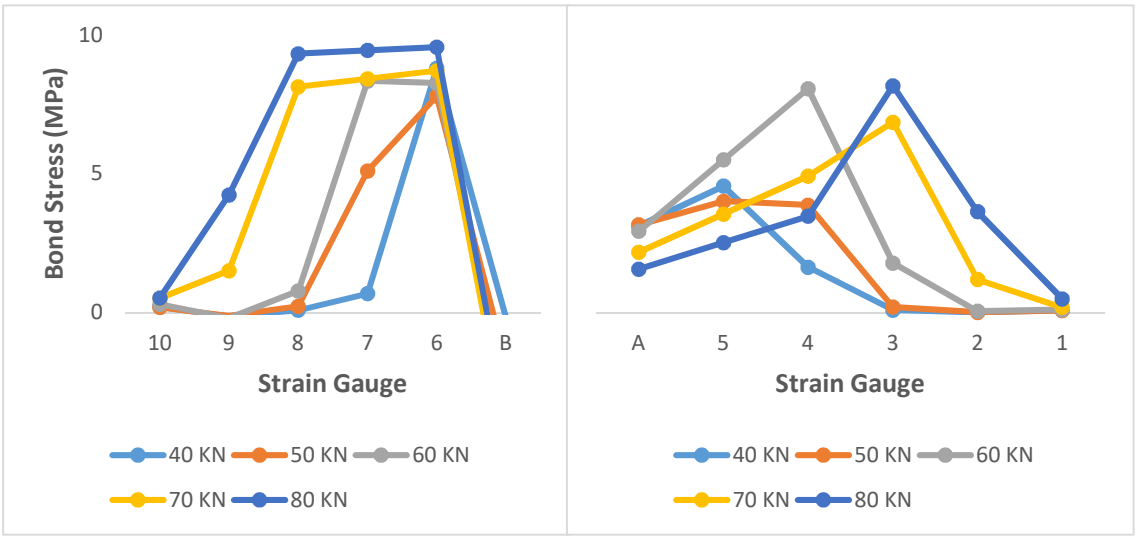

Figure 4.31 Seawater Concrete Bond Stress Distribution, 50 cm Embedment Length

4.6.2 Experimental Development Length

The theoretical development length is calculated based on the CSA S806-12 [72] proposed formula:

$$l_d = 1 \cdot 15 \frac{k_1 k_2 k_3 k_4 k_5}{d_{cs}} \frac{f_F}{\sqrt{f'_c}} A_b \qquad \text{Eq. 4.8}$$

Where:

$l_d = Development\ Length\ (mm)$

$K_1 = Bar\ Location\ Factor = 1$

$K_2 = Concrete\ Density\ Factor = 1$

$K_3 = Bar\ Size\ Factor = 0.8$

$K_4 = Bar\ Fibre\ Factor = 1$

$K_5 = Bar\ Surface\ Profile\ Factor = 1.05$

$f_F = Bar\ Stress\ (MPa)$

$A_b = Bar\ Area\ (mm^2)$

$f'_c = Concrete\ Compressive\ Strength\ (MPa)$

$d_{cs} = Concrete\ Bottom\ Surface\ to\ Bar\ Center\ (mm)$

Based on the above factors and parameters, the theoretical development length is equal to 970 mm, while in the actual beam specimens the embedment lengths were intentionally much lower in order to ensure an anchorage failure. Generally, the experimental development length can be obtained by plotting and extrapolating the change in failure load as a function of embedment length. While it was expected that the longer embedment lengths would result in higher failure loads, the development of diagonal shear cracks near the loading point actually resulted in relatively similar failure loads between the beams as previously discussed. Thus, the experimental development lengths cannot be derived with much certainty with these results.

Nevertheless, an approximation is attempted here for the sake of discussion which should be verified with further testing. The results obtained from the pullout tests presented in Chapter 3 with an embedment length of 80 mm, along with the failure loads presented in this chapter for embedment lengths of 300 to 500 mm, are plotted in Figure 4.32. By passing a trend line through the experimental results and the origin, and extrapolating to the average tensile rupture stress of the bars (1339 MPa), the experimental development length is found to be 1061 and 1069 mm for the normal and seawater concrete, respectively. Given that the failure loads for the higher embedment lengths were lower than expected due to the diagonal crack propagation, the actual development length of the bars is also expected to be less than the extrapolated value shown here and is likely close to that predicted by the design equation. This can be verified through further testing with longer embedment lengths and by shifting the pockets further away from the loading point in future studies. It should also be noted that the pullout test results should generally not be directly compared to the beam-anchorage tests due to the different stress states in the concrete and bar, but are provided here for reference given the small number of beam tests.

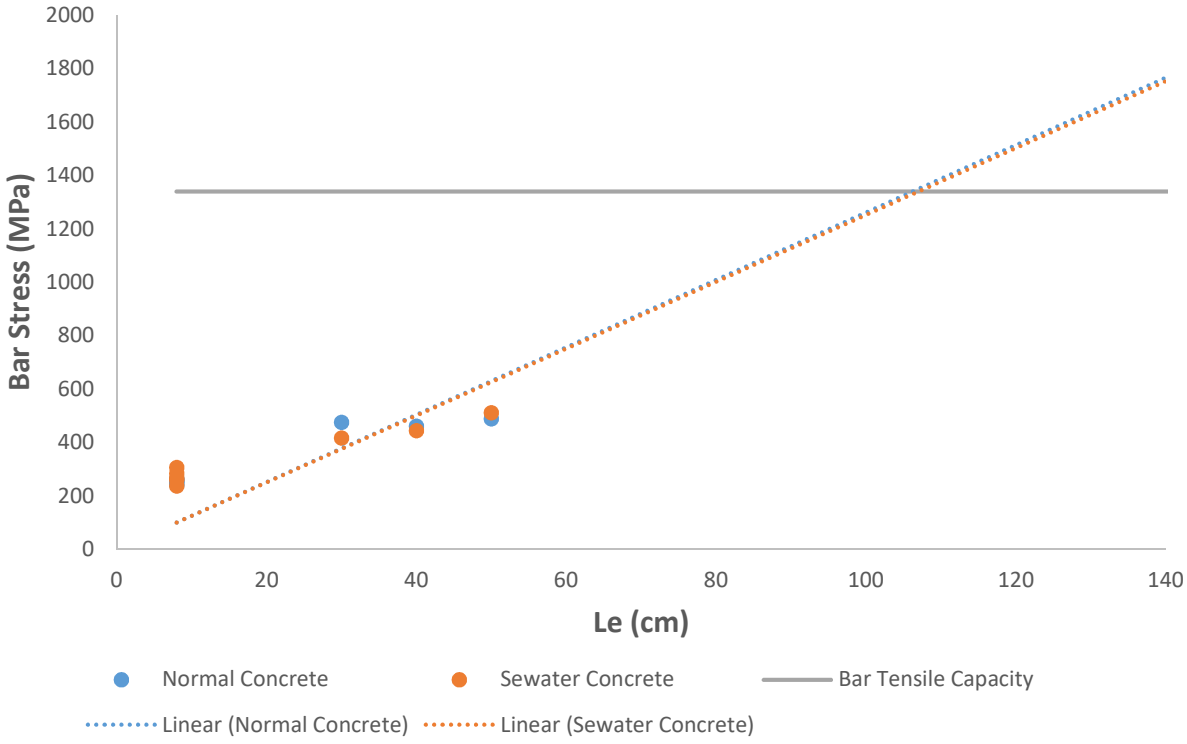

Figure 4.32 Experimental Development Length

It is important to note that a linear trendline implies a uniform bond stress distribution along the embedment length, which is not supported by the experimental results or in the literature. Nevertheless, this simplifying assumption is often used in practice due to challenges associated with accurately characterizing bond stress distributions over long embedment lengths. Further research is recommended to clarify this issue.

The maximum bond stress obtained from the strain gauge measurements was in the range of 8-10 MPa for each of the beams tested. Under a uniform bond stress of 8 MPa, the development length for a 16 mm bar would be 69.6 cm, whereas a triangular distribution varying from 0 to 10 MPa (average of 5 MPa) results in a development length of 111.3 cm. Non-linear functions (e.g. exponential or parabolic) may also be suitable, although the experimental results obtained are not conclusive in this regard. The theoretical development length of 97.0 cm corresponds to an average bond stress of approximately 5.7 MPa, which is fairly reasonable when compared with the experimental results obtained.

4.7 Discussion

According to the test results from the beam anchorage specimens presented in this chapter, the seawater concrete beams showed a similar behaviour overall to the normal concrete specimens. The peak loads and force-slip responses were similar, as were the strain and bond stress distributions. The seawater beams showed more of an increase in load with increasing embedment length, although due to the small number of tests the likely variation in the experimental results is not known.

Moreover, the approximated experimental development lengths were similar for both concrete types and were reasonably close to the theoretical development length (Figure 4.32), especially when considering the likely effect of inclined cracking on the recorded failure loads. This is a promising sign to suggest that seawater concrete conforms with design code requirements for GFRP-reinforced concrete structures, although further research needs to be done to investigate any potential long term issues.

Considering these results together with the pullout test results from Chapter 3, the beam anchorage test results provide further support to suggest that the use of seawater concrete will result in similar performance as conventional concrete for structural elements reinforced with GFRP bars (at least in terms of short term behaviour).

Chapter 5 Conclusions

5.1 Conclusion

The intent of this research was to investigate the potential effects that seawater concrete might have on the bond behaviour of GFRP bars with two different surface configurations. During recent years, concerns about future water security have increased the importance of investigations of the effect of seawater substitution with potable water. Therefore, the construction industry as a huge water consumer cannot stay neutral. The concrete production as a large part of this huge industry is one of the main industrial users of water. As a result, the seawater substitution can offer an acceptable answer to these concerns related for the construction industry, but the effect of seawater on concrete performance should be investigated.

The major known drawback of using seawater is corrosion due to high concentration of chlorides which can initiate the deterioration of steel reinforcement. FRP products have shown a reliable performance against corrosion, given their corrosion-resistant properties. Among all different types, GFRP is one the most widely used material due to its low cost relative to its mechanical properties.

Therefore, in the current study the bond performance of GFRP bars in seawater concrete was investigated through two sets of test methods:

1) Pullout

2) Beam Anchorage

A total of 40 cube specimens were casted, and tested under a pullout test method using a Universal Testing Machine. The specimens showed an acceptable range of peak bond strengths and residual strengths in both seawater and normal concrete. Moreover, it was demonstrated through the ANOVA test that the difference between their performance under this method is not significant.

Through another test method, the bond behaviour was investigated by testing six full-scale specimens to see the effects of seawater on a real structural element. According to the observation from the strain gauges, the seawater concrete showed a very similar behaviour compared to normal concrete where the peak bond strength reached up to about 10 MPa in both cases. Moreover, an approximate experimental development length was calculated according to the bar force from both pullout test and beam anchorage specimens where the values were very close to the theoretical development length offered by the building code.

In conclusion, the use of seawater concrete appears very promising for construction projects in many water-stressed regions of the world, particularly when combined with corrosion-resistant FRP reinforcement.

5.2 Recommendations

For future studies and deeper understanding of the bond behaviour, besides improving the results obtained from the test specimens it is highly recommended to: test larger beams with longer embedment lengths, study the shear behaviour, assess the long term performance and behaviour besides the durability issues and microstructure investigations though the specimens. All above mentioned recommendations contributes to a broader look and understanding on this topic.

Chapter 6 References

[1] E. A. Ahmed, M. Asce, F. Settecasi, and B. Benmokrane, "Construction and Testing of GFRP Steel Hybrid-Reinforced Concrete Bridge-Deck Slabs of Sainte-Catherine Overpass Bridges," vol. 19, no. 6, pp. 1–11, 2014.

[2] B. Benmokrane, E. El-salakawy, A. El-ragaby, and T. Lackey, "Designing and Testing of Concrete Bridge Decks Reinforced with Glass FRP Bars," vol. 11, no. April, pp. 217–229, 2006.

[3] "https://fiberline.com/sites/default/files/media/Brochure." .

[4] "https://www.iaea.org/sites/default/files/publications/magazines/bulletin." .

[5] C. Meyer, "Concrete Materials and Sustainable Development in the United States By," 1992.

[6] A. Rteil, K. Soudki, and T. Topper, "Mechanics of bond under repeated loading," *Constr. Build. Mater.*, vol. 25, no. 6, pp. 2822–2827, 2011.

[7] D. Darwin, J. H. Allen, and J. F. Silva, "Bond and Development of Straight Reinforcing Bars in Tension Reported by ACI Committee 408," pp. 1–49, 2003.

[8] P. J. M. Monteiro, S. A. Miller, and A. Horvath, "Produce and use with care," *Nat. Publ. Gr.*, vol. 16, no. 7, pp. 698–699, 2017.

[9] S. A. Miller, A. Horvath, and P. J. M. Monteiro, "Readily implementable techniques can cut annual CO 2 emissions from the production of concrete by Readily implementable techniques can cut annual CO 2 emissions from the production of concrete by over 20 %."

[10] S. A. Miller, A. Horvath, and P. J. M. Monteiro, "Impacts of booming concrete production on water resources worldwide," *Nat. Sustain.*, vol. 1, no. 1, pp. 69–76, 2018.

[11] "https://www.who.int/en/news-room/fact-sheets/detail/drinking-water#.," *WHO 2015*, 2015. .

[12] F. M. Wegian, "Effect of seawater for mixing and curing on structural concrete," vol. 3260, 2010.

[13] Andrew Maddocks, "Ranking the World's Most Water-Stressed Countries

in 2040." [Online]. Available: https://www.wri.org/blog/2015/08/ranking-world-s-most-water-stressed-countries-2040.

[14] H. Y. Ghorab, M. S. Hilal, and E. A. Kishar, "Effect of mixing and curing waters on the behaviour of cement pastes and concrete part II: properties of cement paste and concrete," *Cem. Concr. Res.*, vol. 20, no. 1, pp. 868–878, 1990.

[15] K. Katano, N. Takeda, Y. Ishizeki, K. Iriya, F. Ash, and L. Sand, "Properties and Application of Concrete Made with Sea Water and Un-washed Sea Sand."

[16] M. Etxeberria, A. Gonzalez-corominas, and P. Pardo, "Influence of seawater and blast furnace cement employment on recycled aggregate concretes ' properties," *Constr. Build. Mater.*, vol. 115, pp. 496–505, 2016.

[17] "MIXING AND CURING WATERS ON THE," vol. 20, no. c, pp. 69–72, 1990.

[18] A. Younis, U. Ebead, P. Suraneni, and A. Nanni, "Fresh and hardened properties of seawater-mixed concrete," *Constr. Build. Mater.*, vol. 190, pp. 276–286, 2018.

[19] S. K. Kaushik and S. Islam, "Suitability of Sea Water for Mixing Structural Concrete Exposed to a Marine Environment," vol. 9465, no. 95, pp. 177–185, 1995.

[20] J. Xiao, C. Qiang, A. Nanni, and K. Zhang, "Use of sea-sand and seawater in concrete construction : Current status and future opportunities," *Constr. Build. Mater.*, vol. 155, pp. 1101–1111, 2017.

[21] T. Nishida, D. Ph, N. Otsuki, D. Ph, M. Asce, and H. Ohara, "Some Considerations for Applicability of Seawater as Mixing Water in Concrete," vol. 27, no. 1980, pp. 1–7, 2015.

[22] R. L. Henry and D. F. Griffin, "THE EFFECT OF SALT IN CONCRETE ON COMPRESSIVE STRENGTH, WATER VAPOR TRANSMISSION, AND CORROSION OF REINFORCING STEEL," p. 44, 1964.

[23] D. A. Abrams, "Tests of impure waters for mixing concrete," *Proc. Am. Concr. Inst.*, vol. 20, no. 2, pp. 442–486, 1924.

[24] M. M. Islam, M. S. Islam, M. Al-Amin, and M. M. Islam, "Suitability of sea water on curing and compressive strength of structural concrete," *J.*

Civ. Eng in., vol. 40, no. 1, pp. 37–45, 2012.

[25] D. L. Narver, "Good concrete made with coral and water," *Civ. Engng*, vol. 24, pp. 654–658, 1964.

[26] H. H. Steinour, "Concrete mix water-how impure can it be?," *J. Portl. Cem. Asso., Res. Dev. Lab.*, vol. 2, no. 3, pp. 32–50, 1960.

[27] T. U. Mohammed, H. Hamada, and T. Yamaji, "Performance of seawater-mixed concrete in the tidal environment," vol. 34, no. September 2001, pp. 593–601, 2004.

[28] Q. Guo, L. Chen, H. Zhao, J. Admilson, and W. Zhang, "The Effect of Mixing and Curing Sea Water on Concrete Strength at Different Ages," vol. 02004, pp. 1–6, 2018.

[29] J. D. Dewar, *The workability and compressive strength of concrete made with sea water*. Cement and Concrete Association, 1963.

[30] Z. Shi, Z. Shui, Q. Li, and H. Geng, "Combined effect of metakaolin and sea water on performance and microstructures of concrete," *Constr. Build. Mater.*, vol. 74, pp. 57–64, 2015.

[31] S. Soon and P. S. Kwon, "Analysis technique for restrained shrinkage of concrete containing chlorides," pp. 475–486, 2011.

[32] S. Khatibmasjedi, F. De Caso, and A. Nanni, "SEACON: Redefining sustainable concrete," in *Sustainable Construction Materials and Technologies*, 2016, vol. 2016-August.

[33] P. J. Jensen, J. F. Lang, and J. Chao, "A Guillotine Tube Rupture Modeling Technique Using RETRAN-02," *Nucl. Technol.*, vol. 76, no. 2, pp. 279–289, 1987.

[34] M. Yan, Y. T. Li, and Y. Zhang, "Research on influence of mixtures on strength of seawater and sea sand concrete," *Shanxi Arch.*, vol. 38, no. 30, pp. 135–136, 2012.

[35] H. Y. Ghorab, M. S. Hilal, and E. A. Kishar, "Effect of mixing and curing waters on the behaviour of cement pastes and concrete part 1 : Microstructure of cement pastes," *Cem. Concr. Res.*, vol. 19, no. 6, pp. 868–878, 1989.

[36] Z. L. Chen, X. N. Tang, G. F. Sun, and Y. L. Liu, "Research on durability and application of seawater concrete," *Ocean Eng.*, vol. 26, no. 4, pp. 102–106, 2008.

[37] M. Makita, Y. Mori, and K. Katawaki, “No Title,” *A.C.I. Publ. SP-65*, pp. 271–289, 1980.

[38] R. Shalon and M. Raphael, “Influence of sea water on corrosion of reinforcement,” *J. Am. Concr. Inst.*, vol. 55, no. 12, pp. 1251–1268, 1959.

[39] N. Otsuki, T. Saito, and Y. Tadokoro, “Possibility of seawater as mixing water in concrete,” *J. Civ. Eng. Archit.*, vol. 6, no. 10, pp. 1273–1279, 2012.

[40] J. G. Dempsey, “Coral and salt water as concrete materials,” *ACI Mater. J.*, vol. 48, no. 10, pp. 157–166, 1951.

[41] A. Younis, U. A. Ebead, and A. Nanni, “A PERSPECTIVE ON SEAWATER / FRP REINFORCEMENT IN CONCRETE A PERSPECTIVE ON SEAWATER / FRP REINFORCEMENT IN CONCRETE STRUCTURES,” no. July, 2017.

[42] B. Benmokrane, A. H. Ali, H. M. Mohamed, A. Elsafty, and A. Manalo, “Laboratory assessment and durability performance of vinyl-ester, polyester, and epoxy glass-FRP bars for concrete structures,” *Compos. Part B*, 2017.

[43] G. Mathys, “Stability of polyester- and vinyl ester-based composites in seawater,” vol. 9, pp. 6073–6077, 2004.

[44] P. Wang, *Effect of Moisture, Temperature, and Alkaline on Durability of E-glass/vinyl Ester Reinforcing Bars*. Université de Sherbrooke., 2005.

[45] C. Zou, J. C. Fothergill, and S. W. Rowe, “The effect of water absorption on the dielectric properties of epoxy nanocomposites,” *IEEE Trans. Dielectr. Electr. Insul.*, vol. 15, no. 1, pp. 106–117, 2008.

[46] M. Robert, P. Cousin, and B. Benmokrane, “Durability of GFRP Reinforcing Bars Embedded in Moist Concrete,” vol. 13, no. April, pp. 66–73, 2009.

[47] S. P. Tastani, S. J. Pantazopoulou, and M. Asce, “Bond of GFRP Bars in Concrete : Experimental Study and Analytical Interpretation,” vol. 10, no. October, pp. 381–391, 2006.

[48] H. El-hassan, T. El-maaddawy, A. Al-sallamin, and A. Al-saidy, “Performance evaluation and microstructural characterization of GFRP bars in seawater-contaminated concrete,” *Constr. Build. Mater.*, vol. 147, pp. 66–78, 2017.

[49] H. El-hassan, T. El-maaddawy, A. Al-sallamin, and A. Al-saidy, "Durability of glass fiber-reinforced polymer bars conditioned in moist seawater-contaminated concrete under sustained load," *Constr. Build. Mater.*, vol. 175, pp. 1–13, 2018.

[50] M. Robert and B. Benmokrane, "Combined effects of saline solution and moist concrete on long-term durability of GFRP reinforcing bars," *Constr. Build. Mater.*, vol. 38, pp. 274–284, 2013.

[51] C. D. Eamon *et al.*, "Life-Cycle Cost Analysis of Alternative Reinforcement Materials for Bridge Superstructures Considering Cost and Maintenance Uncertainties," vol. 24, no. April, pp. 373–380, 2012.

[52] A. Younis, U. Ebead, and S. Judd, "Life cycle cost analysis of structural concrete using seawater , recycled concrete aggregate , and GFRP reinforcement," *Constr. Build. Mater.*, vol. 175, pp. 152–160, 2018.

[53] P. Fellow, Q. City, and Q. Canada, "DESIGN , CONSTRUCTION , AND MONITORING OF THE FIRST WORLDWIDE TWO-WAY FLAT SLAB PARKING GARAGE REINFORCED WITH GFRP BARS," pp. 1–8.

[54] H. M. Mohamed and B. Benmokrane, "Design and Performance of Reinforced Concrete Water Chlorination Tank Totally Reinforced with GFRP Bars : Case Study," vol. 05013001, no. 11, pp. 1–11, 2014.

[55] "Benmokrane, B., El-Salakawy, E., Desgagné, G., and Lackey, T. (2004). 'FRP bars for bridges.' Concr. Int., 26(8), 84–90."

[56] B. Benmokrane, E. El-salakawy, S. El-gamal, and S. Goulet, "Construction and Testing of an Innovative Concrete Bridge Deck Totally Reinforced with Glass FRP Bars : Val-Alain Bridge on Highway 20 East," vol. 12, no. 5, pp. 632–645, 2008.

[57] "Design and Construction of Building Structures with Fibre-reinforced Polymers," 2006.

[58] V. M. C. F. Cunha, J. A. O. Barros, and J. M. Sena-cruz, "Pullout Behavior of Steel Fibers in Self-Compacting Concrete," vol. 22, no. January, pp. 1–9, 2010.

[59] S. Kim and H. Yun, "Cement & Concrete Composites Evaluation of the bond behavior of steel reinforcing bars in recycled fine aggregate concrete," *Cem. Concr. Compos.*, vol. 46, pp. 8–18, 2014.

[60] M. J. Bandelt and S. L. Billington, “Bond behavior of steel reinforcement in high-performance fiber-reinforced cementitious composite flexural members,” *Mater. Struct.*, pp. 71–86, 2016.

[61] M. H. Harajli, “Comparison of Bond Strength of Steel Bars in Normal- and High-Strength Concrete,” vol. 16, no. August, pp. 365–374, 2004.

[62] M. A. Aiello and U. Salento, “Bond Performances of FRP Rebars-Reinforced Concrete,” vol. 1561, no. September 2016, 2007.

[63] M. Baena, L. Torres, A. Turon, and C. Barris, “Composites : Part B Experimental study of bond behaviour between concrete and FRP bars using a pull-out test,” *Compos. Part B*, vol. 40, no. 8, pp. 784–797, 2009.

[64] Z. Achillides and K. Pilakoutas, “Bond Behavior of Fiber Reinforced Polymer Bars under Direct Pullout Conditions,” vol. 8, no. April, pp. 173–181, 2004.

[65] B. Tighiouart, B. U. Benmokrane, and D. Gao, “Investigation of bond in concrete member with fibre reinforced polymer Ž FRP . bars,” 1998.

[66] C. C. Test *et al.*, “Standard Test Method for Bond Strength of Fiber-Reinforced Polymer Matrix Composite Bars to Concrete by Pullout Testing 1,” pp. 1–9, 2019.

[67] W. Lei, M. Yadong, L. Haibo, C. Shuang, and L. Wei, “Bond properties between FRP bars and coral concrete under seawater conditions at 30 , 60 , and 80 ° C,” *Constr. Build. Mater.*, vol. 162, pp. 442–449, 2018.

[68] “ASTM International. D7913/D7913M-14 Standard Test Method for Bond Strength of Fiber-Reinforced Polymer Matrix Composite Bars to Concrete by Pullout Testing. West Conshohocken, PA, 2014.”

[69] R. Chemicals, A. Chemical, S. Specifications, U. S. Pharmacopeia, and N. Formulary, “Standard Practice for the Preparation of Substitute Ocean Water 1,” vol. 98, no. Reapproved 2013, pp. 1–3, 2019.

[70] “ASTM International. D1141-98(2013) Standard Practice for the Preparation of Substitute Ocean Water. West Conshohocken, PA, 2013.”

[71] R. Okelo, A. M. Asce, R. L. Yuan, and M. Asce, “Bond Strength of Fiber Reinforced Polymer Rebars in Normal Strength Concrete,” vol. 9, no. June, pp. 203–213, 2005.

[72] *Design and construction of building structures with fibre-reinforced*. .

Appendix A: Pullout Stress-Slip Curves

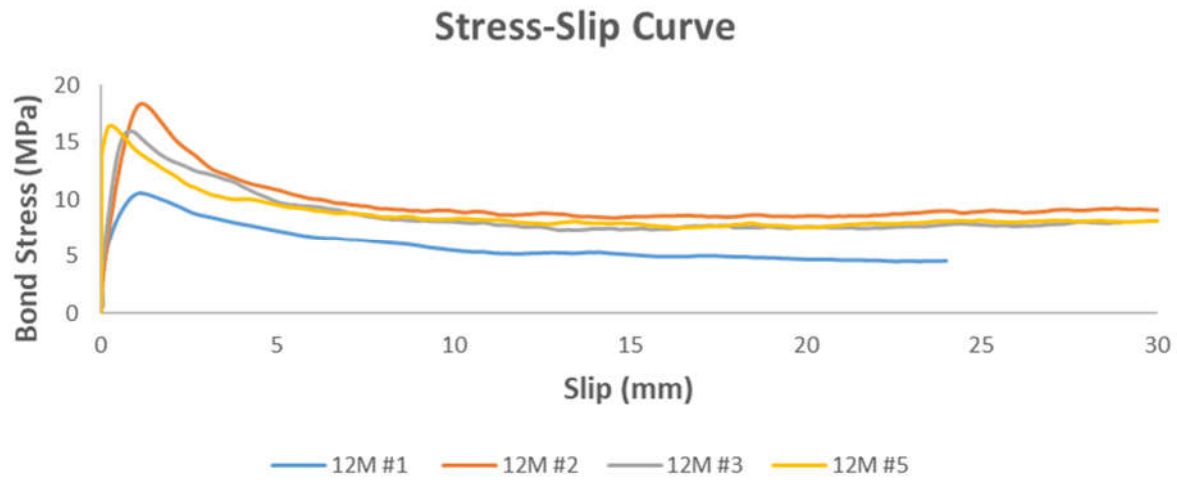

Figure 1 12M Loaded End Curve, Sand Coated Bar with Normal Concrete

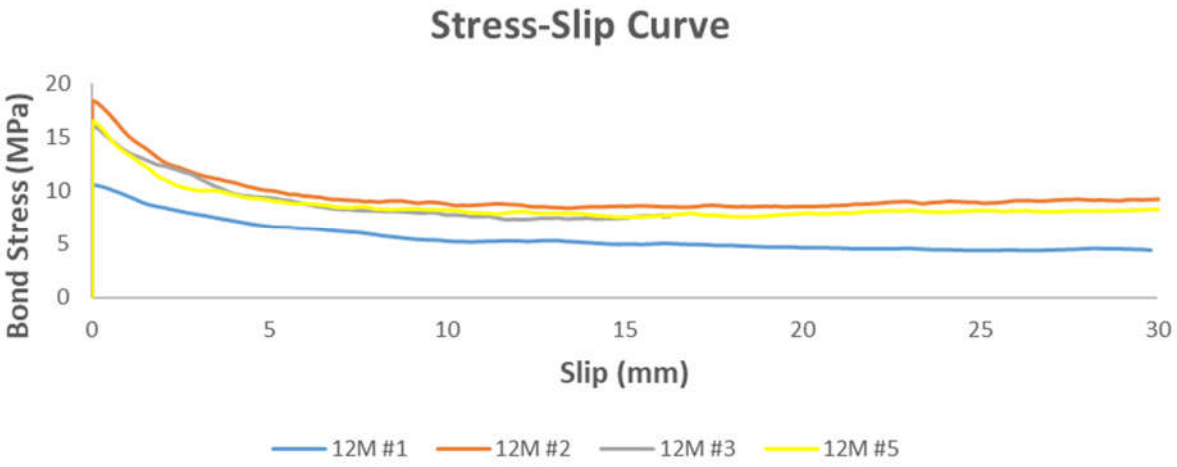

Figure 2 12M Unloaded End Curve, Sand Coated Bar with Normal Concrete

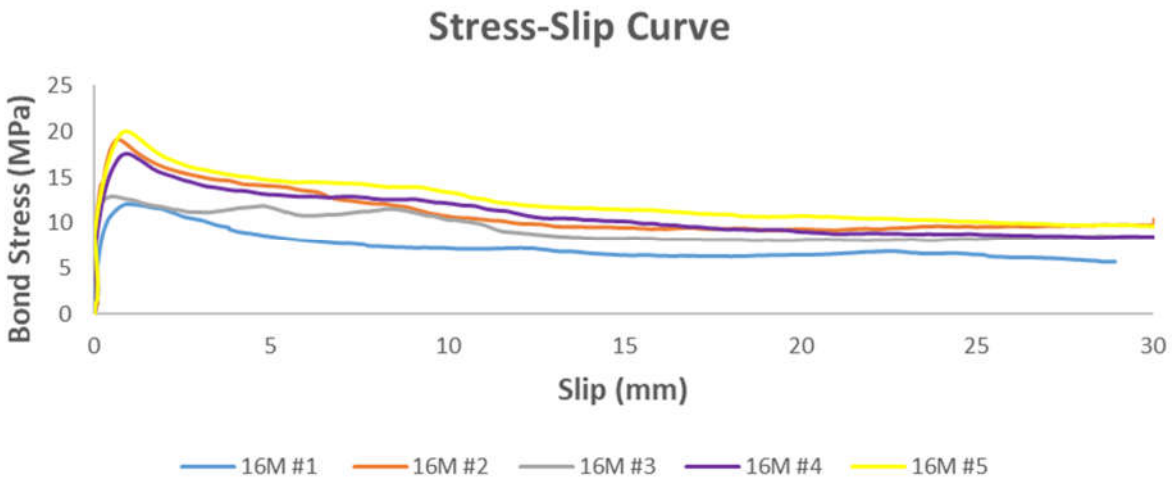

Figure 3 16M Loaded End Curve, Sand Coated Bar with Normal Concrete

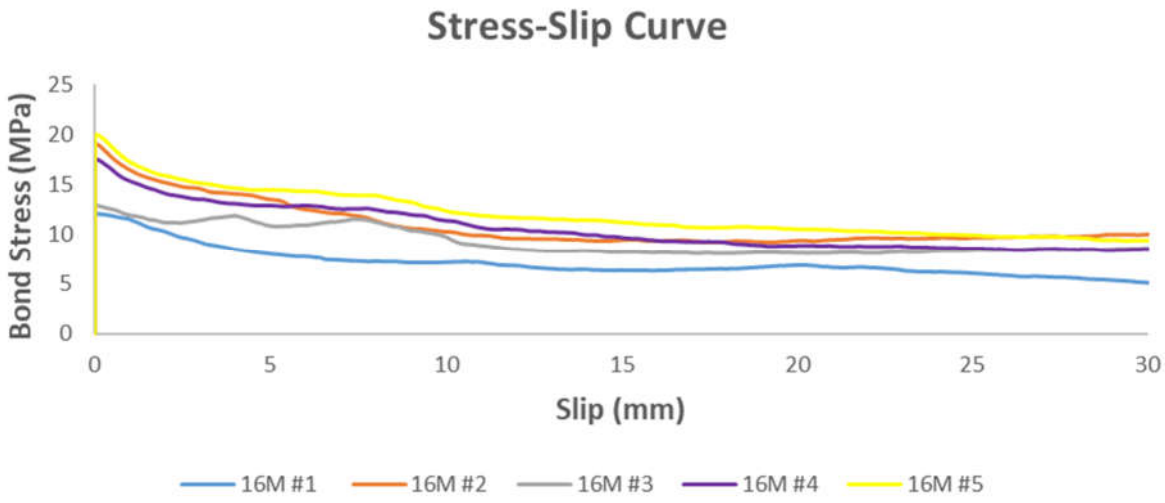

Figure 4 16M Unloaded End Curve, Sand Coated Bar with Normal Concrete

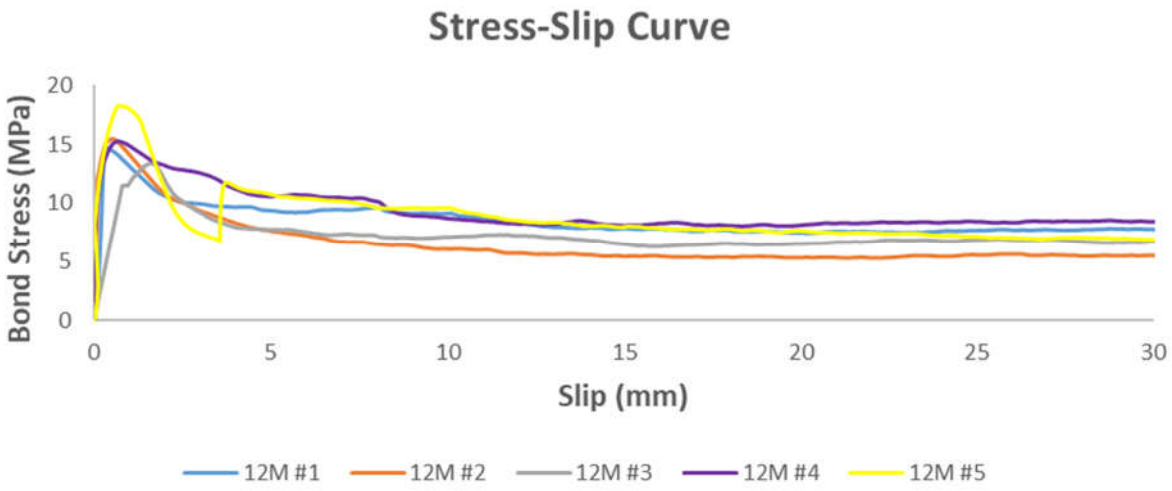

Figure 5 12M Loaded End Curve, Sand-coated Bar with Seawater Concrete

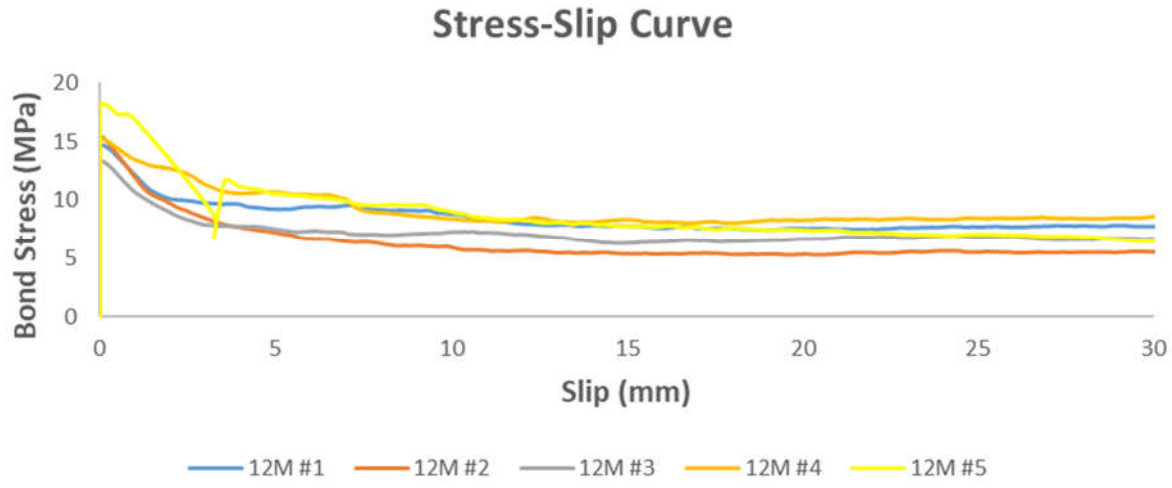

Figure 6 12M Unloaded End Curve, Sand-coated Bar with Seawater Concrete

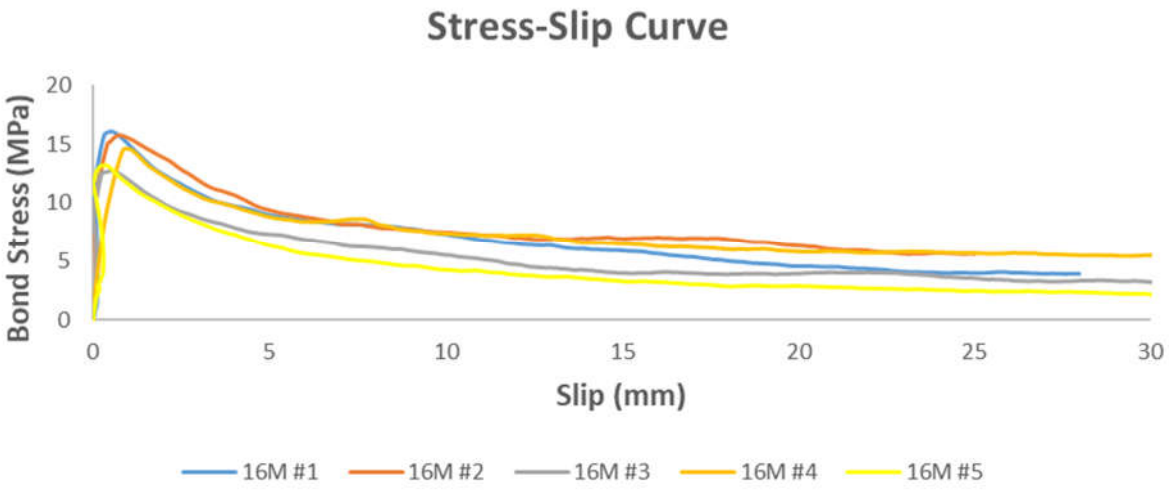

Figure 7 16M Loaded End Curve, Sand-coated Bar with Seawater Concrete

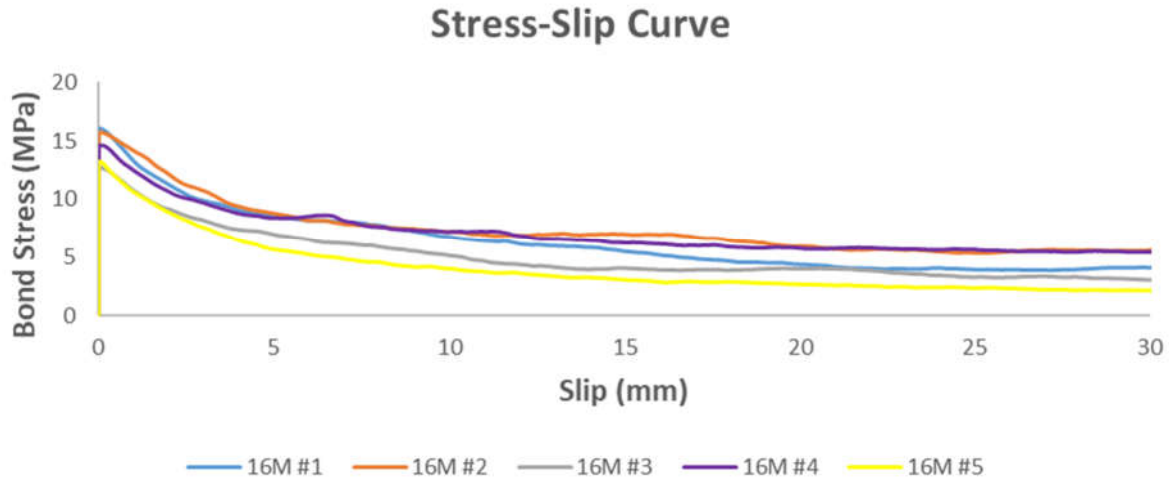

Figure 8 16M Unloaded End Curve, Sand-coated Bar with Seawater Concrete

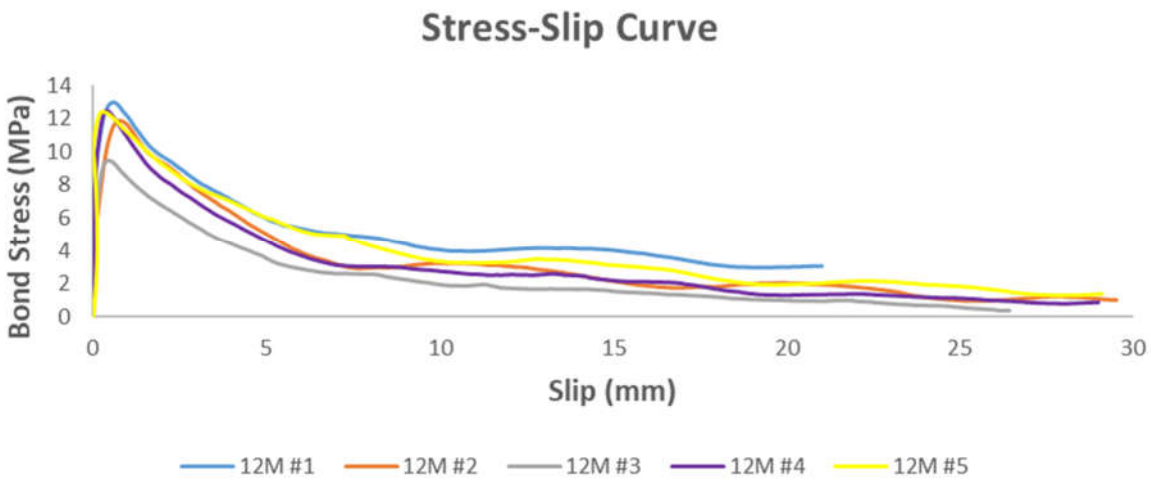

Figure 9 12M Loaded End Curve, Spiral bar with Normal Concrete

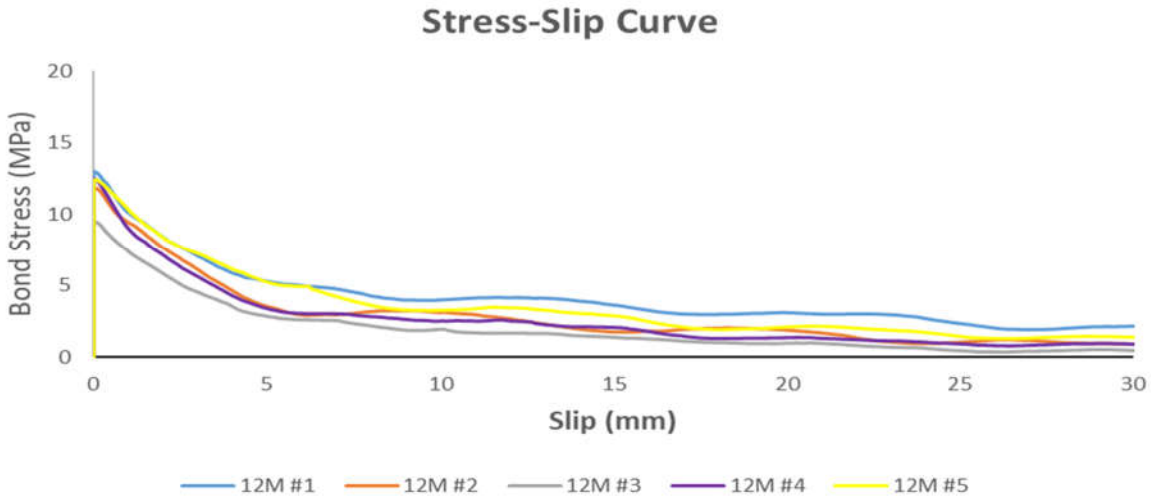

Figure 10 12M Unloaded End Curve, Spiral bar with Normal Concrete

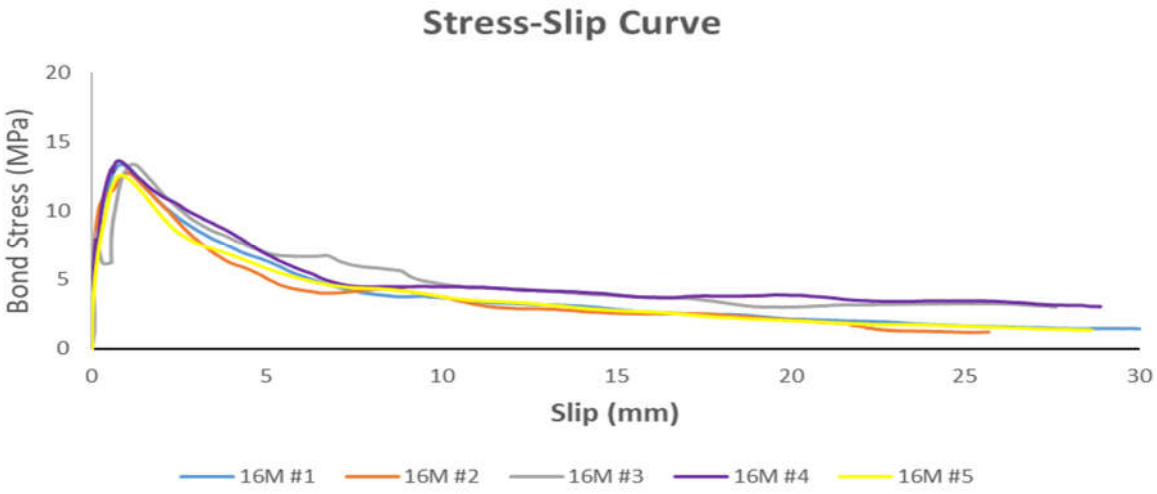

Figure 11 16M Loaded End Curve, Spiral bar with Normal Concrete

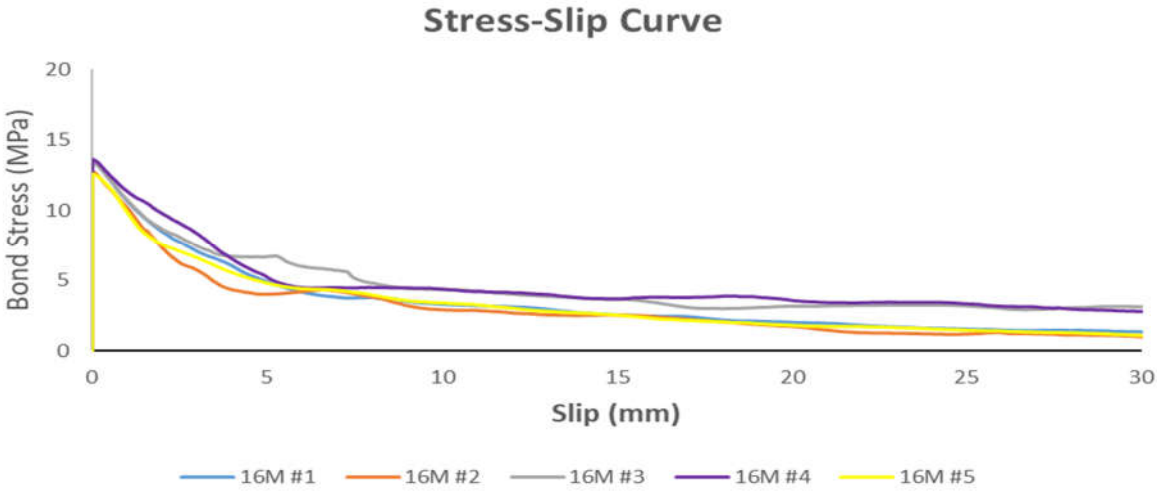

Figure 12 16M Unloaded End Curve, Spiral bar with Normal Concrete

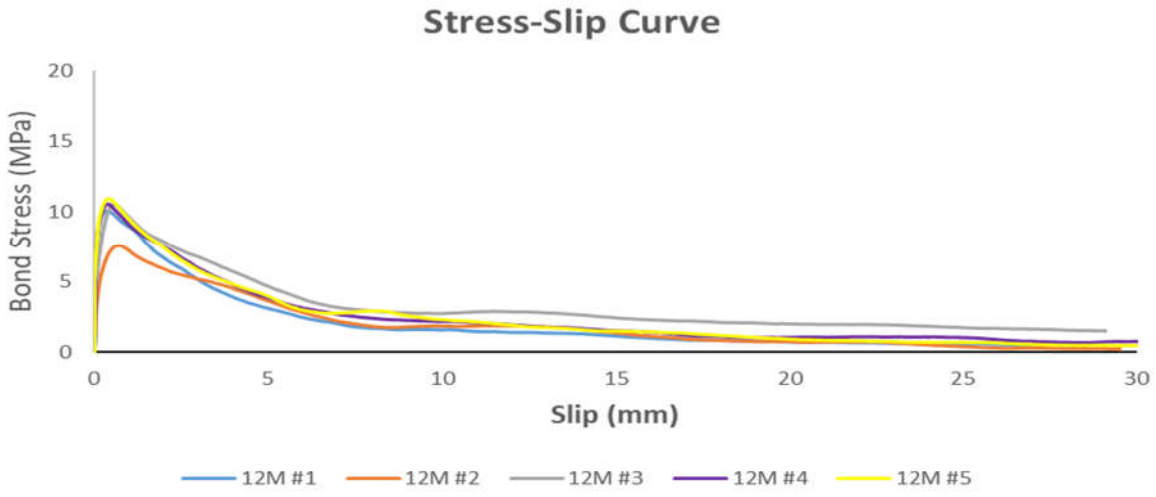

Figure 13 12M Loaded End Curve, Spiral bar with Seawater Concrete

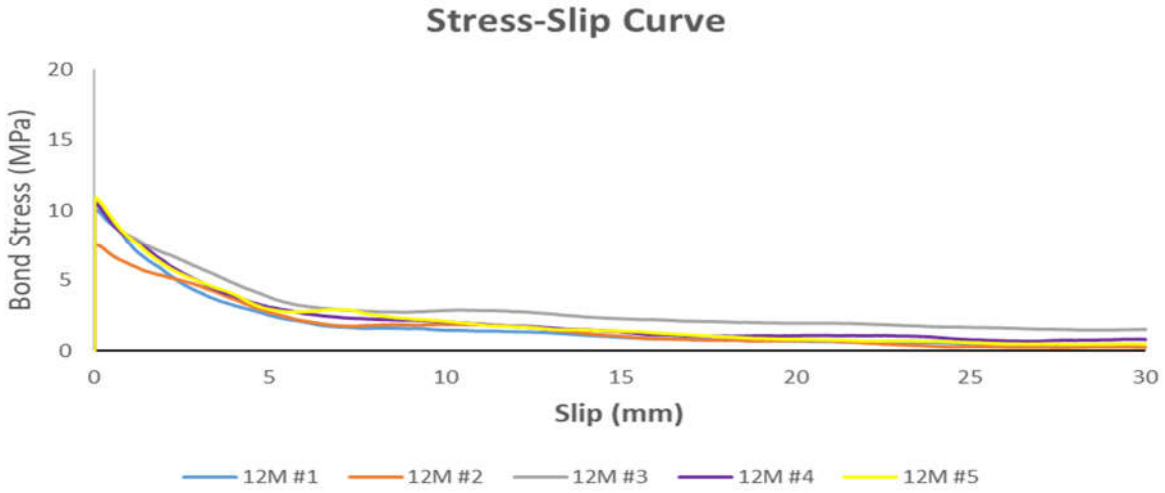

Figure 14 12M Unloaded End Curve, Spiral bar with Seawater Concrete

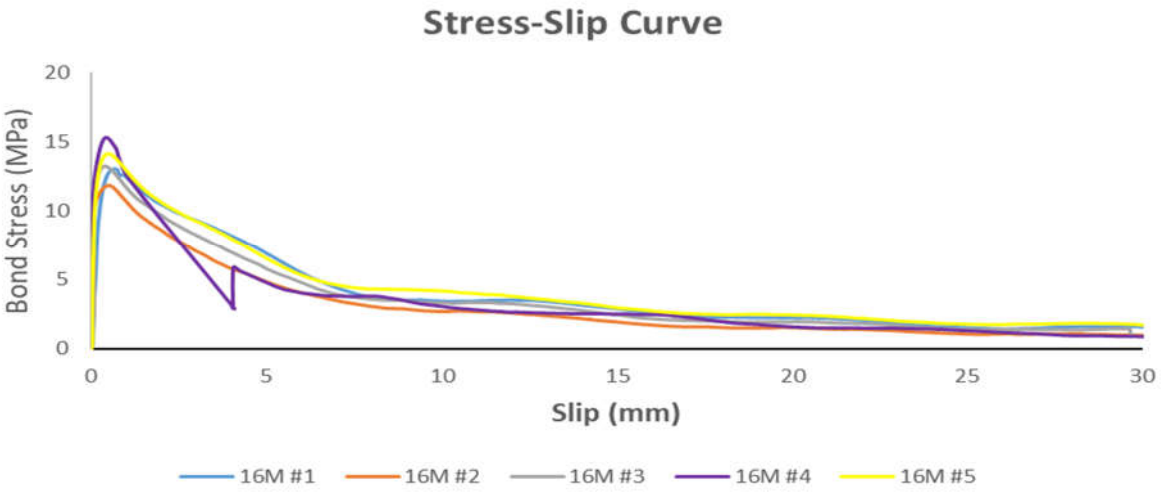

Figure 15 16M Loaded End Curve, Spiral bar with Seawater Concrete

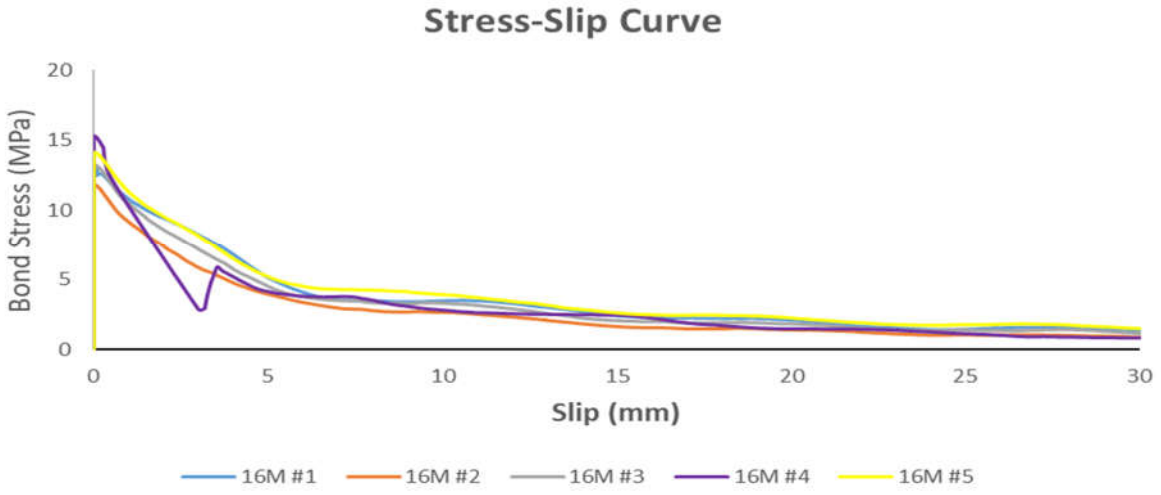

Figure 16 16M Unloaded End Curve, Spiral bar with Seawater Concrete